

A LAGRANGIAN MODEL FRAMEWORK FOR THE SIMULATION
OF FLUID FLOW AND SOLUTE TRANSPORT IN SOILS

ALEXANDER STERNAGEL

A LAGRANGIAN MODEL FRAMEWORK FOR THE
SIMULATION OF FLUID FLOW AND SOLUTE TRANSPORT IN
SOILS

Zur Erlangung des akademischen Grades eines

DOKTORS DER NATURWISSENSCHAFTEN
(Dr. rer. nat.)

von der KIT-Fakultät für
Bauingenieur-, Geo- und Umweltwissenschaften
des Karlsruher Instituts für Technologie (KIT)
genehmigte

DISSERTATION

von
M. Sc. Alexander Sternagel
aus Mainz

Tag der mündlichen Prüfung:
04. April 2023

REFERENT: Prof. Dr. Erwin Zehe
KORREFERENT: Prof. Dr. Alberto Guadagnini

Karlsruhe 2023



This document is licensed under a Creative Commons Attribution 4.0 International License (CC BY 4.0): <https://creativecommons.org/licenses/by/4.0/deed.en>

Dedicated to all my friends and my beloved family,

to my mother and father,
for making every opportunity in life possible for me

and

to Constantin und Dorothee,
for being the third member of your team

and

to Jannika,
for your companionship and all the emotional support
(despite our countless disagreements).

CONTENTS

LIST OF FIGURES	x
LIST OF TABLES	xii
ABSTRACT	xiii
ZUSAMMENFASSUNG	xvi
I INTRODUCTION	
1.1 General motivation	3
1.2 Theoretical background	3
1.2.1 Physical basics of soil water flow and solute transport	3
1.2.2 Particle-based, Lagrangian approach	12
1.3 Objectives of the thesis	14
II SIMULATING PREFERENTIAL SOIL WATER FLOW AND TRACER TRANSPORT USING THE LAGRANGIAN SOIL WATER AND SOLUTE TRANSPORT MODEL	
2.1 Introduction	21
2.2 Concept and implementation of the LAST-Model . . .	24
2.2.1 The Lagrangian model of Zehe and Jackisch (2016) in a nutshell	24
2.2.2 Representation of solute transport in the LAST-Model	25
2.2.3 The macropore domain and representation of preferential flow	25
2.3 Model benchmarking	32
2.3.1 Evaluation of the solute transport and linear mixing approach during well-mixed matrix flow	32
2.3.2 Parameterization and evaluation of the preferential flow domain	33
2.3.3 Simulations with HYDRUS 1-D	35
2.3.4 Sensitivity analyses of selected parameters . . .	36
2.4 Results	39
2.4.1 Simulation of solute transport under well-mixed conditions	39
2.4.2 Evaluation of the preferential flow domain . . .	40
2.4.3 Comparison with HYDRUS 1-D	42
2.4.4 Sensitivity analyses	42
2.5 Discussion and conclusions	47
2.5.1 New routine for solute transport and diffusive mixing	47
2.5.2 Model extension to account for preferential flow in macropores	47

III SIMULATION OF REACTIVE SOLUTE TRANSPORT IN THE CRITICAL ZONE: A LAGRANGIAN MODEL FOR TRANSIENT FLOW AND PREFERENTIAL TRANSPORT	
3.1	Introduction 56
3.2	LAST-Model: concept, theoretical background, numerical implementation 59
3.2.1	Model concept 59
3.2.2	Underlying theory and model equations 59
3.3	Concept and implementation of reactive solute transport into LAST 65
3.3.1	Retardation of solute transport via non-linear sorption between water and solid phase 67
3.3.2	First-order degradation of adsorbed solutes in soil solid phase 69
3.4	Model application tests 71
3.4.1	Characterization of the irrigation experiments 71
3.4.2	Model setups 73
3.5	Results 82
3.5.1	Simulation results at the well-mixed plot site (site 5) after 2 d 82
3.5.2	Simulation results at the preferential-flow-dominated plot site (site 10) after 2 d 83
3.5.3	Simulation results of LAST at the plot site (P4) 86
3.5.4	Simulation results of FLU breakthrough on field site 88
3.6	Discussion 90
3.6.1	Sorption and degradation in the Lagrangian framework 90
3.6.2	Indicators for solute over-mixing from the 7 d plot-scale simulations 93
3.6.3	Comparison of plot-scale simulations over different periods and simulation of FLU breakthrough on the field site 94
3.6.4	General reflections on Lagrangian models for solute transport 95
3.7	Conclusions and outlook 98
IV STEPPING BEYOND PERFECTLY MIXED CONDITIONS IN SOIL HYDROLOGICAL MODELLING USING A LAGRANGIAN APPROACH	
4.1	Introduction 104
4.2	Lagrangian approach for soil hydrological and subscale diffusion processes 107
4.2.1	Underlying concept of the LAST-Model 107
4.2.2	The DIPMI approach: concept to represent subscale diffusion in a Lagrangian model 108
4.3	Testing the DIPMI approach 113

4.3.1	Simulating the experiment of Bowers et al. (2020)	113
4.3.2	Setup of virtual experiment: simulating diffusive pore mixing and leaching of solute during steady state, saturated flow in a soil column	116
4.4	Results and Discussion	118
4.4.1	DIPMI simulations of the experiment of Bowers et al. (2020)	118
4.4.2	Analysis of simulations of the experiment of Bowers et al. (2020)	120
4.4.3	Simulation of the virtual experiment	122
4.4.4	Analysis of the virtual experiment	126
4.5	Conclusions and Outlook	129
V SUMMARY AND DISCUSSION		
5.1	Conclusions and summary of the key findings	133
5.1.1	Part II: Preferential flow and solute transport	133
5.1.2	Part III: Reactive solute transport	134
5.1.3	Part IV: Diffusive mixing on the pore scale	134
5.1.4	What can we learn from these findings?	135
5.2	Outlook	135
5.2.1	Water ages and travel times	136
5.2.2	Root water uptake for evapotranspiration	137
5.3	Discussion: Why are Darcy-Richards models still preferably used?	138
VI APPENDIX A		
A.1	Appendix of Part II	145
A.2	Appendix of Part III	147
BIBLIOGRAPHY		151
ACKNOWLEDGMENTS		165
OWN PUBLICATIONS		166
DECLARATION		167

LIST OF FIGURES

Figure 1.1	Principles of soil water physics	7
Figure 1.2	Principles of solute transport	11
Figure 2.1	Concept of particle binning	25
Figure 2.2	Conceptual visualization of macropore domain	27
Figure 2.3	Macropore distribution at sites Spechtacker and	
	33	34
Figure 2.4	Linear regression of macropore flux rate with	
	radius	35
Figure 2.5	Final simulated and observed vertical bromide	
	mass profiles of the matrix at the two well-	
	mixed sites 23 and 31	39
Figure 2.6	Final simulated and observed vertical bromide	
	mass profiles of the matrix at the two preferential	
	flow sites Spechtacker and 33	41
Figure 2.7	Final simulated bromide concentration and soil	
	moisture profiles of soil matrix without and	
	with macropores at different k_s values	43
Figure 2.8	Final bromide concentration profiles at different	
	k_s values and the proportion of solutes	
	which originate from the macropores	43
Figure 2.9	Final simulated bromide concentration and soil	
	moisture profiles of soil matrix at different	
	macropore diameters and numbers	44
Figure 2.10	Final simulated bromide concentration and soil	
	moisture profiles of soil matrix at different	
	macropore depth distribution configurations	
	and distribution factor configurations	45
Figure 3.1	Concept of particle binning (= Fig. 2.1)	62
Figure 3.2	Conceptual visualization of macropore domain	
	(modified, cf. Fig. 2.2)	64
Figure 3.3	Overview sketch of sorption and degradation	
	processes in the soil domain	66
Figure 3.4	Results of reactive IPU transport simulations at	
	the well-mixed site (site 5) after 2 d	83
Figure 3.5	Results of reactive IPU transport simulations	
	at the preferential-flow-dominated site (site 10)	
	after 2 d	86
Figure 3.6	Results of 7 d and 21 d simulations with bro-	
	midate and IPU at site P4	88

Figure 3.7	Results of FLU breakthrough simulations with FLU concentrations in the tile-drain tube of the field site	89
Figure 4.1	Schematic sketch of the diffusive pore mixing (DIPMI) approach	112
Figure 4.2	Isotopic concentrations in a dual-isotope space for each tension area and time point	120
Figure 4.3	Solute breakthrough curves over 7 d simulated with DIPMI approach	123
Figure 4.4	Vertical concentration profiles of a solute with mean concentrations in three tension areas over 7 d simulated with DIPMI approach	125
Figure A.1	Time series of bromide tracer concentration profiles and centres of mass at different k_s values	145
Figure A.2	Time series of bromide tracer concentration profiles and centres of mass at different macropore diameters (dmac)	146

LIST OF TABLES

Table 2.1	Simulation and tracer experiment parameters at sites 23, 31, Spechtacker and 33	37
Table 2.2	Parameter ranges of sensitivity analyses, configurations of macropore depth distribution and distribution factors	38
Table 3.1	Parameters of IPU plot-scale experiments and simulations, as well as soil hydraulic parameters at sites 5 and 10	78
Table 3.2	Reactive transport parameters of IPU at sites 5, 10, and P4	79
Table 3.3	Parameters of 7 d bromide experiment at the plot-scale site (site P4) and simulation parameters as well as soil hydraulic parameters	80
Table 3.4	Parameters of field-scale FLU breakthrough experiment and simulation parameters as well as soil hydraulic parameters	81
Table 4.1	Experimental and sandy loam parameters by Bowers et al. (2020), and DIPMI simulation parameters	115
Table 4.2	Mean and standard deviation of isotopic concentrations in each tension area and time point	119
Table A.1	Relevant LAST-Model equations and related parameters.	149

ABSTRACT

Physical soil water models are an important instrument of the hydrological toolbox for the assessment of water and solute dynamics in the partially saturated soil zone. Up to now, soil hydrological models have commonly relied on the classical theories of Darcy-Richards and the advection-dispersion-equation (ADE). The theories physically describe (i) soil water fluxes by means of the interplay of gravity and capillarity, as well as (ii) solute transport driven by advection and hydrodynamic dispersion in the soil pore system (cf. Sect. 1.2.1). Under "ideal" conditions both theories have been proven to perform well. "Ideal" refers to the redistribution of soil water and dissolved solutes in a homogeneously structured matrix that is dominated by the capillarity of soil pores. However, it has been also proven that the Darcy-Richards theory and the ADE have limitations under more natural conditions. Soils are usually a composition of various materials and exhibit heterogeneous structures. These structures imply larger voids (macropores) in which capillarity effects lose their dominance. Instead, water flow and solute transport in macropores are mainly gravity-driven and faster (preferential flow) than the theories can assume by the homogeneous, capillarity-dominated pore system. Preferential flow especially occurs during rainfall events when water and dissolved solutes are actively infiltrating.

The significance of subsoil processes, like preferential flow, for hydrological systems and the limitations of the Darcy-Richards theory and the ADE under more natural conditions are the main motivations of this thesis. The objectives of the thesis are in turn (i) to propose a new theoretical concept as alternative to the common theories, and (ii) to develop an integrated model framework for the simulation of a multitude of soil hydrological processes. This framework is called the Lagrangian Soil Water and Solute Transport (LAST) Model. Soil water is represented by discrete water particles of constant mass. The model applies a Lagrangian perspective on the trajectories of the particles through a partially saturated soil domain. Particle displacements along the trajectories are calculated by a non-linear, space domain random walk that combines physics and stochastic. The theoretical concept of the LAST-Model is introduced in Sect. 1.2.2.

In Sect. 2, I extend the basic LAST-Model by routines for solute transport and preferential flow. Water particles are assigned by a solute mass and in this way, solutes are distributed together with the displacement of water particles. For preferential flow, a structural

macropore domain is implemented as a second flow domain. Particles can infiltrate and travel purely by gravity in the macropore domain, independent from the capillary-flow conditions in the soil matrix. As a result, they can bypass the bulk water fractions in the soil matrix before re-infiltrating the matrix and accumulating in greater depths.

In Sect. 3, I modify the solute transport routine to allow for the simulation of the transport of reactive substances. Specific routines for sorption and degradation processes are implemented. Sorption is represented by an explicit solute mass transfer between water particles and the solid phase by means of non-linear Freundlich isotherms, and driven by a concentration gradient. Adsorbed solutes are then assumed to be microbially degraded following first-order decay kinetics.

In Sect. 4, I introduce the diffusive pore mixing (DIPMI) approach as additional routine for the simulation of pore-size-dependent diffusive mixing of water and solutes over the pore space. This approach should produce more reliable descriptions of frequently observed (imperfect) mixing behaviours, in contrast to the common assumption of averaging concentrations over all pore sizes in a single time step.

Each model extension is tested by simulations of field and laboratory experiments as well as sensitivity analyses. Simulation results are compared against observed data and results of a benchmark model that uses the Darcy-Richards theory and the ADE. The most important findings of this thesis can be summarized as:

- The structural macropore domain of LAST is the key for a successful representation of preferential water flow and (reactive) solute transport. In heterogeneous soils, LAST simulations match better the observed redistribution and depth-accumulation of solutes compared to simulations with the Darcy-Richards + ADE model (cf. Sect. 2.5.2). Retardation, degradation and remobilization processes must be taken into account in soil hydrological modelling as they highly influence the fate and breakthrough of reactive substances (cf. Sect. 3.6.1).
- Mixing over the pore space of a control volume is far way from being an instantaneous and perfect process, as often assumed by soil hydrological models. Imperfect, diffusive mixing on the pore scale has a significant influence on macroscopic leaching behaviours and chemical/isotopic compositions of soil water fractions (cf. Sect. 4.4.4).
- The particle-based approach of the LAST-Model framework is a promising tool for further soil- and ecohydrological application fields (cf. Sect. 5.2). However, the Darcy-Richards theory and the ADE remain the commonly used approaches in soil hydrological

modelling, although their limitations are widely approved and several alternative model concepts are available (cf. Sect. 5.3).

ZUSAMMENFASSUNG

Physikalische Bodenwassermodelle sind ein wichtiger Bestandteil des hydrologischen Methodenkatalogs für die Bewertung von Wasser- und Stoffdynamiken in der teilgesättigten Bodenzone. Bisher stützen sich die bodenhydrologischen Modelle im Wesentlichen auf die klassische Darcy-Richards-Theorie und die Advektions-Dispersions-Gleichung (ADG). Diese Theorien beschreiben physikalisch (i) die Wasserflüsse im Boden durch das Zusammenspiel von Schwerkraft und Kapillarität, und (ii) den Transport gelöster Stoffe getrieben durch Advektion und Dispersion im Porensystem des Bodens (vgl. Abschnitt 1.2.1). Unter "idealen" Bedingungen haben sich beide Theorien als verlässlich erwiesen. "Ideal" bezieht sich dabei auf die Verbreitung von Bodenwasser und gelösten Stoffen in einer homogen strukturierten Matrix, die von der Kapillarität der Bodenporen dominiert wird. Es wurde jedoch auch nachgewiesen, dass die Darcy-Richards-Theorie und die ADG unter natürlicheren Bedingungen Limitationen aufweisen. Böden sind üblicherweise aus verschiedenen Materialien zusammengesetzt und weisen heterogene Strukturen auf. Diese Strukturen implizieren größere Hohlräume (Makroporen), in denen Kapillaritätseffekte ihre Dominanz verlieren. Der Wasserfluss und Stofftransport in Makroporen wird stattdessen hauptsächlich durch die Schwerkraft getrieben und ist somit schneller (präferentielles Fließen) als es die Theorien im homogenen Porensystem annehmen können.

Die Wichtigkeit von Untergrundprozessen, wie präferentielles Fließen, für hydrologische Systeme und die Limitationen der Darcy-Richards-Theorie und der ADG unter heterogenen Bedingungen sind die Hauptmotivationen für diese Dissertation. Die Ziele der Dissertation sind daher (i) ein neues theoretisches Konzept als Alternative zu den gängigen Theorien vorzuschlagen und damit (ii) ein integriertes Modellkonzept für die Simulation einer Vielzahl von bodenhydrologischen Prozessen zu entwickeln. Es nennt sich "Lagrangian Soil Water and Solute Transport" (LAST) Modell. Bodenwasser wird repräsentiert durch diskrete Wasserpartikel von konstanter Masse. Das Modell verwendet eine Lagrange-Perspektive auf die Bewegungsbahnen der Partikel durch eine teilgesättigte Bodendomäne. Die Verlagerung der Partikel entlang ihrer Bewegungsbahnen wird dabei berechnet über eine nicht-lineare, räumliche Random-Walk-Gleichung, welche Physik und Stochastik kombiniert. Das theoretische Konzept des LAST-Modells wird in Abschnitt 1.2.2 vorgestellt.

In Abschnitt 2 erweitere ich das grundlegende LAST-Modell mit Routinen für Stofftransport und präferentielles Fließen. Den Wasser-

partikeln wird eine gelöste Stoffmasse zugewiesen. Auf diese Weise werden gelöste Stoffe zusammen mit der Bewegung der Wasserpartikel im Boden verteilt. Für das präferentielle Fließen wird eine strukturelle Makroporendomäne als zweite Fließdomäne implementiert. Die Partikel können in die Makroporendomäne infiltrieren und sich darin, rein durch die Schwerkraft getrieben, bewegen, und das unabhängig von den kapillaren Fließbedingungen in der Bodenmatrix. Dadurch können sie die größten Wasserfraktionen in der Bodenmatrix umfließen, bevor sie wieder in die Bodenmatrix zurück infiltrieren und sich in größeren Tiefen anreichern.

In Abschnitt 3 modifiziere ich die Stofftransportroutine, um die Simulation des Transports von reaktiven Substanzen zu ermöglichen. Zu diesem Zweck werden spezifische Routinen für Sorptions- und Abbauprozesse implementiert. Die Sorption wird durch einen expliziten Stoffmassenaustausch zwischen Wasserpartikeln und der festen Bodenphase mit Hilfe der nichtlinearen Freundlich-Isothermen dargestellt. Getrieben werden die Sorptionsprozesse durch Konzentrationsgradienten. Adsorbierte Stoffmassen werden dann mikrobiell gemäß einer Zerfallskinetik erster Ordnung abgebaut.

In Abschnitt 4 stelle ich den DIPMI ("diffusive pore mixing") Ansatz als zusätzliche Routine für die Simulation von porengrößenabhängigen, diffusiven Mischen von Wasser und gelösten Stoffen im Porenraum vor. Dieser Ansatz soll zu einer zuverlässigeren Beschreibung von häufig beobachteten Mischungsverhalten führen, in Kontrast zu der üblichen Annahme von gemittelten Konzentrationen über den gesamten Porenraum in einem einzigen Zeitschritt.

Jede dieser Modellerweiterungen wird mit Simulationen von Feld- und Laborexperimenten sowie Sensitivitätsanalysen getestet. Die Simulationsergebnisse werden mit beobachteten Daten und den Ergebnissen eines Vergleichsmodells bewertet, welches die Darcy-Richards-Theorie und die ADG verwendet. Die wichtigsten Ergebnisse aller Analysen in dieser Dissertation lassen sich wie folgt zusammenfassen:

- Die strukturelle Makroporendomäne von LAST ist der Schlüssel für eine erfolgreiche Darstellung von präferentiellen Fließmustern und des (reaktiven) Stofftransports. In heterogenen Böden stimmen die LAST-Simulationen besser mit der beobachteten Ausbreitung und Tiefenakkumulation von Stoffmassen überein, im Vergleich zu Simulationen mit dem Darcy-Richards-Modell + ADG (vgl. Abschnitt 2.5.2). Retardations-, Abbau- und Remobilisierungsprozesse müssen in der bodenhydrologischen Modellierung berücksichtigt werden, da sie den Verbleib und den Durchbruch reaktiver Stoffe entscheidend beeinflussen (vgl. Abschnitt 3.6.1).

- Die Durchmischung über den Porenraum eines Kontrollvolumens ist weit davon entfernt ein instantaner und perfekter Prozess zu sein, wie es jedoch oft in bodenhydrologischen Modellen angenommen wird. Die nicht perfekte, diffusive Durchmischung auf der Porenskala hat einen erheblichen Einfluss auf das makroskopische Versickerungsverhalten und die chemische/isotopische Zusammensetzung von Bodenwasserfraktionen (vgl. Abschnitt 4.4.4).
- Der partikelbasierte Ansatz des LAST-Modells ist ein vielversprechendes Instrument für weitere boden- und ökohydrologische Anwendungsfelder (vgl. Abschnitt 5.2). Die Darcy-Richards-Theorie und die ADG bleiben allerdings die am häufigsten verwendeten Ansätze in der bodenhydrologischen Modellierung, obwohl ihre Limitationen allgemein anerkannt sind und mehrere alternative Modellkonzepte zur Verfügung stehen (vgl. Abschnitt 5.3).

Part I

INTRODUCTION

INTRODUCTION

1.1 GENERAL MOTIVATION

Physical modelling is an integral component, together with field and laboratory experiments, for the prediction of soil hydrological processes in the critical zone. This includes specifically the processes along the typical pathway of water and dissolved solutes from soil infiltration, over movement through the partially saturated soil body, to soil storage and breakthrough into aquifers or surface waters. The scope of soil hydrological modelling is to advance the understanding of (i) the water storage dynamics in the critical zone and (ii) the subsoil controls on solute transport. A considerable process understanding is crucial for the assessment of the water supply and the fate of leaching pollutants in ecosystems (e.g. Arias-Estévez et al., 2008; Klaus and Zehe, 2011). The general motivation of my thesis is to provide a novel physical model framework for the simulation of these kinds of soil hydrological processes in the critical zone.

The scope of soil hydrological modelling.

1.2 THEORETICAL BACKGROUND

1.2.1 Physical basics of soil water flow and solute transport

The Darcy-Richards theory for describing partially saturated water dynamics

For the simulation of water dynamics in partially saturated soils, many physically based models rely on the Darcy-Richards equation (Richards, 1931). The theory of Darcy-Richards is regarded as the dominant description of water dynamics in partially saturated soils (Beven and Germann, 2013). I explain the principles of the Darcy-Richards theory for vertical water flow based on an example and the sketches in Fig. 1.1.

Let's assume a 1-D, vertical soil domain with length z (Fig. 1.1a). The soil domain is discretized into several vertical soil layers (= control volumes, grid elements) of constant length Δz . Such a subdivided domain can be called an Euler grid. Each soil layer i stores a certain water volume, which is defined as a soil water content θ_i ($m^3 m^{-3}$). The soil water content of a soil layer may change when water is flowing through it. The rate of change of the soil water content $\Delta\theta_i$ is determined by the inflow q_{i-1} and outflow fluxes q_i ($m s^{-1}$) of the soil layer. The difference between the water volume flowing into

The continuity equation for mass conservation.

and the water volume flowing out of a control volume is equal to the difference of the water content within this control volume in a time step (Kutílek and Nielsen, 1994). This principle implies mass conservation in space and time during partially saturated water flow and is described by the continuity equation (Eq. 1.1, Fig. 1.1c).

$$\frac{\partial \theta}{\partial t} = -\frac{\partial q}{\partial z} \quad (1.1)$$

Capillarity and gravity act upon water in soils.

Water flow is in turn induced by the interplay of the forces of capillarity and gravity, which are the main actors in the physics of partially saturated soils. The soil pores act like capillary tubes applying a capillary force on the water to hold it against gravity (binding force). Gravity in turn is the driving force of water flow, which drags the water out of the soil pores in downward direction. The required forces to bring a unit mass/volume of water into a reference height above a basis ($z = 0$ m), or to hold it within the soil pores in this reference height, are defined as gravity potential Ψ_z and matric potential Ψ_m , respectively. The unit of these potentials can be given (i) per unit water volume as an actual pressure ($\frac{N}{m^2} = \text{Pa}$), or (ii) per unit water weight as a pressure head (m). In the following, I generally refer to pressure heads, if not differently stated.

Water potential gradient enables water flow.

The sum of the gravity potential and the matric potential gives the total water potential H at a depth z (Fig. 1.1b). The gravity potential is positive and contrarily, the matric potential is negative. If the difference of the water potential ΔH over the length of a soil layer Δz is positive (i.e. gravity force exceeds capillary force), water flows in downward direction through the soil layer. The difference of the water potential over a length is called the potential gradient ∇H (Eq. 1.2), with $\nabla = \left(\frac{\partial}{\partial x}, \frac{\partial}{\partial y}, \frac{\partial}{\partial z} \right)$. Here, we only focus on the potential gradient in the one-dimensional z -direction.

$$\nabla H = \frac{\Delta H}{\Delta z} = \frac{\Delta \Psi_m + \Delta \Psi_z}{\Delta z} \quad (1.2)$$

The interplay of matric potential and gravity potential over a vertical soil domain.

If the gravity potential and the matric potential are equal and $H = 0$, the system is in equilibrium and no water is flowing. The interface of the partially saturated soil zone and the saturated zone (groundwater) is usually defined as the basis of the reference height ($z = 0$ m). At this depth, both potentials are 0. With increasing elevation and distance to the saturated zone, the gravity potential increases while the matric potential decreases as the soil pores gradually desaturate. At the soil surface, only small pores with high capillary forces (= high negative matric potentials) are still able to defy gravity and hold water. However,

external influences like rainwater infiltration brings the system out of equilibrium. Infiltrating water gradually saturates the pore space from smaller to larger pores with the result that the negative matric potential increases. As the gravity potential stays constant, the total water potential H increases and gradients of the water potential ∇H over the soil layers finally lead to water fluxes q (m s^{-1}). With these insights, we can formulate a general equation for water fluxes in the partially saturated soil zone, which is commonly denoted as the Darcy-Buckingham equation (Eq. 1.3).

$$q = -K \cdot \nabla H \quad (1.3)$$

K (m s^{-1}) is a proportionality factor called hydraulic conductivity, which I explain later. The Darcy-Buckingham equation (Buckingham, 1907) is only valid to describe the simplified case of stationary flow conditions when $q_{i-1} = q_i$ and $\Delta\theta = 0$. It can be seen as a first advancement of the Darcy equation to partially saturated flow and as an antecedent version of the Darcy-Richards equation. By inserting Eq. 1.2 into 1.3, we obtain the Darcy-Buckingham equation in a potential-based form (Eq. 1.4).

The Darcy-Buckingham equation.

$$q = -K(\Psi_m) \cdot \left[\frac{\partial \Psi_m}{\partial z} + \frac{\partial \Psi_z}{\partial z} \right] \quad (1.4)$$

When assuming that the length of each soil layer Δz is equal and stays constant, then Δz is in turn equal to the difference of the gravity potential over a soil layer and thus, we can re-write the last term to

$$\frac{\partial \Psi_z}{\partial z} = \frac{\Psi_z(i-1) - \Psi_z(i)}{\Delta z} = 1. \quad (1.5)$$

To enable finally the description of partially saturated flow under transient conditions when $q_{i-1} \neq q_i$ and $\Delta\theta \neq 0$, we combine the Darcy-Buckingham equation (Eq. 1.4 + 1.5) with the continuity equation (Eq. 1.1) to obtain the Darcy-Richards equation (Eq. 1.6).

Continuity equation + Darcy-Buckingham equation = Darcy-Richards equation.

$$\frac{\partial \theta}{\partial t} = \frac{\partial}{\partial z} \cdot \underbrace{\left[K(\Psi_m) \cdot \underbrace{\left(\frac{\partial \Psi_m}{\partial z} + 1 \right)}_{=\nabla H} \right]}_{=-q} \quad (1.6)$$

The hydraulic conductivity $K(\Psi_m)$ is a factor that scales the water

Relationship of hydraulic state variables with soil water content is non-linear and dependent on pore-size-distribution.

flow in a partially saturated, porous medium and describes how easy a fluid can pass through the porous medium (Bear, 2013). It depends on the properties of the solid material and the fluid (viscosity, intrinsic permeability). As the water flow primarily takes place in larger, saturated soil pores, the partially saturated hydraulic conductivity is further dependent on the pore-size-distribution and the soil water content. Furthermore, from the fact that the matric potential is also dependent on the water content it follows that K is in turn dependent on the matric potential. These interrelations are represented by the soil water retention curve (red) and the hydraulic conductivity curve (yellow) in Fig. 1.1d. Both curves show the non-linear functions of the change of K and Ψ_m with θ in absolute values. These relationships are commonly parameterized by the model of van Genuchten (1980) and Mualem (1976). The more soil pores are saturated, the larger is the cross section area in the pore space that contributes to the water flow. By gradually approaching the saturated soil water content θ_s , the mean flow velocity increases. In contrast, drying the soil and approaching the residual water content θ_r means that less soil pores contribute to the water flow. The remaining, still saturated and rather small pores apply higher capillary forces on the water, which reduces the mean water flow velocity.

Due to the non-linear character of $K(\theta)$ and $\Psi_m(\theta)$, it exists no closed-form analytical solution to the Darcy-Richards equation. Numerical modelling based on the Darcy-Richards equation is possible by using appropriate solvers that define suitable boundary and initial conditions. Also important is to apply the equation sequentially to infinitesimal increments of the soil domain and simulation time (Dingman, 2015).

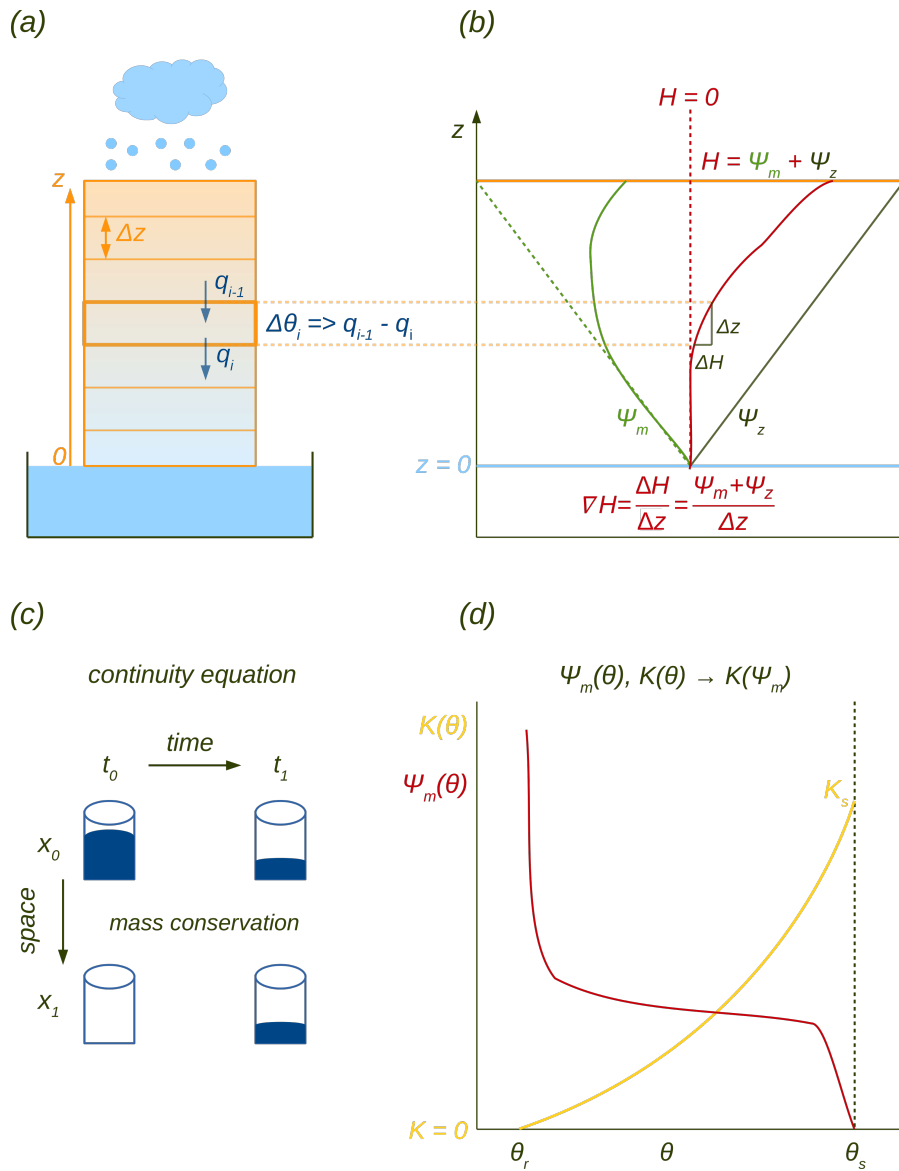


Figure 1.1: Schematic sketches of the principles of the Darcy-Richards theory. (a) Vertical soil domain for partially saturated flow between soil layers, (b) interplay of gravity potential and matric potential over the vertical extent, (c) principle of the continuity equation ensuring mass conservation (Eq. 1.1), (d) soil water retention curve (red) and hydraulic conductivity curve (yellow). This figure is adapted and inspired by the lecture of Conrad Jackisch.

Limitations of the Darcy-Richards theory and alternative model concepts

The Darcy-Richards theory makes assumptions, which are not suitable to describe some of the flow processes that are frequently observed in natural soil systems. The most essential assumptions are:

*Three assumptions
that limit the
applicability of the
Darcy-Richards
theory to more
natural conditions.*

- Capillarity is the dominant factor. The state of the water content θ is exclusively dependent on the matric potential Ψ_m during wetting and drying phases, as the gravity potential gradient is constant (cf. Eq. 1.5, Fig. 1.1b). Infiltrating water only changes the matric potential in the total water potential gradient ∇H (cf. Eq. 1.2), while the gravity potential remains unchanged by definition: $\Psi_z = \rho \cdot g \cdot z$. Gravity potential Ψ_z (Pa) is a product of water density ρ (kg m^{-3}), earth acceleration g (m s^{-2}) and the reference height z (m). The change of the matric potential results in the disturbance of the equilibrium state of potentials, which induces water flow.
- Local equilibrium (well-mixed) conditions of the hydraulic state variables θ and Ψ_m over the macroscopic scale of a vertical soil layer. Microscopic variations (e.g. on the pore scale) are not considered although pore-size-dependent differences of the hydraulic state variables can lead to a wide range of macroscopic flow behaviours (Roth, 2008).
- Expecting local equilibrium further results in the assumption that the pore space sequentially saturates from small to large pores. This implies a homogeneous saturation from θ_r to θ_s according to the soil water retention curve (cf. Fig. 1.1d).

*Darcy-Richards
rather restricted to
ideal conditions.*

Due to these assumptions the Darcy-Richards theory is restricted to rather ideal flow scenarios. An ideal flow scenario would comprise a soil that exhibits a homogeneous matrix without any structural inhomogeneities on the microscale (local equilibrium). Furthermore, water flow is quite slow either during drainage/drying phases or at most, during a continuous, homogeneous infiltration.

*More natural
conditions imply
heterogeneous
structures and
preferential flow.*

However, under more natural conditions, soils are a composition of different materials with highly heterogeneous structures and inhomogeneities such as fissures, cracks and macropores. Especially macropores can have such large diameters that they are free of capillarity. This implies that water can easily infiltrate and move through macropores in a mostly unimpeded manner solely driven by gravity. This flow process is commonly called preferential flow (Jarvis, 2007; Beven and Germann, 2013). During preferential flow, the water flow mainly takes place in a few macropores while the residual water in the smaller pores of the soil matrix is relatively stagnant. This leads to a bypassing of the soil matrix without or only very less interactions between water in the macropores and the smaller pores (= non-equilibrium, not well-mixed). The processes of preferential flow cannot be resolved by models based on the assumptions of the Darcy-Richards theory, which often leads to an underestimation of flow velocities (Zehe, 1999; Neuweiler and Dentz, 2012).

The limitations of the Darcy-Richards theory have been the motivation for the development of several alternative model concepts over the last decades. More popular ones of these alternative concepts comprise, e.g.:

- Bundle-of-tubes/discretization approaches (e.g. Talbot and Ogden, 2008; Ogden et al., 2017). The soil water content domain is discretized into tubes or bins. Each bin is a continuum in the vertical dimension and characterized by specific hydraulic properties. Infiltration and redistribution of wetting fronts are calculated explicitly by means of a soil moisture velocity equation based on capillary and gravitational forces. Bins can interact by diffusive interbin flow.
- Viscous film flow approaches (e.g. Germann, 2018). The propagation of wetting fronts is described by film flows along the vertical walls of soil pores. The flux density is only dependent on the water film thickness and a contact length of the film with the solid. Momentum dissipation due to shear forces reduces the water flux density. The concept does not need any information about soil hydraulic functions or pore-size-distributions but its parameterization requires velocity and water content data from experiments.
- Particle-based, Lagrangian approaches (e.g. Zehe and Jackisch, 2016; Jackisch and Zehe, 2018). Introduced for the first time by Ewen (1996a) and Ewen (1996b). Soil water is represented by a great number of discrete particles. Particles travel through a vertical soil domain driven by capillarity and gravity. The displacement of particles is calculated by a random walk approach. Spatial particle densities in control volumes give the water content profile over the vertical domain.

The model framework, which I present in this thesis, is a representative of the particle-based, Lagrangian approaches and is based on the previous work of Zehe and Jackisch (2016). In Sect. 1.2.2, I introduce the basic principles of this model concept in more detail.

The advection-dispersion-equation for solute transport

Water flow in soils is often accompanied by the transport of solutes dissolved in the soil water. In soil hydrological modelling, the transport of dissolved solutes through soils is dominantly described by the advection-dispersion-equation (ADE). The ADE bases on similar theoretical and physical principles as the Darcy-Richards equation. For the vertical transport of conservative solutes in partially saturated soils without any sinks or sources of solute masses, the ADE is defined

Limitations of Darcy-Richards motivate development of alternative models.

The advection-dispersion-equation (ADE) as dominant concept for solute transport in soils.

as follows:

$$\frac{\partial C_w}{\partial t} = \underbrace{-v \cdot \frac{\partial C_w}{\partial z}}_{= \text{advection}} + \underbrace{\frac{\partial}{\partial z} \left(D_e \cdot \frac{\partial C_w}{\partial z} \right)}_{= \text{hydrodyn. dispersion}} \quad \text{with } v = \frac{q}{\theta} \quad (1.7)$$

Solute transport and the temporal change of the solute concentration in the water phase C_w (kg m^{-3}), within a control volume of the Eulerian soil domain, is caused by the joint processes of advection and hydrodynamic dispersion (the parameter D_e will be explained later on). In line with the equation of continuity (cf. Eq. 1.1) in the Darcy-Richards theory, the principle of mass conservation also applies for solute transport (Kutílek and Nielsen, 1994). The difference of solute masses entering and leaving a spatial control volume is equal to the solute mass stored within the control volume per time step.

Advection alone causes uniform displacement of all solute particles.

The first term of the ADE describes the displacement of dissolved solutes due to advection along with the average water flux. This advective solute displacement is determined by the mean vertical velocity v (m s^{-1}) of the flow field. The mean flow velocity can be calculated by the quotient of the local Darcy-Richards flux q and the soil water content θ in a control volume. Advection alone would result in uniform transport lengths for all dissolved solute particles in a time step, determined by the mean flow velocity v . It comes to a vertical displacement but not to an actual mixing of solute particles (Bear, 2013).

Hydrodynamic dispersion = mechanical dispersion + molecular diffusion.

The second term of the ADE describes an additional solute displacement, beyond the uniform, advective transport length. This effect is called hydrodynamic dispersion and enables the actual mixing of solute particles. It represents the macroscopic fingerprint of the subscale movements of individual solute particles through the soil pore space. Such individual solute particle movements are basically the result of the two subscale phenomena of (i) mechanical dispersion and (ii) molecular diffusion. Mechanical dispersion occurs due to the presence of flow through a porous medium. The heterogeneity of the geometry and topology of the pore system implies tortuous flow paths for particles around the soil grains (Fig. 1.2). This in turn results in a distribution of local flow velocities and different transport lengths of individual particles that cause the spreading of solute masses over an ever-increasing volume of the pore space. Simultaneously with mechanical dispersion, variations of solute concentrations in the water phase further induce additional displacements of solute particles. Such concentration gradients are depleted by the subscale mixing of solute particles. This effect is referred to molecular diffusion (or Brownian motion) (Bear, 2013).

All the subscale phenomena involved in the hydrodynamic dispersion process are lumped together in the ADE by a macroscopic, effective dispersion coefficient D_e ($m^2 s^{-1}$). It basically represents the ability of a porous system to enable the process of hydrodynamic dispersion and is dependent on the properties of the porous medium, the fluid and the solute. The effective dispersion coefficient is hence similarly defined as the hydraulic conductivity in the Darcy-Richards equation (cf. Eq. 1.6).

Dispersion coefficient as lumped, macroscopic representation of subscale processes.

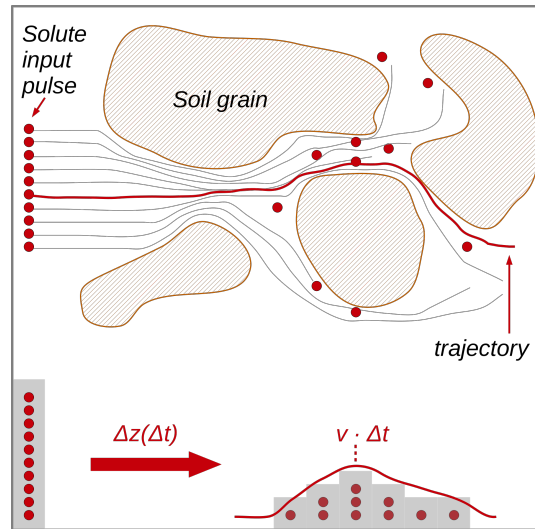


Figure 1.2: Scheme of solute transport in soils. An initial solute input pulse occupies an ever-increasing extent of the soil domain over time due to the effects of advection and hydrodynamic dispersion. Hydrodynamic dispersion causes individual trajectories of solute particles and leads to displacements lengths Δz distributed around an expected transport length according to the mean advective flow velocity v .

Further similarities shares the ADE with the Darcy-Richards theory in regard of theoretical assumptions and their limitations for describing transport processes in natural, heterogeneous soil systems. The ADE assumes well-mixed conditions in respect of the hydrodynamic dispersion coefficient D_e over the macroscopic scale of a control volume (Dentz and Lester, 2022). This implies a Gaussian distribution of displacement lengths (Fig. 1.2). The hydrodynamic dispersion coefficient describes the variance of this distribution $Var[z] = 2 \cdot D_e \cdot t$ (m^2) around an expected average transport length $\langle z \rangle = v \cdot t$ (m). The relation of both gives a measure for the distribution of transport lengths

ADE assumes well-mixed transport behaviour.

(Eq. 1.8).

$$\frac{\text{Var}[z]}{\langle z \rangle} = \frac{2 \cdot D_e \cdot t}{v \cdot t} = \frac{2 \cdot D_e}{v} = \alpha \quad (1.8)$$

The constant α (m) is called dispersivity and represents the lengths of the macroscopic heterogeneities of the porous medium. It is a medium specific measure and together with the mean flow velocity, it defines the hydrodynamic dispersion coefficient (Eq. 1.9).

$$D_e = \frac{1}{2} \cdot \alpha \cdot v \quad (1.9)$$

Limitations of the ADE.

However, preferential flow in heterogeneous soils implies not well-mixed conditions with a rapid transport of solutes that takes place much faster than the actual mixing process, which cannot be sufficiently described in the ADE by only one constant, macroscopic dispersion coefficient. Furthermore, the ADE assumption that the variation of subscale flow velocities, and finally also breakthrough curve shapes, follow a symmetrical Gaussian distribution does not hold under heterogeneous, non-Fickian transport conditions in natural systems (Zehe et al., 2021).

1.2.2 Particle-based, Lagrangian approaches as alternative to the common theory

What do the terms "particle-based" and "Lagrangian" actually mean in this context?

Meaning of terms "particle-based" and "Lagrangian".

"Particle-based" means that the soil water is not considered as an entirety but is represented by a large number of discrete particles. Each particle is defined by a constant mass and volume. They are allowed to move freely through the soil domain. The sum of the number of water particles per control volume (= particle density) gives a local soil water content. The term "Lagrangian" in turn refers to a Lagrangian perspective. The model acts like a mobile observer that travels along the trajectories of the water particles as they move through the soil domain. In this way, it is able to describe the history of individual particles and to track the position of each particle at every time.

In contrast to Darcy-Richards methods, Lagrangian approaches may not calculate water flux densities to describe changes of soil water contents. They describe the movement of discrete water particles through the soil domain and calculate local particle densities to infer

soil water contents. The movement of the particles is determined by the joint effects of advection and diffusion (cf. Sect. 1.2.1). Re-writing the Darcy-Richards equation into a soil-moisture-based form gives an equation that reflects these effects (Eq. 1.10).

$$\frac{\partial \theta}{\partial t} = \underbrace{\frac{\partial K(\theta)}{\partial z}}_{v(\theta)} + \frac{\partial}{\partial z} \left(\underbrace{K(\theta) \cdot \frac{\partial \Psi}{\partial \theta}}_{D(\theta)} \cdot \frac{\partial \theta}{\partial z} \right) \quad (1.10)$$

This general equation can be used to describe the movement of water particles. The first term represents the advective movement $v(\theta)$ in downward direction driven by gravity and is a function of the partially saturated hydraulic conductivity $K(\theta)$ only. This parameter serves as a lumped measure representing the complex inhomogeneities of the flow system (tortuosity, friction, variations of pore sizes and velocities) that act against free gravity. The second term describes diffusive water flow driven by local differences of the soil water content and controlled by a water diffusivity $D(\theta)$ ($m^2 s^{-1}$). It is a mathematical description of how well a fluid can freely diffuse over a porous medium (Kutlík and Nielsen, 1994). It is determined by the properties of the porous material and the fluid, and is calculated by $K(\theta)$ multiplied by the slope of the soil water retention curve $\frac{\partial \Psi}{\partial \theta}$. The slope represents how strong the water content reacts on a change of the matric potential. The more inert this reaction, the stronger the soil can hold water and the larger is the water saturated area that contributes to diffusion.

Advection and diffusion determine particle movements.

In this form, Eq. 1.10 is equivalent to the Fokker-Planck equation (Risken, 1984), as it basically describes the temporal evolution of a system under the influence of a drag force (advection/drift) and a random force (diffusion). Due to this formal equivalence, we can formulate Eq. 1.11 for the vertical displacement Δz of water particles in a time step Δt .

$$\Delta z(\Delta t) = - \underbrace{\left(\frac{K(\theta(t))}{\theta(t)} + \frac{\partial D(\theta(t))}{\partial z} \right)}_{= \text{advection}} \cdot \Delta t + Z \underbrace{\sqrt{2 \cdot D(\theta(t))}}_{= \text{diffusion}} \cdot \Delta t \quad (1.11)$$

According to that, individual particle displacements follow the general form of a Langevin equation and correspond to the ADE (cf. Eq. 1.7). The first part again corresponds to advection and contains an additional drift term that corrects the advective movement of particles in case of spatially variable dispersivity properties in the soil domain

Non-linear, spatial random walk for particle displacement.

(for more information see Sects. 2.2.1 and 3.3.2). The second part of the equation is a non-linear, spatial random walk that represents the diffusion process (Zehe and Jackisch, 2016). A random number Z , standard normally distributed, governs the diffusion direction of particles in the vertical dimension of the soil domain dependent on its algebraic sign. In this way, the random walk method reflects the undirected nature of Brownian motion that is involved in the diffusion process. Non-linear further means that both the advection and the diffusion term changes non-linearly with changing particle densities (= soil water content), which in turn refers to the characteristics of the water retention curve and the hydraulic conductivity curve (cf. Fig. 1.1d).

Advantages of the particle-based, Lagrangian approach

Particles can move freely dependent on pore sizes.

Water particles are represented as discrete and independent entities. This allows them to move freely over the entire soil domain. This mutual independence of water particles enables the resolution of the hydraulic state variables on the microscale of the pore space. That means, it can be assumed that particles are stored in different pore sizes and that the size of a pore determines the flow velocity of a particle. Smaller pores with lower soil water contents imply a decreased particle velocity according to the water retention curve and hydraulic conductivity curve (cf. Fig. 1.1d). In the same way, specific particles can move with an enhanced velocity in macropores to represent preferential flow. The dispersion term can be neglected for those specific particles and their movement is exclusively governed by gravity and by terms of, e.g. the saturated hydraulic conductivity K_s or other velocities. The majority of particles still moves slowly in the matrix following the "normal" hydraulic state variables at the actual soil water content.

Any information can be added to particles.

Another advantage of the approach is the possibility to add different information to the water particles. For instance, a water particle can carry a solute mass and together with the water particle, the solute is moving through the soil domain. In this way, it is possible to describe water flow and solute transport as a combined process by the random walk method, without the need for an additional solute transport equation.

1.3 OBJECTIVES OF THE THESIS

Objective 1: Introducing the LAST-Model framework.

One objective of my thesis is to extend and optimize the particle-based, Lagrangian approach of Zehe and Jackisch (2016) and to develop a framework for the simulation of a multitude of physical soil- and ecohydrological processes. The framework is called the Lagrangian

Soil Water and Solute Transport (LAST) Model. The intention is to strengthen the general understanding of the complex, interacting processes in the vadose zone during water flow and solute transport, such as preferential flow phenomena.

In the following sections, I present three studies in which I describe how several routines are implemented to extend gradually the scope of the LAST-Model framework. In Sect. 2, I start with the implementation of solute transport and a macropore domain to enable the simulation of preferential flow and solute transport processes. In Sect. 3, I extend the previous solute transport routine by adding sorption and degradation processes to account for the transport of reactive substances. In Sect. 4, I finally implement a routine for a more realistic description of diffusive mixing processes of waters and solutes on the microscale of the pore space. In Sect. 5.2, I give an outlook on why the particle-based approach is a promising tool for the research on further soil- and ecohydrological topics, e.g. water ages and related travel times, or evapotranspiration processes with root water uptake.

Three studies for three extension steps of the LAST-Model framework.

Another objective of my thesis is to provide an alternative model concept in contrast to common Darcy-Richards and ADE approaches. The presented LAST-Model framework belongs to a set of novel soil hydrological models. Their development over the last decades has been strongly motivated by the evidence that the Darcy-Richards theory fails to predict flow under more natural, heterogeneous soil conditions. Besides their equal motivation, the novel approaches have in common that they still have only minor impact on the hydrological research and practical applications. Their alternative concepts are by now not able to displace the theory of Darcy-Richards and the ADE, which remain the main physical basis of most soil hydrological models despite their well-known limitations.

Objective 2: Alternative concept in contrast to Darcy-Richards theory and ADE.

In the discussion of my thesis (Sect. 5.3), I come back to this issue and discuss reasons why the Darcy-Richards approaches are so persistent and why alternative model concepts may have problems to replace the common theory.

Part II

SIMULATING PREFERENTIAL SOIL WATER FLOW AND TRACER TRANSPORT USING THE LAGRANGIAN SOIL WATER AND SOLUTE TRANSPORT MODEL

This study is published in the scientific journal Hydrology and Earth System Science (HESS). The remainder of part II is a reprint of:

Sternagel, A., R. Loritz, W. Wilcke, and E. Zehe (2019). "Simulating preferential soil water flow and tracer transport using the Lagrangian Soil Water and Solute Transport Model." In: Hydrology and Earth System Sciences 23.10, pp. 4249–4267. <https://doi.org/10.5194/hess-23-4249-2019>.

SIMULATING PREFERENTIAL SOIL WATER FLOW AND TRACER TRANSPORT USING THE LAGRANGIAN SOIL WATER AND SOLUTE TRANSPORT MODEL

ABSTRACT

We propose an alternative model concept to represent rainfall-driven soil water dynamics and especially preferential water flow and solute transport in the vadose zone. Our LAST-Model (Lagrangian Soil Water and Solute Transport) is based on a Lagrangian perspective on the movement of water particles (Zehe and Jackisch, 2016) carrying a solute mass through the subsurface which is separated into a soil matrix domain and a preferential flow domain. The preferential flow domain relies on observable field data like the average number of macropores of a given diameter, their hydraulic properties and their vertical length distribution. These data may either be derived from field observations or by inverse modelling using tracer data. Parametrization of the soil matrix domain requires soil hydraulic functions which determine the parameters of the water particle movement and particularly the distribution of flow velocities in different pores sizes. Infiltration into the matrix and the macropores depends on their respective moisture state and subsequently macropores are gradually filled. Macropores and matrix interact through diffusive mixing of water and solutes between the two flow domains which again depends on their water content and matric potential at the considered depths.

The LAST-Model is evaluated using tracer profiles and macropore data obtained at four different study sites in the Weiherbach catchment in south Germany and additionally compared against simulations using HYDRUS 1-D as benchmark model. While both models show an equal performance at two matrix flow dominated sites, simulations with LAST are in a better accordance with the fingerprints of preferential flow at the two other sites compared to HYDRUS 1-D. These findings generally corroborate the feasibility of the model concept and particularly the implemented representation of macropore flow and macropore-matrix exchange. We thus conclude that the LAST-Model approach provides a useful and alternative framework for a) simulating rainfall-driven soil water and solute dynamics and fingerprints of preferential flow as well as b) linking model approaches and field experiments. We also suggest that the Lagrangian perspective offers promising opportunities to quantify

water ages and to evaluate travel and residence times of water and solutes by a simple age tagging of particles entering and leaving the model domain.

2.1 INTRODUCTION

Until now, the most commonly used hydrological models have been following an Eulerian perspective on the flow processes with a stationary observer balancing dynamic changes in a control volume. The alternative Lagrangian perspective with a mobile observer travelling along the trajectory of a solute particle through the system (Currie, 2002) has up to now only been used to simulate advective-dispersive transport of solutes (Delay and Bodin, 2001; Zehe et al., 2001; Berkowitz et al., 2006; Koutsoyiannis, 2010; Klaus and Zehe, 2011). However, this particle tracking approach is mostly embedded in frameworks with Eulerian control volumes which still characterize the dynamics of the carrying fluid. Lagrangian descriptions of the fluid dynamics itself are only realized in a few models. But such a particle tracking framework may offer many advantages, especially at the coping of the challenges induced by preferential water flow and solute transport in structured heterogeneous soils.

Preferential flow has become a major issue in hydrological research since the benchmark papers of Beven and Germann (1982), Flury et al. (1994) and Uhlenbrook (2006). The term of preferential flow is used to summarize a variety of mechanisms leading to a rapid water movement in soils. The most prominent one is the flow through non-capillary macropores (Beven and Germann, 2013) where water and solutes travel in a largely unimpeded manner due to the absence of capillary forces and bypass the soil matrix (Jarvis, 2007). Macropores can be classified into e.g. earth worm burrows, channels from degraded plant roots or shrinkage cracks and all of them are not static in space nor time (e.g. Blouin et al., 2013; Nadezhdina et al., 2010; Palm et al., 2013; van Schaik et al., 2013; Schneider et al., 2018). Especially in rural areas and in combination with agrochemicals, macropore flow can be a dominant control on stream and groundwater pollution (e.g. Flury, 1996; Arias-Estévez et al., 2008). To understand such water and solute movements a combination of plot-scale experiments and computer models is commonly used (Zehe et al., 2001; Šimůnek and Genuchten, 2008; Radcliffe and Simunek, 2010; Klaus et al., 2013). One of the most frequently used approaches to simulate water flow dynamics and solute transport is to use the Darcy-Richards and the advection-dispersion equation. Both equations fundamentally assume that solute transport is controlled by the interplay of advection and dispersion (Beven and Germann, 2013) and that the underlying soil water dynamics are dominated by capillary-driven diffusive flow. While the second assumption is well justified in homogeneous soils, it frequently fails in soils with macropores. Consequently, we separate at least two flow regimes in soils: the slow diffusive flow in the soil matrix and the rapid advective flow in the macropores. Partial mixing

between these two flow regimes is non-trivial as it depends on the hydraulic properties of the macropore walls, the water content of the surrounding soil, actual flow velocities, hydrophobicity of organic coatings and much more. The inability of the Richards equation to simulate partial mixing between both flow regimes is well known and a variety of different models have been proposed to address this problem (Šimůnek et al., 2003; Beven and Germann, 2013). But most of them are still fundamentally based on the Darcy-Richards equation like the most prominent and well-established double-domain models like for instance the HYDRUS model of Šimůnek and Genuchten (2008).

A promising alternative approach is provided by particle-based Lagrangian models for subsurface fluid dynamics. The first implementation of such a model for soil water dynamics is the SAMP model proposed by Ewen (1996a,b). SAMP represents soil water by a large number of particles travelling in an one-dimensional soil domain by means of a random walk which is based on soil physics and soil water characteristics. A more recent example is the two-dimensional MIP model of Davies et al. (2013) developed for hillslopes. Fluid particles travel according to a distribution function of flow velocities which needs to be estimated from tracer field experiments. Exchange of particles among the different pathways is conceptualized as random process following an exponential distribution of mixing times. Inspired by the SAMP model, Zehe and Jackisch (2016) conceptualized a Lagrangian model describing soil water flow by means of a non-linear space domain random walk. In line with Ewen (1996a,b), they estimated the diffusivity and the gravity-driven drift term of the random walk based on the soil water retention curve ($\psi(\theta)$) and the soil hydraulic conductivity curve ($k(\theta)$).

The particle-based Lagrangian model of Zehe and Jackisch (2016) initially assumed that all particles travel at the same diffusivity and velocity corresponding to the actual soil water content. But a comparison to a Richards solver revealed that this straightforward, naive random walk implementation highly overestimates infiltration and redistribution of water in the soil. The solution for this overestimation was to account for variable diffusive velocities. Now, particles in different pore sizes travel with various diffusivities, which are determined based on the shape of the soil hydraulic conductivity curve. This approach reflects the idea that the actual soil water content is the sum of volume fractions that are stored in different pore sizes and that the different pore sizes constitute flow paths which differ in both advective and diffusive velocities.

Recently, this model was advanced by Jackisch and Zehe (2018)

with the implementation of a second dimension which contains spatially explicit macropores to simulate preferential flow. Within a macropore the velocity of each particle is described by interactions of driving and hindering forces. Driver is the potential energy of a particle while energy dissipation due to friction at the macropore walls dissipates kinetic energy and accordingly reduces particle velocities. With this approach, Jackisch and Zehe (2018) tried to make maximum use of observables for model parametrization. The assets of their echoRD model are a self-controlling macropore film flow and its ability to represent 2-D infiltration patterns. The drawback of echoRD is the huge computational expense. The simulation time is about 10 to 200 times longer than real-time.

The huge computational expense of the echoRD model is one main motivation for us to develop a Lagrangian approach which balances necessary complexity with greatest possible simplicity. The other motivation is the inability of all models mentioned above to simulate solute transport appropriately. This is essential for a rigorous comparison of the model with tracer data and to get closer to the simulation of reactive transport. Thus, the main objectives of this study are to:

1. Present a new routine for solute transport and diffusive mixing for well-mixed matrix flow conditions which is implemented into the model of Zehe and Jackisch (2016) and to test this approach against tracer data from plot-scale experiments carried out in the Weiherbach catchment (Zehe and Flüßler, 2001a).
2. Extend the model by implementing a macropore domain accounting for preferential flow of water and solutes and related exchange with the matrix domain. In contrast to the echoRD model, we maintain the one-dimensional approach to keep the computational expense moderate.

The structure of our LAST-Model (Lagrangian Soil Water and Solute Transport) is hence similar to a double-domain approach. The main asset is that flow and transport in both domains and their exchange are described by the same stochastic physics and that the macropore domain can be parameterized by observable macropore geometries. This fact may help to overcome the limiting assumptions of the Darcy-Richards and the advection-dispersion equation. The refined LAST-Model is tested by extensive sensitivity analyses to corroborate its physical validity. Further, it is also tested with four tracer infiltration experiments at different study sites in the Weiherbach catchment which are either dominated by well-mixed conditions (sites 23, 31) or preferential flow in macropores (sites Spechtacker, 33). For comparison, these four experiments are also simulated with HYDRUS 1-D.

2.2 CONCEPT AND IMPLEMENTATION OF THE LAST-MODEL

2.2.1 *The Lagrangian model of Zehe and Jackisch (2016) in a nutshell*

The basis of our development is the Lagrangian model of Zehe and Jackisch (2016). It describes infiltration and water movement through a spatially explicit one-dimensional soil domain dependent on the effects of gravity and capillarity in combination with a spatial random walk concept. Water is represented by particles with constant mass and volume. The density of soil water particles in a grid element represents the actual soil water content $\theta(t)$ ($m^3 m^{-3}$), which reflects in turn the sum of the volume fractions of soil water that are stored in pores of strongly different sizes. Water particles travel at different velocities in these pores, which are characterized by the shape of the hydraulic conductivity and water diffusivity curve. The curves are subdivided into N_B bins, starting from the residual moisture θ_r stepwise to the actual moisture $\theta(t)$ using a step size of $\Delta\theta = \frac{\theta(t) - \theta_r}{N_B}$ (Fig. 2.1). The particle displacement within the bins is described by Eq. 2.1:

$$z_i(t + \Delta t) = z_i(t) - \left(\frac{k(\theta_r + i \cdot \Delta\theta)}{\theta(t)} + \frac{\delta D(\theta_r + i \cdot \Delta\theta)}{\delta z} \right) \cdot \Delta t + Z \sqrt{2 \cdot D(\theta_r + i \cdot \Delta\theta) \cdot \Delta t}, \quad (2.1)$$

$$i = 1, \dots, N,$$

where z is the vertical position (m), k the hydraulic conductivity ($m^2 s^{-1}$), i the number of the current bin, D the water diffusivity ($m^2 s^{-1}$), i.e. the product of the hydraulic conductivity $k(\theta)$ and the slope of the soil water retention curve with the relation $\frac{\delta\psi}{\delta\theta}$ (m), t the simulation time (s), Δt the simulation time step and Z a random, uniformly distributed number in the range $[-1,1]$. The equation comprises two terms. The first one represents gravity-driven downward advection of each particle based on the hydraulic conductivity, and the second one is the diffusive term driven by capillarity. According to Fig. 2.1 and Eq. 2.1, particles in coarse pores travel more rapidly at a higher hydraulic conductivity due to wet conditions. In smaller pores or during drier conditions the flow velocities are so small that the particles are in fact immobile. This binning of particle velocities and diffusivities also opens the opportunity to simulate rainfall infiltration under non-equilibrium conditions. To this end, infiltrating rainfall event water is treated as a second type of particle, which initially travels at gravity-driven, rapid velocities in the largest pore fraction and experiences a slow diffusive mixing with the pre-event water particles of the matrix during a characteristic mixing time. Test simulations revealed that the Lagrangian model can simulate water dynamics under equilibrium conditions in good accordance with a

Darcy–Richards approach for three different soils.

For a detailed description of the underlying model concept and the derivation of the equations, see the study of Zehe and Jackisch (2016).

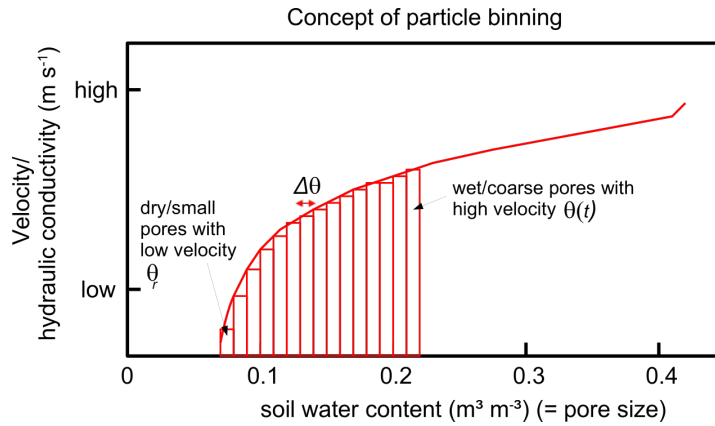


Figure 2.1: Concept of particle binning. All particles within a grid element are subdivided into bins (red rectangles) of different pore sizes. Depending on their related bin, the particles travel at different flow velocities.

2.2.2 Representation of solute transport in the LAST-Model

In a first step we implement a routine for solute transport into the particle model by assigning a solute concentration C ($kg\ m^{-3}$) to each particle. This implies that a particle carries a solute mass, which is equal to its concentration times its volume. Due to the particle movements through the matrix domain, the dissolved mass experiences advective transport in every time step. Diffusive mixing among all particles is calculated after each displacement step by summing up the entire solute mass in a grid element and dividing it by the number of all present water particles. The underlying assumption of perfect mixing among all particles in a grid element requires a diffusive mixing time corresponding to the molecular diffusion coefficient, which is smaller than the time step Δt . The latter is ensured by a sufficiently fine subdivision of the soil matrix.

2.2.3 The macropore domain and representation of preferential flow

The second and main model extension is the implementation of a one-dimensional preferential flow domain considering the influence of macropores on water and solute dynamics. This requires four main steps.

1. Design of a physically based structure of the preferential flow domain

2. Conceptualization of the infiltration and partitioning of water into the two domains
3. Description of advective flow in the macropores
4. Conceptualization of water and tracer exchange between the macropore and the matrix domain

2.2.3.1 *The preferential flow domain*

We define a one-dimensional macropore or preferential flow domain (pfd) which is surrounded by a one-dimensional soil matrix domain with vertically distinct boundaries. In line with other Lagrangian models, we represent water as particles with constant mass and volume corresponding to their domain affiliation. As the vertical extent and volume of the pfd are much smaller than those of the matrix domain, the corresponding particles must be much smaller to ensure that an adequate number of particles travel within the pfd for a valid stochastic approach.

The pfd comprises a certain amount of macropores. Each macropore has the shape and structure of a straight circular cylinder with a predefined length L_M (m) and diameter d_{mac} (m) containing spherically shaped particles (Fig. 2.2a). Two of the most important geometrical properties of the pfd are the macropore diameter and the total number of macropores n_{mac} (-), as they scale exchange fluxes and determine several other characteristics like the total macropore volume. The macropore number, lengths and diameters can be directly measured in field experiments as described in Sect. 2.3.2. From these observable parameters it is further possible to calculate additional pfd parameters like the total volume, stored water mass at saturation, the circumference and the flux rate. As we assume purely gravity-driven flow, the flux rate, the hydraulic conductivity of the pfd k_{pfd} ($m^2 s^{-1}$) and the advective velocity of a particle within the pfd v ($m^2 s^{-1}$) are assumed to be equal and can be calculated by the diameter as also described in Sect. 2.3.2.

Our one-dimensional approach can of course not account for the lateral positions of the macropores, but the pfd allows a depth distribution of macropores, which is important for calculating the depth-dependent exchange with the matrix (Sect. 2.2.3.4). To calculate the water content and tracer concentrations, the macropores of the pfd are vertically subdivided into grid elements of a certain length dz_{pfd} (m). Therefore, water contents and solute concentrations are regarded as averaged over these grid elements. Within a grid element of a macropore we assume cubic packing of a number of particles N (cf. Fig. 2.2a), each having a mass m_p (kg) which is derived from the total water mass stored in a macropore when fully saturated. Based on this

mass and the water density, the pfd particles are also geometrically defined by a diameter D_P (m) and volume $V_P(m^3)$. In a cubic packing the particles are arranged in the way that the centres of the particles form the corners of a cube. The concept of cubic packing facilitates the calculation of the proportion of particles having contact with the lateral surface of a grid element. The rectangle in Fig. 2.2a describes such a lateral surface of a grid element, with a height corresponding to the grid element length dz_{pfd} and the circumference C (m) as length, which can be obtained when a macropore grid element is cut open and its surface is laid flat. The number of particles which can be packed into this rectangle then have contact with the lateral surface of this grid element. The proportion of these contact particles to the total number of particles roughly corresponds to the hydraulic radius scaling the wetted cross section with the wetted contact area in a macropore. Within the mixing process only the contact particles are able to infiltrate via the interface into the soil matrix.

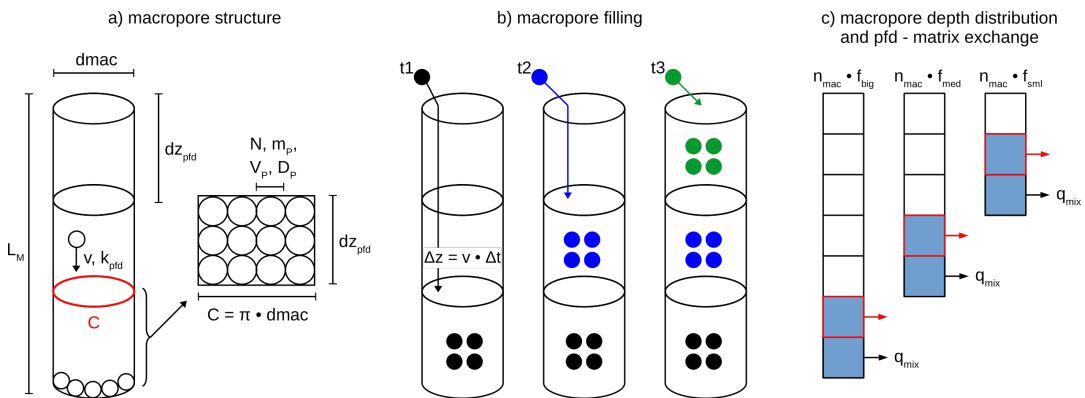


Figure 2.2: Conceptual visualization of (a) the macropore structure and cubic packing of particles in the rectangle of a cut-open and laid-flat grid element cylinder (cf. Sect. 2.2.3.1), (b) the macropore filling with gradual saturation of grid elements, exemplarily shown for three points in time (t_1 – t_3) whereby at each time new particles (differently coloured related to the current time) infiltrate the macropore and travel into the deepest unsaturated grid element (cf. Sect. 2.2.3.3) and (c) the macropore depth distribution and diffusive mixing from macropores into a matrix (cf. Sect. 2.2.3.4).

2.2.3.2 Infiltration and partitioning of water into the two domains

As a one-dimensional approach does not allow an explicit, spatial distribution of the incoming precipitation water over the soil surface, we use an implicit, effective infiltration concept. The infiltration and distribution of water are controlled by the actual soil moisture and the flux densities driven by the hydraulic conductivity and the hydraulic potential gradient of the soil matrix as well as by friction and gravity within the macropores (Weiler, 2005; Nimmo, 2016; Jackisch and Zehe,

2018). For example, a soil matrix with a low hydraulic conductivity increases the proportion of water infiltrating the macropores as it preferentially uses pathways of low flow resistance.

In our model, we use a variable flux condition at the upper boundary of the soil domain dependent on the precipitation intensity. Incoming precipitation water accumulates in an initially empty fictive surface storage from which infiltrating water masses and related particle numbers are calculated. To this end, we distinguish several cases. In Case 1, the top soil grid elements of the soil matrix and the pfd are initially unsaturated and the infiltration capacity of the soil matrix is smaller than the incoming precipitation flux density. Water infiltrates the soil matrix and the excess water is redistributed to the pfd and infiltrates it with a macropore-specific infiltration capacity. Case 2 applies when the top matrix grid element is saturated and water exclusively infiltrates the pfd until all macropores are also saturated. Case 3 occurs when both the top matrix layer and the pfd are saturated, leading to an accumulation of precipitation water in the surface storage. As soon as the water contents in the first soil matrix grid element and in the pfd are subsequently decreasing due to downward water flow or drainage of the macropores, infiltration again occurs according to Case 1. The incoming precipitation mass (m_{rain}) and the infiltrating water masses into the matrix (m_{matrix}) and the pfd (m_{pfd}) are calculated with Eqs. 2.2 - 2.4. Please note that these equations present infiltrating masses and not fluxes because the model generally works with discrete particles and their masses.

$$m_{rain} = q_{rain} \cdot \rho_w \cdot \Delta t \cdot A \quad (2.2)$$

$$m_{matrix} = \left(\frac{k_{m1} + k_s}{2} \right) \cdot \left(\frac{\psi_1 - \psi_2}{dz} + 1 \right) \cdot A \cdot \rho_w \cdot \Delta t \quad (2.3)$$

$$m_{pfd} = k_{pfd} \cdot \pi \cdot \left(\frac{dmac}{2} \right)^2 \cdot \rho_w \cdot \Delta t \cdot nmac, \quad (2.4)$$

where q_{rain} ($m s^{-1}$) is the precipitation flux density or the intensity, k_{m1} ($m s^{-1}$) the actual hydraulic conductivity of the first grid element of the matrix, k_s ($m s^{-1}$) the saturated hydraulic conductivity of the matrix and $\psi_1 - \psi_2$ (m) the matric potential difference between the surface and the first grid element right beneath the surface, dz (m) the grid element length in the matrix domain (0.1 m), k_{pfd} ($m s^{-1}$) the saturated hydraulic conductivity of a macropore (cf. Sect. 2.3.2), $dmac$ (m) the diameter of a macropore and $nmac$ (–) the total number of macropores within the pfd, ρ_w ($kg m^{-3}$) the water density, Δt (s) the

simulation time step and A (m^2) the plot area. According to Eq. 2.3, the infiltration rate into the matrix is based on Darcy's law, and thus we are generally able to account for an extra pressure due to a ponded surface, e.g. in Case 3. But in our simulation cases, ponding heights are small and have only a marginal effect. After the precipitation water has infiltrated into the two domains, the masses are converted to particles which are initially stored in the first grid elements of the matrix and pfd. They are now ready for the displacement process.

2.2.3.3 *Advective flow in the macropores*

In the pfd, we assume a steady-state balance between gravity and dissipative energy loss at the macropore walls. This implies purely advective flow characterized by a flow velocity v which can be inferred from either tracer or infiltration experiments on macroporous soils as described by Shipitalo and Butt (1999), Weiler (2001) and Zehe and Blöschl (2004). The particle displacement in our pfd is described by Eq. 2.5:

$$\Delta z = v \cdot \Delta t. \quad (2.5)$$

As all particles in the pfd travel at the same velocity, their displacement depends on the time step. Generally, our model can work with variable time stepping as Lagrangian approaches are not subject to time step restrictions or numerical stability criteria. Here, we select the time step such that the particle displacement per time step equals the maximum depth of the pfd, and subsequently excess particles are shifted upwards to the deepest unsaturated grid element. In this way, we gradually fill the macropores from the bottom to the top, comparable to the filling of a bottle with water. This simple volume-filling method was applied before in other models, e.g. in the SWAP model of van Dam et al. (2008) or in the study of Beven and Clarke (1986). Fig. 2.2b shows an example of the macropore-filling concept: in each of the three points in time (t_1 – t_3), new particles, shown by the different colours, infiltrate the macropore, and subsequently they are displaced with Δz to the bottom of the macropore, initially saturating the deepest grid element (t_1). In the following points in time t_2 and t_3 the new particles do not fit into the respective saturated grid elements anymore and are then shifted to the next deepest unsaturated grid element. In line with the matrix, particle densities are calculated in each grid element to obtain the actual soil water content and tracer concentrations of the pfd.

2.2.3.4 Water and tracer exchange between the macropore and the matrix domain

Commonly, macropore–matrix interactions are challenging to observe within field experiments. One approach is to evaluate the isotopic composition of water in the two domains (Klaus et al., 2013). In theory it is often assumed that the interactions and water dynamics at the interface between macropores and the matrix are mainly controlled by the matric head gradients and the hydraulic conductivity of both domains, which depend on an exchange length and the respective flow velocities (Beven and Germann, 1981; Gerke, 2006).

Our model approach is also based on these assumptions as illustrated in Fig. 2.2c. We restrict exchange to the saturated parts of the pfd, assuming downward particle transport to be much larger than the lateral exchange, and we neglect diffusive exchange between solutes in the matrix and the pfd. We are aware that these simplifications might constrain the generality of our model. For instance, we also neglect the effect of a reverse diffusion from the matrix into the macropores. This effect can influence water and solute dynamics when the propagation of a pressure wave pushes matrix water into empty macropores, mainly in deeper-saturated matrix areas (Beven and Germann, 2013). We rely on those simplifications (a) to keep the model simple and efficient and (b) because the focus of our model is on unsaturated soil domains and during rainfall-driven conditions the macropores are most of the time largely filled due to their small storage volume.

The distribution of different macropore depths and the definition of distribution factors can be derived from datasets containing information on macropore networks observed in field experiments as described in Sect. 2.3.2. Based on these datasets, the current version of our model divides the total amount of macropores n_{mac} in the pfd into three depths. To this end, the total number is multiplied by a distribution factor f for big (f_{big}), medium (f_{med}) and small (f_{smi}) macropores (cf. Fig. 2.2c).

The saturated grid elements (blue filled) of the largest macropores are coupled to the respective grid elements of the medium and small macropores. In this example, the red and black framed grid elements of the three macropore sizes are coupled due to their saturation state and depth order. This coupling ensures a simultaneous diffusive water flow out of the respective grid elements of all three macropore depths. The mixing fluxes q_{mix} ($m s^{-1}$) in the actual grid elements are calculated by Eq. 2.6:

$$q_{mix} = \frac{2 \cdot k_s \cdot k_{mi}}{(k_s + k_{mi})} \cdot \frac{\psi_i}{d_{mac}} \cdot C \cdot dz_{pfd}. \quad (2.6)$$

Thus, diffusive mixing fluxes are calculated with the harmonic mean of the saturated hydraulic conductivity of the matrix k_s ($m s^{-1}$) and the current hydraulic conductivity of the respective matrix grid element k_{mi} ($m s^{-1}$) multiplied by the relation of the matric potential ψ_i (m) of the actual matrix grid element and the macropore diameter d_{mac} (m) as exchange length and the circumference C (m) of the macropore grid element. We use the harmonic mean here because we assume a row configuration at the calculation of the lateral diffusive mixing fluxes between macropore and matrix as there is a vertical interface between the two domains.

The mixing masses are again converted into particle numbers with the two different particle masses. Due to the higher masses of the matrix particles a much lower number of particles enters the matrix. This has to be taken into account by choosing an adequate number of total particles present in the matrix, i.e. at least 1 million at moderately saturated hydraulic conductivities. In addition, it is ensured that the number of particles leaving a grid element of the pfd is lower than the maximum possible number of particles having contact with the lateral surface (cf. Sect. 2.2.3.1) dependent on its current soil water content. Please note that up to now our model has worked with a no-flow condition at the lower boundary of the pfd, but the model structure is generally capable of adding an additional diffusive drainage with particles leaving the macropores at their lower boundary.

2.3 MODEL BENCHMARKING

2.3.1 *Evaluation of the solute transport and linear mixing approach during well-mixed matrix flow*

The bases of the first evaluation of our solute transport and linear mixing approach are data from tracer experiments conducted by Zehe and Flühler (2001a) in the Weiherbach catchment to investigate mechanisms controlling flow patterns and solute transport. The Weiherbach Valley is located in the southwest of Germany and has a total extent of 6.3 km^2 . The basic geological formations comprise Triassic Muschelkalk marl and Keuper sandstone covered by Pleistocene Loess layers with a thickness of up to 15 m. The hillslopes exhibit a typical Loess catena with erosion-derived Colluvic Regosols at lower slopes and Calcaric Regosols or Luvisols at the top and mid slopes. Land use is dominated by agriculture. For further details on the Weiherbach catchment, please see the work of Plate and Zehe (2008).

In this catchment, a series of irrigation experiments with bromide as tracer were performed at 10 sites. At each site, a plot area of $1.4 \text{ m} \times 1.4 \text{ m}$ was defined and the initial soil water content and the soil hydraulic functions were measured. The plot area was then irrigated by a block rainfall of approx. 10 mm h^{-1} with a tracer solution containing 0.165 kg m^{-1} bromide. After 1 d, soil profiles were excavated and soil samples were collected in a $0.1 \text{ m} \times 0.1 \text{ m}$ grid down to a depth of 1 m and their corresponding bromide concentrations measured.

Thus, in every 10 cm soil depth interval, 10 samples were taken and, for the comparison with our one-dimensional simulation results, the bromide concentrations were averaged over each sample depth. Note that the corresponding observations provide the tracer concentration per dry mass of the soil C_{dry} , while the LAST-Model simulates concentrations in the water phase C_w . We thus compare simulated and observed tracer masses at the respective depths. More details on the tracer experiments can be taken from Zehe and Flühler (2001a,b). For the evaluation of our solute transport and linear mixing approach, we select the two sites 23 and 31, where flow patterns reveal a dominance of well-mixed matrix flow without any considerable influence of macropores. Thus, we use the LAST-Model without an active pfd for the simulations at the study sites 23 and 31.

The soil at the two sites can be classified as Calcaric Regosol (WRB, 2014). In line with the experiments, our model uses a spatial soil matrix discretization of 0.1 m and the soils initially contain in total 1 million water particles but with no tracer masses. Initial soil water

contents and all further experimental and model parameters as well as the soil properties at these sites are listed in Tab. 2.1.

2.3.2 *Parameterization and evaluation of the preferential flow domain*

In a next step, our pfd model extension is again evaluated with the help of the results of two additional field tracer experiments of Zehe and Flübler (2001a). This time, we select study sites Spechtacker and 33, which show numerous worm burrows inducing preferential flow. The sites are also located in the Weiherbach catchment and the sprinkling experiments were equally conducted with the application of a block rainfall containing bromide on a soil plot. The soils can be classified as Colluvic Regosol (WRB, 2014).

Additionally, the patterns of the worm burrows were extensively examined at these study sites. Horizontal layers at different depths of the vertical soil profiles were excavated (cf. introduction of van Schaik et al., 2013) and in each layer the amount of present macropores counted as well as the diameters and depths measured. These detailed measurements provided an extensive dataset of the macropore network at study sites Spechtacker and 33. Based on this dataset, we can obtain those data we need for the derivation of a mean macropore diameter, macropore depth distribution and distribution factors. We focus on a mean macropore diameter of 5 mm at the Spechtacker site because worm burrows with a diameter range of roughly 4–6 mm are dominant here, and at site 33 we select a mean diameter of 6 mm. Fig. 2.3 shows the mean number of macropores with these diameters at each depth at both sites. Based on this distribution, we can identify and select three considerable macropore depths at the Spechtacker site (0.5, 0.8 and 1.0 m) and two macropore depths at site 33 (0.6 and 1.0 m) (cf. Tab. 2.1). At these depths, we count circa 11, 3 and 2 macropores ($n_{\text{mac}} = 16$) at the Spechtacker site as well as 30 and 16 macropores ($n_{\text{mac}} = 46$) at site 33, respectively. With these distributions we are able to calibrate our distribution factors f in a way that a multiplication of the total number of macropores by these factors results in the correct number of macropores at the respective depths. The obtained distribution factors are listed in Tab. 2.1.

Moreover, Zehe and Flübler (2001a) measured saturated water flow through a set of undisturbed soil samples containing macropores of different radii at the Spechtacker study site with the assumption that flow through these macropores dominated. In line with the law of Hagen and Poiseuille, they found a strong proportionality of the flux through the macropores to the square of the macropore radius, while frictional losses were 500 to 1000 times larger. This dependence of the flux rate on the macropore radius can be described by the

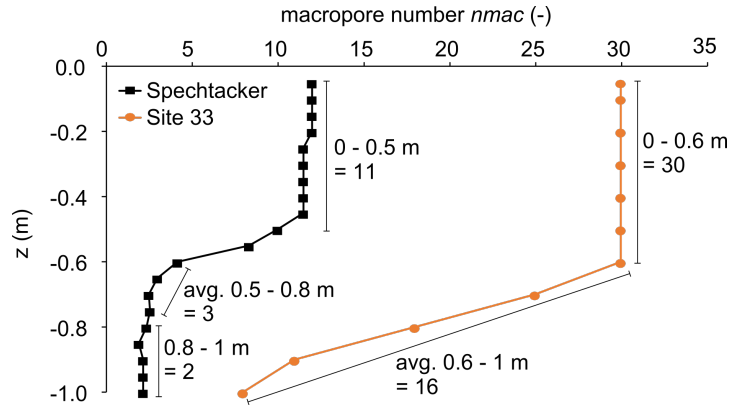


Figure 2.3: Distribution of macropore numbers with average diameters of 5 mm (Spechtacker) and 6 mm (site 33) along the vertical soil profiles at the two study sites. The arrows highlight the derivation of the macropore numbers at different depths (cf. Sect. 2.3.2), whereby “avg.” means that at these depths the macropore numbers are averaged because there was no clear macropore pattern observed.

linear regression shown in Fig. 2.4. Based on this linear regression, the hydraulic conductivity of the macropores k_{pfd} was calculated as a function of the macropore radius $\frac{d_{mac}}{2}$ (termed r_M in Zehe and Flühler, 2001a) as we assume the hydraulic conductivity k_{pfd} is equal to the flux rate q_M of the macropore (Eq. 2.7):

$$k_{pfd} = 2884.2 \cdot \left(\frac{d_{mac}}{2} \right)^2. \quad (2.7)$$

For more details on the two study sites and their macropore network, see also the studies of Ackermann (1998) and Zehe (1999). Here, we select a spatial pfd discretization of 0.05 m and assume that macropores initially contain no particles and hence also no water or tracer masses. The total possible number of particles, which can be stored in the pfd is 10,000 particles. All further experimental and simulation parameters, soil properties as well as information about the macropore network at sites Spechtacker and 33 are listed in Tab. 2.1.

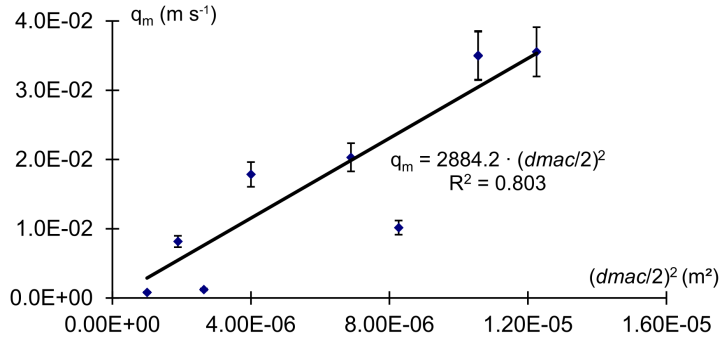


Figure 2.4: Linear regression of the flux rate within the macropore on the macropore radius ($d_{mac}/2$) at the Spechtacker study site (edited figure, adopted from Zehe and Flüßler, 2001a). This relation was derived from measurements of saturated flow through undisturbed soil columns containing worm burrows.

2.3.3 Simulations with HYDRUS 1-D

The simulations with HYDRUS 1-D are performed with the same soil properties, model setups and initial conditions introduced in Sect. 2.3.1 and 2.3.2 as well as shown in Tab. 2.1. The simulations of the well-mixed sites 23 and 31 are performed with a van Genuchten–Mualem single-porosity model for water flow and an equilibrium model for solute transport. For the simulations at the preferential flow sites Spechtacker and 33 we use dual-porosity models for water flow (“Durner, dual van Genuchten–Mualem”) and solute transport (“Mobile–Immobile Water”). This means HYDRUS assumes two differently mobile domains to account for preferential flow. The theory of that approach describes preferential flow in the way that the effective flow space is decreased due to the immobile fraction and thus the same volume flux is forced to flow through this decreased flow space, resulting in higher porewater velocities and consequently also in a deeper percolation of water and solutes (Šimůnek and Genuchten, 2008). For the parameterization of these two domains we select an immobile soil water content $Th_{mob.}$ of $0.2 \text{ m}^3 \text{ m}^{-3}$. We hence assume that about 80 %–90 % of the total soil water amounts at the two sites are stored in the matrix and are therefore in fact immobile compared to the remaining 10 %–20 %, which are assumed to flow through macropores. Zehe and Jackisch (2016) elaborated this rate of an immobile fraction and a mobile fraction in the fine-grained soils of the Weiherbach catchment. For all simulations we choose an atmospheric condition with a surface layer and variable infiltration fluxes at the upper boundary as well as a free drainage condition at the lower boundary.

2.3.4 Sensitivity analyses of selected parameters

The sensitivity analyses of the model with the pfd extension are conducted by varying several parameters describing the soil matrix and the pfd in a realistic, evenly spaced value range. To this end, the saturated hydraulic conductivity of the matrix k_s , the diameter d_{mac} and the number n_{mac} of the macropores are the selected parameters, which are deemed to be most sensitive and crucial for the model behaviour and the simulation results. The probably most sensitive parameter is k_s as it controls the infiltration capacities of both domains, the displacement within the soil matrix as well as the diffusive mixing fluxes. Besides the saturated hydraulic conductivity of the matrix, we also assume that the total number and diameter of the macropores are probably of great importance for the model results because they are crucial for the development of the new pfd (cf. Sect. 2.2.3.1). Moreover, based on the derived three depths and distribution factors at the Spechtacker site (cf. Sect. 2.3.2), we arbitrarily select different configurations of the macropore depth distribution and the distribution factors to evaluate the behaviour of the model related to various numbers of macropores at different depths. The depth distribution of macropores thereby comprises deep (Configuration 1), medium (Configuration 2) and shallow (Configuration 3) distributions. At the distribution factors there are four different configurations. A realistic distribution comprising more small than big macropores is represented by Configurations A and D, a homogeneous distribution is shown by Configuration B and a rather uncommon distribution with more big than small macropores is illustrated by Configuration C. All parameter ranges and the detailed configurations of the sensitivity analyses are listed in Tab. 2.2. All model runs of the sensitivity analyses are performed at the Spechtacker site using 22 mm of rainfall in 140 min with a subsequent drainage duration of 1 d. Additional parameters like soil properties, antecedent moisture and concentration states, and bromide concentration of precipitation water remain constant (cf. Tab. 2.1).

Table 2.1: Simulation and tracer experiment parameters (average values) as well as soil hydraulic parameters following Schäfer (1999) at sites 23, 31, Spechtacker and 33, where k_s is the saturated hydraulic conductivity of the matrix, θ_s the saturated soil water content, θ_r the residual soil water content, α the inverse of an air entry value, n a quantity characterizing pore size distribution, s the storage coefficient and ρ_b the bulk density. In general, all these observable parameters can be freely adjusted in our model and are hence independent of other variables. All other calculated parameters presented in the text are dependent on these observable parameters.

Parameter	Site 23	Site 31	Spechtacker	Site33
Irrigation duration (hh:mm)	02:10	02:10	02:30	02:20
Irrigation intensity ($mm\ h^{-1}$)	10.36	10.91	11.1	9.7
Br concentration of irrigation water ($kg\ m^{-3}$)			0.165	
Recovery rate (%)	77	76	95	96
Initial soil moisture in 15 cm (%)	20.5	25.3	27.4	22.3
Initial soil moisture in 30 cm (%)	25.3	15.9	-	-
Initial soil moisture in 45 cm (%)	28.1	13	-	-
Initial soil moisture in 60 cm (%)	29.6	13.4	-	-
Simulation time t (s)		86,400 (= 1 d)		
Time step Δt (s)		120		
Particle number in matrix (-)		1 million		
Particle number in pfd (-)	-	-	10 k	10 k
Soil type	Calcaric Regosol	Calcaric Regosol	Colluvic Regosol	Colluvic Regosol
k_s ($m\ s^{-1}$)	0.5×10^{-7}	0.5×10^{-6}	2.5×10^{-6}	2.5×10^{-6}
θ_s ($m^3\ m^{-3}$)	0.44	0.44	0.4	0.4
θ_r ($m^3\ m^{-3}$)	0.06	0.06	0.04	0.04
α (m^{-1})	0.4	0.4	1.9	1.9
n (-)	2.06	2.06	1.25	1.25
s (-)	0.26	0.45	0.38	0.38
ρ_b ($kg\ m^{-3}$)	1300	1300	1500	1500
nmac (-)	-	-	16	46
dmac (m)	-	-	0.005	0.006
Grid element length in pfd dz_{pfd} (m)	-	-	0.05	0.05
mac. big (m)	-	-	1	1
mac. med (m)	-	-	0.8	0.6
mac. sml (m)	-	-	0.5	-
f_{big} (-)	-	-	0.13	0.35
f_{med} (-)	-	-	0.19	0.65
f_{sml} (-)	-	-	0.68	-

Table 2.2: Parameter ranges of the sensitivity analyses and configurations of macropore depth distribution and distribution factors (cf. Fig. 2.10)

Parameter	Value range			
k_s ($m s^{-1}$)	10^{-6} - 10^{-5} (step: 1×10^{-6})			
dmac (m)	0.0035 - 0.008 (step: 0.0005)			
nmac (-)	11 - 20 (step: 1)			
mac. depth distr. config.	1	2	3	
mac. big (m)	-1	-0.8	-0.6	
mac. med (m)	-0.8	-0.6	-0.4	
mac. sml (m)	-0.6	-0.4	-0.2	
distr. factors config.	A	B	C	D
f_{big} (-)	0.13	0.3	0	0.5
f_{med} (-)	0.19	0.3	0.2	0.3
f_{sml} (-)	0.68	0.3	0.8	0.2

2.4 RESULTS

2.4.1 Simulation of solute transport under well-mixed conditions

The well-mixed sites 23 and 31 show a high similarity due to their spatial proximity (Fig. 2.5a, b). The shape and courses of the simulated tracer mass profiles coincide well with the observed ones over the entire soil domain, with RMSE values of 0.23 and 0.28 g, respectively. The observed values are within the uncertainty range, represented by the rose shaded areas. This area reflects the uncertainty arising from a variation of k_s values of the soil matrix in the observed range of 10^{-7} – 10^{-6} m s^{-1} at site 23 and 10^{-6} – 10^{-5} m s^{-1} at site 31.

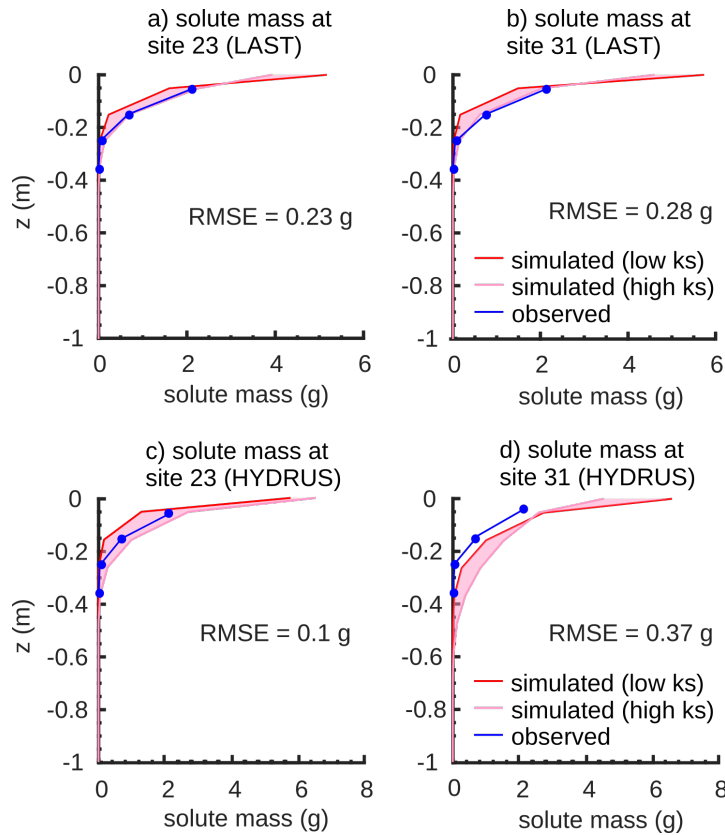


Figure 2.5: Final simulated and observed vertical bromide mass profiles of the matrix at the two well-mixed sites 23 and 31 (a, b) with RMSE values simulated with the LAST-Model. In comparison, final simulated and observed vertical bromide mass profiles at the two well-mixed sites 23 and 31 (c, d) with RMSE values simulated with HYDRUS 1-D. The rose shaded area shows the uncertainty area of measured k_s values.

Note that in the experiments the tracer mass was not directly measured at the soil surface, but the observations represent averages across 10 cm depth increments, starting at a depth of 5 cm. A comparison of

the simulated masses close to the surface is thus not meaningful. This difference between simulated and observed profiles near to the surface suggests that the coarse resolution of the sampling grid is a likely reason for the relatively low recovery rates of 77 % and 76 % at the two sites (cf. Tab. 2.1). Overall, we conclude that manipulating k_s within the observed uncertainty leads to an unbiased simulation ensemble compared to the observed tracer data at matrix-flow-dominated sites.

2.4.2 Evaluation of the preferential flow domain

Our model with the new preferential flow domain is tested against two tracer experiments on macroporous soils at sites Spechtacker and 33. At the Spechtacker site, the simulated and observed tracer mass distributions are generally in good accordance (Fig. 2.6a) with a RMSE of 0.3 g, and again the values are within the uncertainty range. In this case, the rose area shows the standard deviation of measured macropore numbers (± 4) and diameters (± 1 mm) from the mean values (cf. Tab. 2.1) at the Spechtacker site. Especially in deeper soil regions from 0.35 to 1 m, the shape and the magnitude of values correspond well. In the upper soil parts from 0.05 to 0.15 m the model slightly overestimates the tracer masses. Between 0.15 and 0.35 m soil depth both profiles exhibit the greatest differences and even contrary courses. In general, the simulated mass profile at site 33 corroborates the results of the Spechtacker site (Fig. 2.6b). The simulated and observed tracer masses are also in good accordance with a RMSE value of 0.15 g. In contrast to the Spechtacker site, varying the macropore numbers and diameters within the standard deviation (± 4 ; ± 1 mm) has just slight effects on the mass profile at this site. However, especially in deeper soil regions from 0.6 to 1 m the values correspond well, while the greatest differences occur between 0.25 and 0.45 m as the simulated mass profile is not able to completely depict the observed hump in this area.

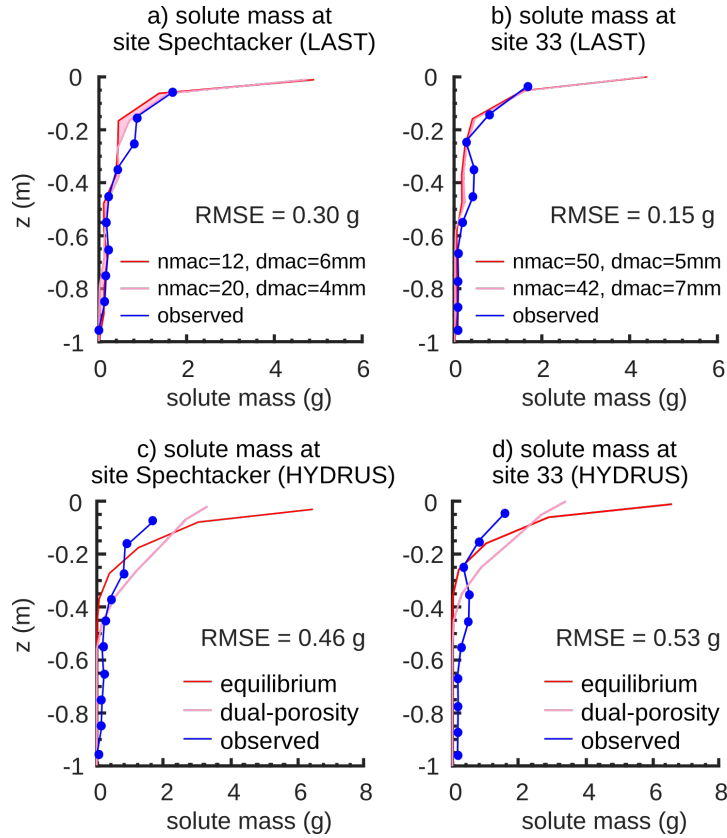


Figure 2.6: Final simulated and observed vertical bromide mass profiles of the matrix at the two preferential flow sites Spechtacker and 33 (a, b) with RMSE values simulated with the LAST-Model. The rose area shows the standard deviation of measured macropore numbers and diameters from the mean values at site Spechtacker ($n_{mac} = 16$, $d_{mac} = 5$ mm) and site 33 ($n_{mac} = 46$, $d_{mac} = 6$ mm) (cf. Tab. 2.1). In comparison, final simulated and observed vertical bromide mass profiles at the two preferential flow sites Spechtacker and 33 (c, d) with RMSE values simulated with HYDRUS 1-D. The rose mass profile is simulated with a dual-porosity approach to account for preferential flow (cf. Sect. 2.3.3) and, for comparison, the red mass profile is simulated with an equilibrium approach.

2.4.3 Comparison with HYDRUS 1-D

The mass profiles at the well-mixed sites 23 and 31 simulated with HYDRUS 1-D show similar patterns and are in accordance with the observed profiles with RMSE values of 0.1 g at site 23 and 0.37 g at site 31 (Fig. 2.5c, d). Especially at site 23 the simulated mass profile is centred within the uncertainty range of the measured k_s values (rose shaded area; cf. Sect. 2.4.1). At site 31, HYDRUS 1-D slightly overestimates the tracer masses over the entire soil domain, but here the shapes of the profiles also coincide well. In contrast, at the two preferential flow sites Spechtacker and 33 the mass profiles simulated with HYDRUS 1-D and the dual-porosity approach (rose profile) are not in good accordance with the observed profiles with RMSE values of 0.46 and 0.53 g, respectively (Fig. 2.6c, d). In the first 40 cm there is an overestimation of the simulated tracer masses, while in the deeper soil regions HYDRUS 1-D is not able to reproduce well the tail of the mass profiles with their heterogeneous courses. A comparison with the results of HYDRUS with an equilibrium model (red profile) reveals that the dual-porosity approach is generally able to predict a deeper percolation of solutes through the mobile domain.

2.4.4 Sensitivity analyses

2.4.4.1 Sensitivity to saturated hydraulic conductivity k_s

The concentration profile range of the matrix reveals a strong sensitivity of the simulated profiles to k_s when we neglect macropores (Fig. 2.7a). Especially in the upper soil part, the differences arising from low and high k_s values are clearly detectable. Lower values imply that the soil matrix has a smaller infiltration capacity and therefore less water is infiltrating the matrix. Consequently, without macropores solutes do not penetrate into depths greater than 0.2 m. The presence of macropores significantly alters the sensitivity of the concentration and soil moisture profiles (Fig. 2.7b, c). Again, the profile shapes clearly depend on the k_s values, but now water and solutes reach greater depths of down to 0.8 m by flowing through the macropores. At low k_s values (red curve) the reduced matrix infiltration capacity leads to an increased infiltration of water and solute into the macropores. Subsequently, the solutes bypass the matrix until they diffusively mix into the matrix at greater depths. In contrast, at high k_s values the matrix infiltration capacity is increased. This leads in turn to a reduced infiltration into the macropores, and instead the majority of water and solute masses infiltrate the matrix and remain in the top soil. This effect is reflected by the blue curves in Fig. 2.7 with higher solute concentrations near the soil surface and decreased concentrations at greater depths in comparison to low k_s values.

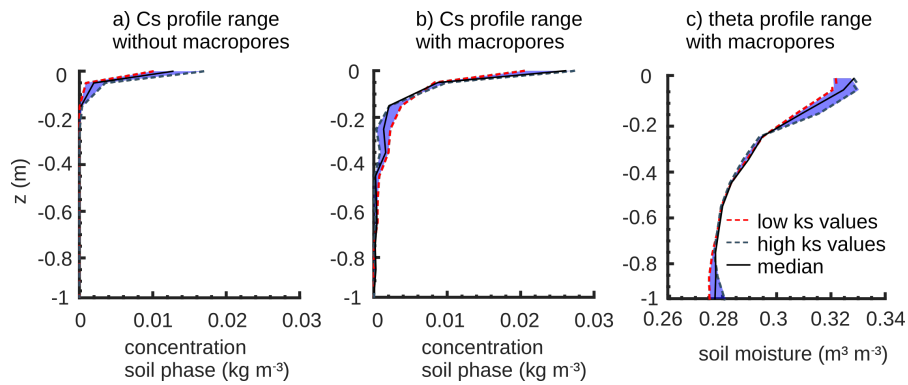


Figure 2.7: Final simulated bromide concentration (C_s) and soil moisture (theta) profiles of the soil matrix (a) without and (b, c) with macropores at different k_s values. The blue area shows the possible range of simulated profiles with different k_s values.

Finally, the yellow curves in Fig. 2.8 show the proportion of solutes within the matrix, which originates from the macropores. In general, at all k_s values and depths below 0.2 m the entire solute amount within the matrix travelled through the macropores. Differences are restricted to the upper soil part. Here the largest proportion of solutes has directly infiltrated the matrix without having been in the macropores before. The pfd proportion decreases from low to high k_s values, confirming again the important influence of the k_s values on the infiltration capacities and the distribution of water and solutes.

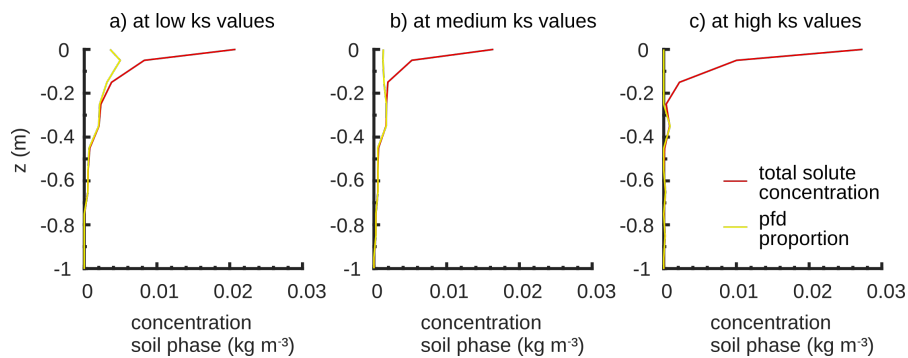


Figure 2.8: Final bromide concentration profiles at (a) low, (b) medium and (c) high k_s values and the proportion of solutes which originate from the macropores.

2.4.4.2 Sensitivity to macropore number n_{mac} and diameter d_{mac}

The model results sensitively respond to a variation of macropore diameters. In the upper soil part, the solute concentrations and moisture are slightly higher, when macropores are small (Fig. 2.9a, b). In this case, the macropores collect only smaller amounts of water and solutes and the majority has directly infiltrated the soil matrix. Wider macropores transport larger amounts of water and solutes to greater depths, where they diffusively mix into the subsoil matrix. This deep redistribution is reflected by the characteristic profile shapes and the higher concentration and moisture values in the deep soil.

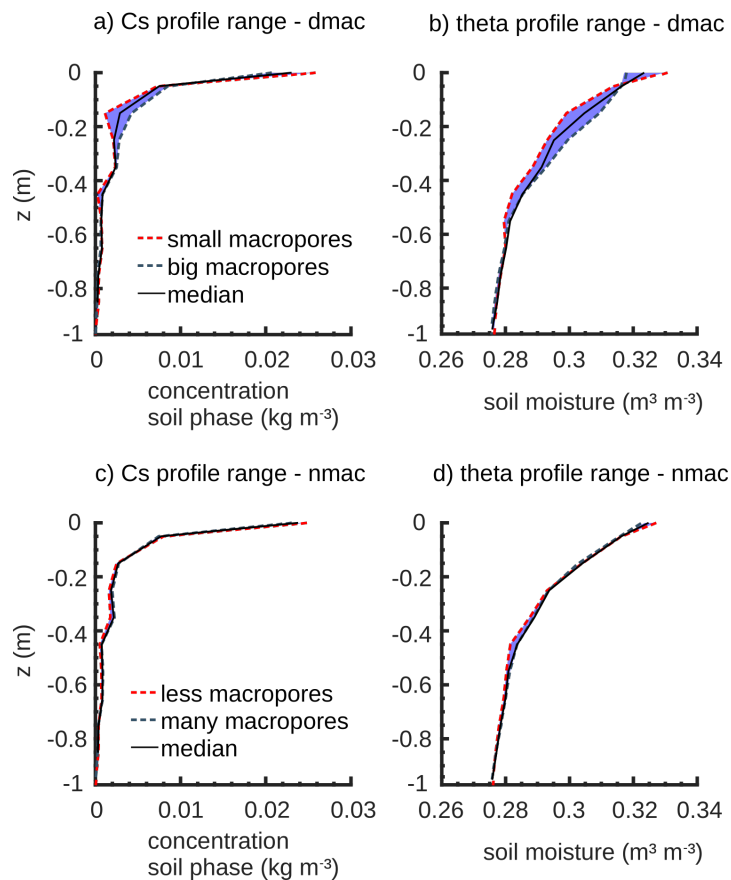


Figure 2.9: Final simulated bromide concentration (C_s) and soil moisture (θ) profiles of the soil matrix at different macropore diameters (d_{mac}) (a, b) and macropore numbers (n_{mac}) (c, d).

Furthermore, the influence of different macropore numbers on the concentration and moisture profiles is marginal (Fig. 2.9c, d). This implies that the model does not respond to every geometrical parameter equally sensitively. The macropore number scales less than the diameter at the calculation of the further macropore measures. However, this could change when working with higher precipitation intensities.

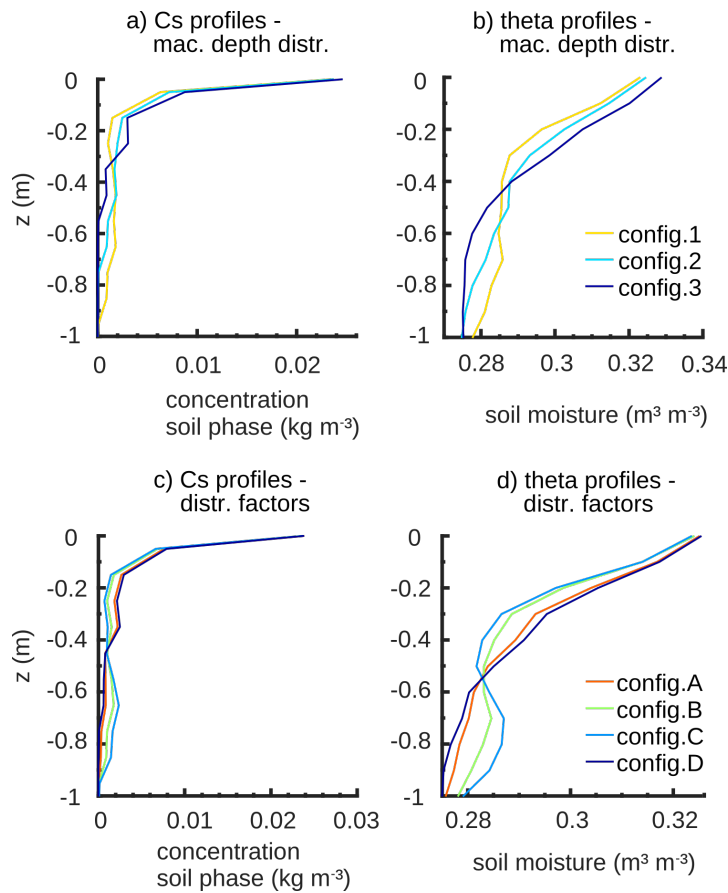


Figure 2.10: Final simulated bromide concentration (Cs) and soil moisture (theta) profiles of the soil matrix at three different macropore depth distribution configurations (a, b) and at four different distribution factor configurations (c, d) (cf. Tab. 2.2).

Simulations with different macropore depth configurations again reveal a clear sensitivity of the model (Fig. 2.10a, b). A steady decrease in the deep redistribution of the concentration and moisture values from the deep (Configuration 1) to shallow depth configuration (Configuration 3) is obvious. Shallow macropores distribute the total amount of water and solutes mainly in the upper soil part, while deep macropores relocate this distribution to greater depths of down to 1 m. The results of the distribution factor configurations again corroborate the previous findings (Fig. 2.10c, d). Configuration B produces a homogeneous solute concentration profile from 0.2 m to the total depth. Both more realistic Configurations A and D comprise more small than big macropores. This increased number of small macropores ensures higher water and solute amounts in the first 0.5 m of the soil matrix due to an enhanced mixing in this area. Finally, the rather uncommon Configuration C with more big than small macropores shows converse results. Solute concentrations and moisture contents are strongly in-

creased at great depths from 0.7 to 1 m because of increased diffusive mixing fluxes in these parts.

2.5 DISCUSSION AND CONCLUSIONS

We extend the Lagrangian model of Zehe and Jackisch (2016) with routines to consider transport and linear mixing of solutes within the soil matrix as well as preferential flow through macropores and related interactions with the soil matrix. The evaluation of the model with data of tracer field experiments, the comparison with results of HYDRUS 1-D and the sensitivity analyses reveal the feasibility and physical validity of the model structure as well as the robustness of the solute transport and linear mixing approach. The LAST-Model provides a promising framework to improve the linkage between field experiments and computer models to reduce working effort and to improve the understanding of preferential flow processes.

2.5.1 *New routine for solute transport and diffusive mixing*

The initially performed simulations of the bromide mass profiles at the two well-mixed sites 23 and 31 support the validity of the straightforward assumptions of the underlying solute transport routine with its perfect mixing approach (Fig. 2.5a, b). In the presented version, our mixing routine works with a short mixing time to ensure an instantaneous mixing between event and pre-event particles to account for the well-mixed conditions at the selected sites. However, the model allows us to select longer mixing times or even a distribution of various mixing times to consider imperfect mixing among different flow paths.

The simulation results at the well-mixed sites 23 and 31 are confirmed by the commonly approved HYDRUS 1-D model. The simulated tracer mass profiles and RMSE values of both models are in good accordance at these sites (Fig. 2.5). The capability of predicting the solute dynamics is hence a big asset of our approach, and it is a solid base to realize the second model extension with the implementation of the preferential flow domain.

2.5.2 *Model extension to account for preferential flow in macropores*

The results of the evaluation of the pfd extension show that our model is furthermore capable of simulating tracer experiments on macroporous soils and depicting well their observed one-dimensional tracer mass profiles with the typical fingerprint of preferential flow (Fig. 2.6a, b). Especially the tracer masses in the subsoil match well between simulated and observed data. This corroborates our assumptions concerning the macropore structure and the approach to describing macropore–matrix exchange, which proved to be feasible for predicting solute distribution patterns due to preferential flow and related long transport lengths. In this context, we stress that the

approach to simulating macropore–matrix exchange (cf. Fig. 2.2c) does not rely on an extra leakage parameter, but follows the theory of deriving an effective diffusive exchange between the domains (cf. Eq. 2.6).

In contrast, the HYDRUS 1-D model performance is clearly inferior and does not match the fingerprints of preferential flow in the mass profiles at sites Spechtacker and 33 (Fig. 2.2c, d). Especially the penetration of bromide through macropores into greater depths is ignored by HYDRUS 1-D, although we selected dual-porosity models for both water flow and solute transport (cf. Sect. 2.3.3). The better performance of our LAST-Model at the two preferential flow sites compared to HYDRUS is further reinforced by the RMSE values, which are significantly different. The results imply that, when working with a dual-porosity approach, HYDRUS and the underlying theory of two differently mobile domains is indeed able to depict a generally deeper penetration of solutes, but it is not sufficient to exactly simulate the heterogeneous course and shape of the observed tracer mass profiles in preferential flow-dominated soil domains.

The results of our LAST-Model mainly deviate from the observations in the upper soil parts. However, these deviations are within the uncertainty ranges revealed by the sensitivity analyses (Figs. 2.7, 2.9). Further, the model reveals difficulties in the simulation of bromide masses between 0.15 and 0.35 m soil depth at the Spechtacker site (Fig. 2.6a). Possible reasons could be the influence of (a) lateral endogeic worm burrows, which are completely unknown and not represented in the model and (b) a nearby plough horizon. Both reasons result in a disturbance of the soil structure, leading to an increased uncertainty of soil properties in this region.

At site 33, our model is not able to sufficiently reproduce the hump of the observed mass profile between 0.25 and 0.45 m soil depth (Fig. 2.6b). A possible explanation for this issue could be the fact that the tracer experiment and the examination of the macropore network were performed on different dates. It is likely that uncertainties arise from this temporal discrepancy with a mismatch between observed macropore geometries and recovered tracer patterns due to natural soil processes as well as anthropogenic soil cultivation during this time lapse. Another possible explanation could be the fact that up to now the exchange has only been simulated for saturated parts of the pfd (cf. Sect. 2.2.3.4) and hence the transport of solute masses from the pfd into the matrix is delayed. A test of this idea requires a refinement of the model in future research. Moreover, varying macropore numbers and diameters in the range of the standard deviation reveals just slight effects on the simulated mass profile at site 33 and is thus less sensitive compared to the results at the Spechtacker site. The

reason for this phenomenon is probably the higher total number of macropores ($n_{\text{mac}} = 46$) and thus a larger macropore volume at site 33. In relation to this larger volume, the variation of macropore numbers and diameters in the quite narrow range of the standard deviation (± 4 , ± 1 mm) has only a minor influence on the total water and tracer masses transported through the macropore network and thus on the resulting mass profile at site 33.

Note that the conversion of solute masses into an integer number of particles results in small errors, leading to a small amount of solutes not entering the system and remaining in the fictive surface storage. To mitigate this model effect, a high number of total particles present in the matrix is necessary, at least 1 million. Besides many displacement steps of each particle, the total number of particles is important to render the random walk approach statistically valid (Uffink, 1990), although too high particle numbers will decrease the computational efficiency. Thus, we conclude that our extension of the Lagrangian particle model of Zehe and Jackisch (2016) is a promising tool for a straightforward one-dimensional estimation of non-uniform solute and water dynamics in macroporous soils. However, before the suitability of our model approach to simulate preferential flow of non-interacting tracers is generalized, further field experiments on a variety of differently structured soils are necessary. In the presented model version, we assume that a macropore distribution with maximally three different depths is a sufficient approximation of the observed macropore networks at study sites Spechtacker and 33 (cf. Sect. 2.3.2, Fig. 2.3). Nevertheless, as a variable macropore depth distribution might be observed at other sites, the implementation of the macropore depth distribution must be kept flexible for other soils in future model parameterizations. Besides the parameterization with experimental data, it is also possible to set up our model by using pedotransfer functions for the soil hydraulic properties and to vary the parameters of the pfd by inverse modelling, which needs prior knowledge of the depth of typical macropore systems (e.g. worm burrow networks) and literature data to parameterize macropore flow velocities. This method would reduce time and the amount of work, but it could result in equifinality as shown by Klaus and Zehe (2010) or Wienhöfer and Zehe (2014).

Some of our assumptions, like the macropore geometry, the simple volume filling or the depth distribution of macropores, were applied in a similar way in dual-porosity models before (Beven and Germann, 1981; Workman and Skaggs, 1990; van Dam et al., 2008), and a few previous studies even also worked with physically and geometrically separated domains (e.g. Russian et al., 2013). Thus, our model extension can be seen as an advancement of double-

domain approaches by assuming simple volume-filling for macropore flow and particle tracking for matrix flow instead of relying on the Darcy–Richards equation. With these results, our model is one of the first, which proves that simulations based on a Lagrangian perspective of both solute transport and dynamics of the carrying fluid itself are possible and very applicable. Also, the vertically distributed exchange between both domains seems feasible and does not rely on extra parameters like a leakage coefficient, e.g. as used in dual models (Gerke, 2006). The concept of cubic particle packing within the macropores (cf. Fig. 2.2a, Sect. 2.2.3.1) is strongly motivated by the hydraulic radius and can thus be transferred to flow in further kinds of macropore geometries, including flow between two parallel walls as occurs in soil cracks or corner flow in rills (Germann, 2018).

Another remarkable result is the high model sensitivity towards the saturated hydraulic conductivity k_s of the soil matrix (Figs. 2.7, 2.8). Especially its direct influence on the infiltration process is crucial. As k_s determines the initialization, infiltration fluxes and distribution of incoming precipitation masses to the two domains, it has a direct impact on the deep displacement of water and solutes. Therewith, our findings highlight the importance of infiltration processes for macroporous soils and the challenge in implementing them properly in models, which have also been stressed by other studies (Beven and Germann, 1981; Weiler, 2005; Nimmo, 2016).

Our model shows further a remarkable sensitivity to the presence of a population of macropores, while differences in macropore properties comparatively have little impact. Generally, wider macropores collect and transport more water and solutes to greater depths than small ones (Fig. 2.9a, b). In contrast, high numbers of macropores do not necessarily result in a greater and deeper percolation of solutes (Fig. 2.9c, d). Jackisch and Zehe (2018) also reported this aspect and explain it with the distribution of the irrigation supply to all macropores, and this supply can drop below the diffusive mixing fluxes from the macropores into the matrix. However, this implies that the number of macropores becomes more sensitive at much larger irrigation rates.

Where and to which extent water and solutes are diffusively mixed from the macropores into the matrix clearly depend on the depth distribution of the macropores and the distribution of the mixing masses among the various depths (Tab. 2.2, Fig. 2.10). This concept of the distribution of macropore depths and mixing masses is important to meet the natural condition of a high spatial heterogeneity of the macropore network. Generally, the results of our sensitivity analyses are in line with the findings of Loritz et al. (2017) as they reveal a significant impact of the implementation of macropore flow on the

model behaviour and its complexity.

Please note that we are aware of the fact that some results of the sensitivity analyses are straightforward and expectable. Nevertheless, we think that their presentation is necessary to allow the reader to check whether our Lagrangian approach with the macropore domain reproduces these results as the model concept is new. To this end, please also see further sensitivity analyses in the Appendix [A.1](#).

We overall conclude that the modified one-dimensional structure of our model is robust and provides a high computational efficiency with short simulation times, which is a big advantage of our model. In line with the underlying Lagrangian model of Zehe and Jackisch (2016), we also used the MATLAB programming language to develop the two model extensions. The model simulation at the Spechtacker site with the selected parameterization (cf. Tab. 2.1) only runs for about 5 min, even on a personal computer with moderate computing power. Without an active pfd, as is the case for the simulations at study sites 23 and 31, the model runs even faster. When performing these simulations on a high performance computer or workstation, one could probably also run several model simulations in parallel within minutes.

Moreover, the efficiency allows for the implementation of further routines with as yet still appropriate simulation times. In this way, the model could prospectively consider retardation and adsorption effects as well as first-order reactions during the transport of non-conservative substances like pesticides. Until now, the solute movement of conservative tracers like bromide has only been determined by the water flow without any consideration of molecular diffusion or particle interactions, although some evidence suggests a non-conservative behaviour of bromide tracers under certain conditions (e.g. Whitmer et al., 2000; Dusek et al., 2015). In our case, we believe that the event scale and the short simulation times allow for the assumption of a conservative behaviour of bromide.

Moreover, the model can be extended to two-dimensional for simulations on hillslope or even catchment scales. In this regard, our model also offers the promising opportunity to quantify water ages and to evaluate travel and residence times of water and solutes by a simple age tagging of particles. This can shed light on the chemical composition and generation of runoff fluxes as well as on the inverse storage effect. This effect describes a greater discharge fraction of recent event water at a high catchment water storage than at low storage (Hrachowitz et al., 2013; Harman, 2015; Klaus et al., 2015; van der Velde et al., 2014; Sprenger et al., 2018a).

Part III

SIMULATION OF REACTIVE SOLUTE TRANSPORT IN THE CRITICAL ZONE: A LAGRANGIAN MODEL FOR TRANSIENT FLOW AND PREFERENTIAL TRANSPORT

This study is published in the scientific journal Hydrology and Earth System Science (HESS). The remainder of part III is a reprint of:

Sternagel, A., R. Loritz, J. Klaus, B. Berkowitz, and E. Zehe (2021). "Simulation of reactive solute transport in the critical zone: a Lagrangian model for transient flow and preferential transport." In: Hydrology and Earth System Sciences 25.3, pp.1483–1508. <https://doi.org/10.5194/hess-25-1483-2021>.

SIMULATION OF REACTIVE SOLUTE TRANSPORT IN THE CRITICAL ZONE: A LAGRANGIAN MODEL FOR TRANSIENT FLOW AND PREFERENTIAL TRANSPORT

ABSTRACT

We present a method to simulate fluid flow with reactive solute transport in structured, partially saturated soils using a Lagrangian perspective. In this context, we extend the scope of the Lagrangian Soil Water and Solute Transport Model (LAST) (Sternagel et al., 2019) by implementing vertically variable, non-linear sorption and first-order degradation processes during transport of reactive substances through a partially saturated soil matrix and macropores. For sorption, we develop an explicit mass transfer approach based on Freundlich isotherms because the common method of using a retardation factor is not applicable in the particlebased approach of LAST. The reactive transport method is tested against data of plot- and field-scale irrigation experiments with the herbicides Isoproturon and Flufenacet at different flow conditions over various periods. Simulations with HYDRUS 1-D serve as an additional benchmark. At the plot scale, both models show equal performance at a matrix-flow-dominated site, but LAST better matches indicators of preferential flow at a macropore-flow-dominated site. Furthermore, LAST successfully simulates the effects of adsorption and degradation on the breakthrough behaviour of Flufenacet with preferential leaching and remobilization. The results demonstrate the feasibility of the method to simulate reactive solute transport in a Lagrangian framework and highlight the advantage of the particle-based approach and the structural macropore domain to simulate solute transport as well as to cope with preferential bypassing of topsoil and subsequent re-infiltration into the subsoil matrix.

3.1 INTRODUCTION

Reactive substances like pesticides are subject to chemical reactions within the critical zone (Kutílek and Nielsen, 1994; Fomsgaard, 1995). Their mobility and life span depend greatly on various factors like (i) the spectrum of transport velocities, (ii) the sorption to soil materials (Knabner et al., 1996), and (iii) microbial degradation and turnover (cf. Sect. 3.3). The multitude and complexity of these factors are a considerable source of uncertainty in pesticide fate modelling. It is still not fully understood how pesticides are transported within different soils and particularly how preferential flow through macropores impacts the breakthrough of these substances into streams and groundwater (e.g. Flury, 1996; Arias-Estévez et al., 2008; Frey et al., 2009; Klaus et al., 2014).

To advance our understanding of reactive solute transport (RT) of pesticides, particularly the joint controls of macropores, sorption, and degradation, a combination of predictive models and plot-scale experiments is often used (e.g. Zehe et al., 2001; Šimůnek et al., 2008; Radcliffe and Simunek, 2010; Klaus and Zehe, 2011; Klaus et al., 2013). Such methods allow for the assessment of the environmental risks arising from the wide use of reactive substances (Pimentel et al., 1992; Carter, 2000; Gill and Garg, 2014; Liess et al., 1999). Combining the Richards and advection–dispersion equations is one common approach used to simulate water flow dynamics and (reactive) solute transport in the partially saturated soil zone. This approach has been implemented, for example, in the well-established models HYDRUS (Gerke and Genuchten, 1993; Šimůnek et al., 2008), MACRO (Jarvis and Larsbo, 2012), and Zin AgriTra (Gassmann et al., 2013). However, this approach has well-known deficiencies in simulating preferential macropore flow and imperfect mixing with the matrix in the vadose zone (Beven and Germann, 2013). As both processes essentially control environmental risk due to transport of reactive substances, a range of adaptations has been proposed to improve this deficiency (Šimůnek et al., 2003). One frequently used adaptation is the dual-domain concept, which describes matrix and macropore flow in separated, exchanging continua to account for local disequilibrium conditions (Gerke, 2006). However, studies show that even these dual-domain models can be insufficient to quantify preferential solute breakthrough into the subsoil (Sternagel et al., 2019) or into tile drains (Haws et al., 2005; Köhne et al., 2009a,b). A different approach is to represent macropores as spatially connected, highly permeable flow paths in the same domain as the soil matrix (Sander and Gerke, 2009). This concept has been shown to operate well for preferential flow of water and bromide tracers at a forested hillslope (Wienhöfer and Zehe, 2014) and for bromide and Isoproturon transport through worm burrows

into a tile drain at a field site (Klaus and Zehe, 2011). Nevertheless, this approach is based on the Richards equation and is thus limited to laminar flow conditions with sufficiently small flow velocities corresponding to a Reynolds number smaller than 10 (e.g. Bear, 2013; Loritz et al., 2017).

Particle-based approaches offer a promising alternative to simulate reactive transport. These approaches work with a Lagrangian perspective on the movement of solute particles in a flow field, rather than by solving the advection–dispersion equation directly. They have been particularly effective in quantifying solute transport alone, while the movement of the fluid carrying solutes is still usually integrated in systems based on Eulerian control volumes (e.g. Delay and Bodin, 2001; Zehe et al., 2001; Berkowitz et al., 2006; Koutsoyiannis, 2010; Klaus and Zehe, 2010; Wienhöfer and Zehe, 2014). In the context of saturated flow in fractured and heterogeneous aquifers, Lagrangian descriptions of fluid flow are already commonly and successfully applied. For example, the continuous-time random walk (CTRW) approach accounts for non-Fickian transport of tracer particles within the water flow through heterogeneous, geological formations via different flow paths with an associated distribution of velocities and thus travel times (Berkowitz et al., 2006, 2016; Hansen and Berkowitz, 2020). However, Lagrangian modelling of fluid flow in the vadose zone is more challenging due to the dependence of the velocity field on the temporally changing soil moisture states and boundary conditions. This explains why only a relatively small number of models use Lagrangian approaches for solute transport and also for water particles (also called water “parcels”) to characterize the fluid phase itself (e.g. Ewen, 1996a,b; Bücken-Gittel et al., 2003; Davies and Beven, 2012; Zehe and Jackisch, 2016; Jackisch and Zehe, 2018). Sternagel et al. (2019) proposed that these water particles may optionally carry variable solute masses to simulate non-reactive transport. Their Lagrangian Soil Water and Solute Transport Model (LAST) combines the assets of the Lagrangian approach with an Euler grid to simulate fluid motion and solute transport in heterogeneous, partially saturated 1-D soil domains. It allows discrete water particles to travel at different velocities and carry temporally variable solute masses through the subsurface domain. The soil domain is subdivided into a soil matrix and a structurally defined preferential flow/macropore domain (cf. Sect. 3.2). A comparison of HYDRUS 1-D and the LAST-Model based on plot-scale tracer experiments showed that both models perform similarly in the case of matrix-flow-dominated tracer transport; however, under preferential flow conditions, LAST better matched observed tracer profiles, indicating preferential flow (Sternagel et al., 2019).

While the results of Sternagel et al. (2019) demonstrate the feasi-

bility of the Lagrangian approach to simulate conservative tracer transport, even under preferential flow conditions during 1 d simulations, a generalization of the Lagrangian approach to reactive solute transport and larger timescales is still missing. The main objectives of this study are thus as follows:

1. We develop a method for reactive transport, i.e. the sorption and degradation of solutes within the Lagrangian framework under well-mixed and preferential flow conditions, and implement this into the LAST-Model. We initially test the feasibility of the method by simulating plot-scale experiments with a bromide tracer and the herbicide Isoproturon (IPU) during 2 d (Zehe and Flühler, 2001a) and use corresponding simulations of the commonly applied model HYDRUS 1-D as a benchmark.
2. We perform plot-scale simulations to explore the transport behaviour of bromide and IPU with the Lagrangian approach over 7 and 21 d to evaluate its performance on longer timescales. For this purpose, we make use of data from another plot-scale irrigation experiment (Klaus et al., 2014).
3. We conduct simulations of breakthrough experiments with Flufenacet (FLU) on a tile-drain field site over a period of 3 weeks (Klaus et al., 2014), to examine the breakthrough behaviour and remobilization of reactive substances.

3.2 THE LAST-MODEL: CONCEPT, THEORETICAL BACKGROUND, AND NUMERICAL IMPLEMENTATION

3.2.1 *Model concept*

The LAST-Model combines a Lagrangian approach with an Euler grid to simulate fluid motion and solute transport in heterogeneous, partially saturated 1-D soil domains. Discrete water particles with a constant water mass and volume carry temporally variable information about their position and solute concentrations through defined domains for soil matrix and macropores that are subdivided into vertical grid elements (Euler grid). Prior to simulation, the initial water content of each grid element is converted to a corresponding water mass with the grid element volume and water density. The water mass of each grid element is summed to a total water mass in the entire soil domain and then divided by the total number of particles. In this way, the water particles in the soil domain are initially defined by a certain water mass. During the simulation, the number of water particles is counted in each time step, and a new particle density per grid element is computed. By multiplying this water particle density with the particle mass and water density, a new soil water content per grid element and time step can be obtained (Zehe and Jackisch, 2016). Different fractions of the water particles in a grid element correspond to the sub-scale distribution of the water content among soil pores of different sizes. Consequently, different water particle fractions travel at different velocities (cf. Fig. 3.1). Their displacements are determined by the hydraulic conductivity and water diffusivity in combination with a spatial random walk (cf. Sect. 3.2.2, Eq. 3.5). This approach accounts for the joint effects of gravity and capillary forces on water flow in partially saturated soils. The use of an Euler grid allows for the necessary updating of soil water contents based on changing particle densities and related time-dependent changes in the velocity field. The space domain approach also reflects the fact that spatial concentration patterns and thus travel distances are usually observed in the partially saturated zone. The Euler grid is hence necessary to calculate spatial concentration profiles and to properly describe specific interactions between the matrix and the macropore domain.

3.2.2 *Underlying theory and model equations*

3.2.2.1 *Transient fluid flow in the partially saturated zone*

The LAST-Model (Sternagel et al., 2019) is based on the Lagrangian approach of Zehe and Jackisch (2016), which was introduced to simulate infiltration and soil water dynamics in the partially saturated zone using a non-linear random walk in the space domain. The results

of test simulations confirmed the ability of the Lagrangian approach to simulate water dynamics under well-mixed conditions in different soils, in good accord with simulations using a Richards equation solver. We refer the reader to the study of Zehe and Jackisch (2016) for further details on the model concept.

Derivation of particle displacement equation

Our starting point is the soil-moisture-based form of the Richards equation:

$$\frac{\delta\theta}{\delta t} = \frac{\delta K(\theta)}{\delta z} + \frac{\delta}{\delta z} \left(D(\theta) \cdot \frac{\delta\theta}{\delta z} \right) \quad (3.1)$$

with $D(\theta) = K(\theta) \cdot \frac{\delta\psi}{\delta\theta}$.

By multiplying the hydraulic conductivity K in the first term of Eq. 3.1 by $\frac{\theta}{\theta}$ ($= 1$), we obtain

$$\frac{\delta\theta}{\delta t} = \frac{\delta}{\delta z} \left[\frac{K(\theta)}{\theta} \cdot \theta \right] + \frac{\delta}{\delta z} \left(D(\theta) \cdot \frac{\delta\theta}{\delta z} \right). \quad (3.2)$$

Rewriting this equation leads to the divergence-based form of the Richards equation:

$$\frac{\delta\theta}{\delta t} = \frac{\delta}{\delta z} \left[\frac{K(\theta)}{\theta} - \frac{\delta D(\theta)}{\delta z} \cdot \theta \right] + \frac{\delta^2}{\delta z^2} (D(\theta) \cdot \theta), \quad (3.3)$$

where z is the vertical position (positively upward) in the soil domain (m), K the hydraulic conductivity ($m s^{-1}$), D the water diffusivity ($m^2 s^{-1}$), ψ the matric potential (m), $\theta(t)$ the soil water content ($m^3 m^{-3}$), and t the simulation time (s).

Eq. 3.3 is formally equivalent to the Fokker–Planck equation (Risken, 1984). The first term of the equation corresponds to a drift/advection term characterizing the advective downward velocity v ($m s^{-1}$) of fluid fluxes driven by gravity:

$$-v(\theta) = \frac{K(\theta)}{\theta} - \frac{\delta D(\theta)}{\delta z}. \quad (3.4)$$

The second term of Eq. 3.3 represents diffusive fluxes driven by the soil moisture or matric potential gradient and controlled by diffusivity $D(\theta)$ (cf. Eq. 3.1). Eq. 3.3 can then be solved by a non-linear random walk of volumetric water particles (Zehe and Jackisch, 2016). The non-linearity arises due to the dependence of K and D on soil moisture and

hence the particle density. The vertical displacement of water particles is described by the Langevin equation:

$$z_i(t + \Delta t) = z_i(t) - \left(\frac{K(\theta_r + i \cdot \Delta\theta)}{\theta(t)} + \frac{\delta D(\theta_r + i \cdot \Delta\theta)}{\delta z} \right) \cdot \Delta t + Z \sqrt{2 \cdot D(\theta_r + i \cdot \Delta\theta) \cdot \Delta t}, \quad (3.5)$$

$$i = 1, \dots, N_B,$$

where the second term describes downward advection/drift of water particles driven by gravity on the basis of the hydraulic conductivity K ($m s^{-1}$). The term $\frac{\delta D(\theta_r + i \cdot \Delta\theta)}{\delta z}$ corrects this drift term for the case of spatially variable diffusion and is hence added as upward velocity, contrary to the downward drift term (Roth and Hammel, 1996). The third term of Eq. 3.5 describes diffusive displacement of water particles determined by the soil moisture gradient and controlled by diffusivity $D(\theta)$ ($m^2 s^{-1}$) in combination with the random walk concept. Here, the expression $(\theta_r + i \cdot \Delta\theta)$ represents the aforementioned fraction of the actual soil water content $\theta(t)$ (cf. Sect. 3.2.1) that is stored in a certain pore size of the soil domain. Note that i is the number of a bin of N_B total bins representing the certain pore size in which the particle is stored, θ_r the residual soil moisture, $\Delta\theta$ the size/water content range of a bin, and Z a random number from a standard normal distribution.

Model assumptions

The above-described distribution of water particle displacements to different pore sizes/bins (“binning”) was the key to simulating soil water dynamics in the case of pure matrix flow, in agreement with the Richards equation and field observations (Zehe and Jackisch, 2016). This binning of particle displacements is defined by the water diffusivity and hydraulic conductivity curve. These curves are separated into N_B bins, using a step size of $\Delta\theta = \frac{\theta(t) - \theta_r}{N_B}$ from the residual moisture θ_r to the actual moisture $\theta(t)$ (Fig. 3.1). Zehe and Jackisch (2016) found that 800 bins are sufficient to resolve both curves. This particle binning concept enables also the simulation of non-equilibrium conditions in the water infiltration process. To that end, a second type of particles (event particles) is introduced to treat infiltrating event water. These particles initially travel, purely by gravity, in the largest pores and experience a slow mixing with pre-event particles in the soil matrix during a characteristic mixing time. This nonequilibrium flow in the matrix is laminar, as Eq. 3.5 is based on the theory of the Richards equation (Eq. 3.1). An adaptive time stepping is used to fulfil the Courant criterion to ensure that particles do not travel farther than the length of a grid element dz in a time step.

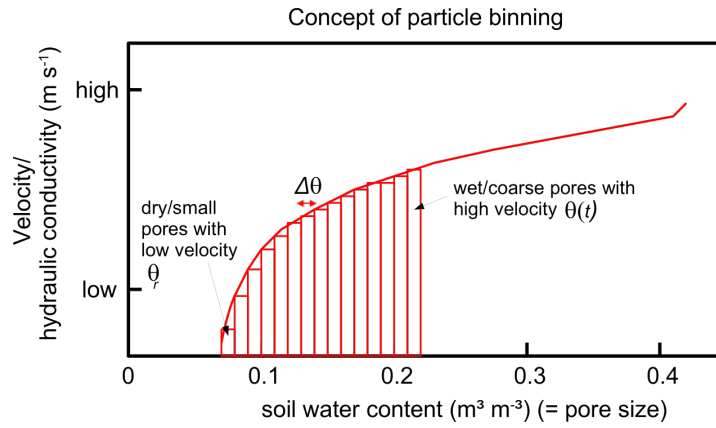


Figure 3.1: Particle binning concept. All particles within an element of the Euler grid are distributed to bins (i.e. red rectangles) representing fractions of the actual soil water content stored in different pore sizes. Displacements of these particle fractions are determined by the corresponding flow velocities and diffusivities (figure taken from Sternagel et al., 2019).

3.2.2.2 Transport of conservative solutes and the macropore domain

In our previous work (Sternagel et al., 2019), we extended the scope of the Lagrangian approach (i) to account for simulations of water and solute transport in soils as well as (ii) by a structural macropore/preferential flow domain and included both extensions in the LAST-Model. We tested this extended approach using bromide tracer and macropore data of plot-scale irrigation experiments at four study sites and compared it to simulations of HYDRUS 1-D. At two sites dominated by well-mixed matrix flow, both models showed equal performance, but at two preferential-flow-dominated sites, LAST performed better. We refer to Sternagel et al. (2019) for additional details on the model and results.

Solute transport

Each water particle is characterized by its position in the soil domain, water mass, and a solute concentration. This means that there is no second species of particles representing solutes. Each water particle is tagged by a solute mass that is defined by the product of solute concentration and water particle volume. Hence, we do not use a separate, specific equation for the transport of solutes in LAST. Solutes are displaced together with the water particles according to the varying particle displacements defined by Eq. 3.5. Subsequent to the displacement, diffusive mixing and redistribution of solutes among all water particles in an element of the Euler grid is calculated by summing their solute masses and dividing this total mass amount by the number of water particles present. Due to this perfect solute mixing process, the solute mass carried by a water particle may vary in space and time. In

this context, it is important to recall that the use of an Euler grid to calculate soil water contents and solute concentrations in Lagrangian models may lead to the problem of artificial over-mixing (e.g. Boso et al., 2013; Cui et al., 2014; Berkowitz et al., 2016). This is because water and solutes are assumed to mix perfectly within the elements of the Euler grid, which may lead to a smoothing of gradients in the case of coarse grid sizes. This might lead to overestimates of concentration dilution while solutes infiltrate into and distribute within the soil domain (Green et al., 2002, cf. Sect. 3.6.2).

Macropore domain

LAST offers a structured preferential flow domain consisting of a certain number of macropores (Fig. 3.2a). Macropores are classified into the three depth classes – deep, medium, or shallow – to reflect the corresponding variations of macropore depths observed at a study site. With this approach, we may account for a depth-dependent exchange of water and solutes between the matrix and macropore domains. The parameterization of the preferential flow domain may hence largely rely on observable field data, such as the number of macropores of certain diameters, their length distribution, and hydraulic properties. When such field observations are not available, the parameters can be estimated by inverse modelling using tracer data. The actual water content and the flux densities of the topsoil control infiltration and distribution of water particles to both domains. The soil water content determines the matric potential and hydraulic conductivity of the soil matrix, while flow in macropores is controlled by friction and gravity. After the infiltration, macropores gradually fill from the bottom to the top by assuming purely gravity-driven, advective flow in the macropore domain (Fig. 3.2b). Interactions among macropores and the matrix are represented by diffusive mixing and exchange of water and solutes between both flow domains, which depends also on the matric potential and water content (Fig. 3.2c).

We provide a detailed description of Fig. 3.2 with the structure of the macropore domain and the infiltration and filling of macropores, as well as exchange processes between macropores and the matrix, in the Appendix A.2.

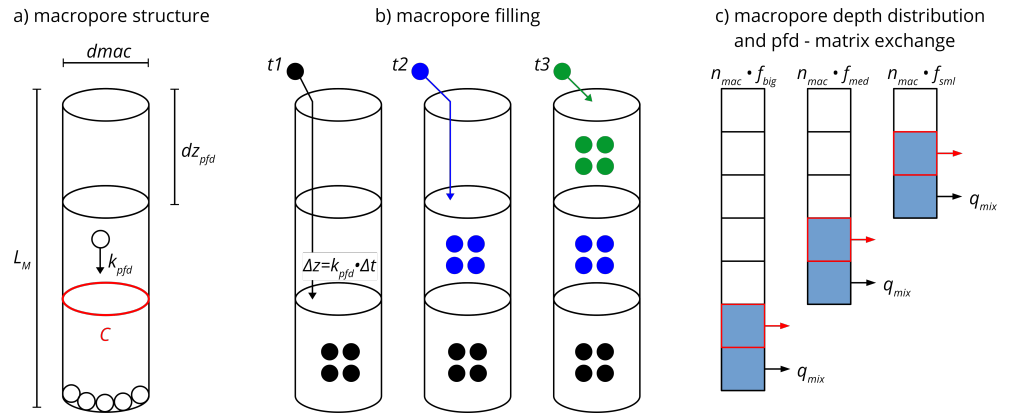


Figure 3.2: Conceptual visualization of (a) the structure of a single macro pore, (b) the macro pore filling with gradual saturation of grid elements, exemplarily shown for three points in time ($t_1 - t_3$), whereby at each time new particles (differently coloured related to the current time) infiltrate the macro pore and travel into the deepest unsaturated grid element, and (c) the macro pore depth distribution and diffusive mixing of water from saturated parts of macropores (blue filled squares) into the matrix (cf. Sect. 3.2.2.2). The figure was adapted from Sternagel et al. (2019).

3.3 CONCEPT AND IMPLEMENTATION OF REACTIVE SOLUTE TRANSPORT INTO THE LAST-MODEL

The main objective of this study is to present a method to simulate fluid flow with reactive solute transport in structured, partially saturated soils, using a Lagrangian perspective. The method is illustrated through the implementation of a routine into the LAST-Model, to simulate the movement of reactive substances through the soil zone under the influence of sorption and degradation processes (Fig. 3.3). This is achieved by assigning an additional reactive solute concentration C_{rs} (kg m^{-3}) to each water particle. A water particle can hence carry a reactive solute mass m_{rs} (kg), which is equal to the product of reactive solute concentration and its water volume. Transport and mixing of the reactive solute masses within a time step are simulated in the same way as for the conservative solute (cf. Sect. 3.2.2.2) (Sternagel et al., 2019). After the solute mixing and mass redistribution among water particles, the reactive solute mass of each particle can change due to a non-linear mass transfer (adsorption, desorption) between water particles and the sorption sites of the adsorbing solid phase, which are determined by the substance-specific and site-specific Freundlich isotherms (cf. Sect. 3.3.1). The adsorbed reactive solute mass in the soil solid phase can then be reduced by degradation following first-order kinetics driven by the half-life of the substance (cf. Sect. 3.3.2). These two reactive solute processes take place in the soil matrix as well as in the wetted parts of the macropores, and their intensity can vary with soil depth as detailed in the following sections.

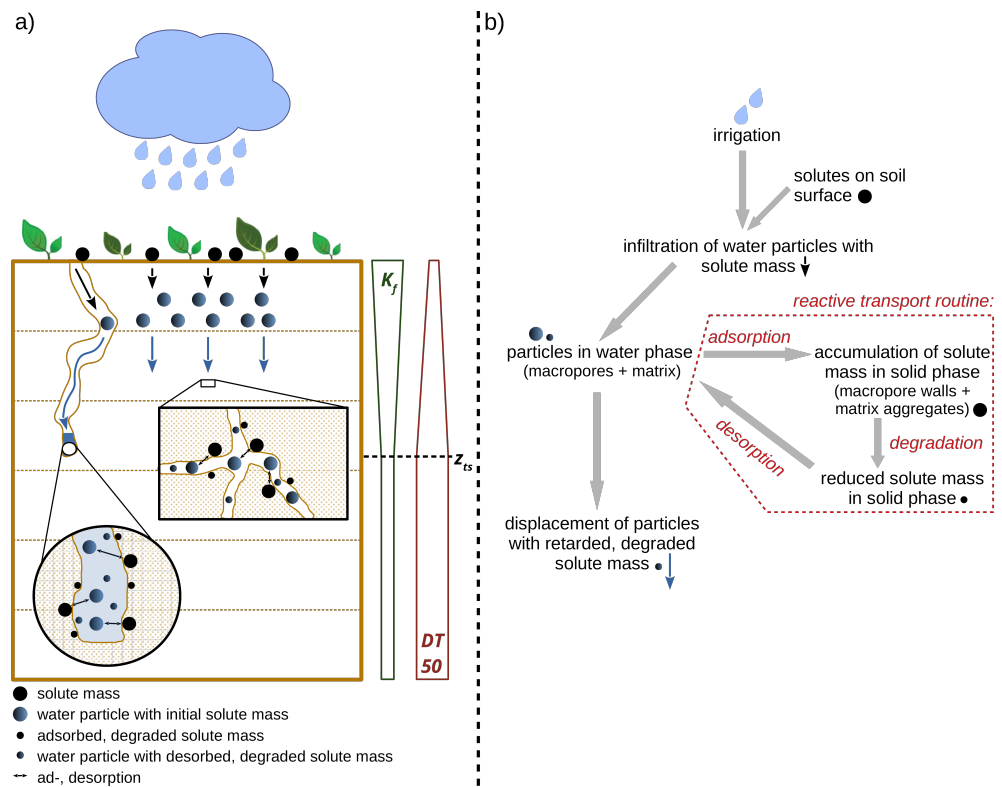


Figure 3.3: (a) Overview sketch of sorption and degradation processes in the soil domain. Down to the predefined depth z_{ts} (m), we assume the topsoil with linearly decreasing K_f and linearly increasing DT_{50} values to account for the depth dependence of sorption and degradation, respectively. Below z_{ts} in the subsoil, we assume constant values. (b) Flow chart to illustrate the sequence of reactive solute transport. The pictograms of the sketch are assigned to the respective positions and steps of the flow chart.

3.3.1 Retardation of solute transport via non-linear sorption between water and solid phase

3.3.1.1 Implementation of retardation

The interplay of adsorption and desorption characterizes the retardation process and implies that the transport velocity of a reactive solute is smaller than the fluid velocity. This is commonly represented by reducing the solute transport velocity by a retardation factor. This retardation factor describes the ratio between the fluid velocity and the solute transport velocity based on the slope of a sorption isotherm. However, this concept is not applicable in our framework because solute masses are carried by the water particles and travel hence at the same velocity as water. We thus explicitly represent sorption processes by a related, explicit transfer of solute masses between the water and soil solid phase. The mass exchange rates are variable in time, as the solute concentrations in the water and solid phase also vary between time steps. In each time step, the solute mass exchange between both phases is calculated by using the non-linear Freundlich isotherms of the respective solute and rate equations (Eq. 3.6 for adsorption, Eq. 3.7 for desorption).

$$m_{rs}(t) = m_{rs}(t - \Delta t) - \left(K_f \cdot C_{rs}^{beta} \right) \left(\frac{m_p}{\rho} \right), \quad (3.6)$$

where m_{rs} (kg) is the reactive solute mass of a particle, $K_f \left(\left[\frac{kg}{kg} \right]^{\frac{1}{beta}} \right)$ the Freundlich coefficient/constant, C_{rs} ($kg\ m^{-3}$) the reactive solute concentration of a particle, $beta$ (-) the Freundlich exponent, m_p (kg) the water mass of a particle, ρ ($kg\ m^{-3}$) the water density, t (s) the current simulation time, and Δt (s) the time step. Note that K_f and $beta$ are both empirical constants that determine the shape and slope of the sorption isotherm of a respective substance. Both are often described as dimensionless coefficients, but K_f can actually adopt different forms to balance the units of the equation, particularly when $beta$ is not equal to 1.

The reversed desorption of adsorbed solutes from the soil solid phase to the water particles, in the case of a reversed solute concentration gradient between water and solid phase, is equally calculated (Eq. 3.7). It uses the solute concentration in the sorbing solid phase $C_{rs,solid}$ ($kg\ m^{-3}$), which requires the adsorbed solute mass and the volume of the phase V_{soil} (m^3). In this way, the total desorbed solute mass is calculated for an entire grid element and must be divided by the present particle number N_p (-) to equally distribute the desorbed solute mass among the water particles. The sorption process is hence controlled by a local concentration gradient between water and the

solid phase within an element of the Euler grid.

$$m_{rs}(t) = m_{rs}(t - \Delta t) + \frac{\left(K_f \cdot C_{rs, solid}^{beta}\right) \cdot V_{soil}}{N_p} \quad (3.7)$$

3.3.1.2 Assumptions for the parameterization of the sorption process

Generally, sorption is a non-linear process, which reflects the limited availability of adsorption sites and, hence, exchange rate limitations. This may cause imperfect sorption, which can lead to the observation of early mass arrivals and longtailings in breakthrough curves (e.g. Leistra, 1977). Thus, our approach calculates the non-linear adsorption or desorption of solute masses, as a function of the solute concentration or loading of the sorption surfaces of the sorbent. Hence, in a given time step, the higher the solute concentration in the solid phase, the fewer the solute masses that can be additionally adsorbed from the water phase, and vice versa. In the approach developed here, the sorption process proceeds only until a concentration equilibrium between both phases is reached. At this point, there is no further adsorption or desorption of solute masses until the concentration of one phase is again disequilibrated by, for example, the infiltration of water into the water phase or by solute degradation in the solid phase. In the case that the concentration of a reactive solute in the water phase is higher than its solubility, the excess solute masses leave the solution and are adsorbed to the soil solid phase.

With regard to pesticides, the major pesticide sorbent is soil organic matter, and its quantity and quality determine to a large fraction the soil sorption properties (Farenhorst, 2006; Sarkar et al., 2020). Several studies revealed that in the topsoil, enhanced sorption of pesticides occurs due to the often high content of organic matter, which may reflect bioavailability by an increased number of sorption sites in the non-mineralized organic matter (e.g. Clay and Koskinen, 2002; Jensen et al., 2004; Boivin et al., 2005; Rodríguez-Cruz et al., 2006). This implies that the conditions in the topsoil generally facilitate the sorption of dissolved solutes. While different depth profiles of the K_f value could be implemented depending on available data, to account for this depth dependence of sorption processes, here we apply a linearly decreasing distribution of the K_f value over the grid elements of the soil domain between two predefined upper and lower value limits for the topsoil. The depth of the topsoil (z_{ts}) can be adjusted individually and for our applications; here, we set it to 50 cm. Below this soil depth, we assume the subsoil and apply constant K_f values. The exact K_f parameterizations of the respective model setups at the different sites are explained in Sect. 3.4.2.1 and 3.4.2.2 and summarized in Tab. 3.2.

Sorption in macropores

While sorption generally controls pesticide leaching in the soil matrix, the processes are different in macropores. Sorption in macropores is often limited because the timescale of vertical advection is usually much smaller than the time required by solute molecules to diffuse to the macropore walls (Klaus et al., 2014). However, sorption may occur to a significant degree once water is stagnant in the saturated parts of the macropores (Bolduan and Zehe, 2006). This stagnancy facilitates the possibility for sorption of reactive solutes between macropore water and the macropore walls. The macropore sorption processes are also described and quantified by the Freundlich approach and Eq. 3.6.

3.3.2 *First-order degradation of adsorbed solutes in soil solid phase*

3.3.2.1 *Implementation of degradation*

Reactive solutes such as pesticides are commonly biodegraded and therewith transformed into metabolite/child compounds by the metabolism or co-metabolism of microbial communities that are present mainly on the surfaces of soil particles. The immobilization of a reactive substance, due to adsorption, favours degradation when the residence time in the adsorbing solid phase is sufficiently long for metabolization. Many pesticides are subject to co-metabolic degradation, which often follows first-order kinetics and can hence be characterized by an exponential decay function

$$C_t = C_0 \cdot e^{-kt}, \quad (3.8)$$

where C_t ($kg\ m^{-3}$) is the concentration of the pesticide after the time t (s), C_0 ($kg\ m^{-3}$) the initial concentration, and k (s^{-1}) the degradation rate constant.

Based on the first-order kinetics of Eq. 3.8, we apply a mass rate equation (Eq. 3.9) for the degradation of adsorbed solute masses on the macroscopic scale of an element of the Euler grid:

$$m_{sp}(t + \Delta t) = m_{sp}(t) \cdot \left(1 - \left(k_d \cdot \frac{\Delta t}{86,400} \right) \right), \quad (3.9)$$

where $m_{sp}(t)$ and $m_{sp}(t + \Delta t)$ (kg) are the reactive solute masses in the soil solid phase of the current time step and of the next time step after degradation and Δt (s) the time step. The kinetics of this degradation process are determined by the half-life DT₅₀ (d) of the respective substance, with the relationship between DT₅₀ and a daily

degradation k_d (d^{-1}) given by

$$k_d = \frac{\ln(2)}{DT50}. \quad (3.10)$$

3.3.2.2 Assumptions for the parameterization of the degradation process

Turnover and degradation of pesticides depend in general on the substance-specific chemical properties and the microbial activity in soils (Holden and Fierer, 2005). Microbial activity in soil depends on many factors, including organic matter content, pH, water content, temperature, redox potential, and carbon / nitrogen ratio. As these factors are usually highly heterogeneous in space, considerable research has focused on spatial differences in pesticide turnover potentials. Some of these studies determined that pesticide turnover rates typically decrease within the top metre of the soil matrix (e.g. El-Sebai et al., 2005; Bolduan and Zehe, 2006; Eilers et al., 2012). This is because the topsoil provides conditions that facilitate enhanced microbial activity (Fomsgaard, 1995; Bending et al., 2001; Bending and Rodriguez-Cruz, 2007). The simplest way to account for such a depth-dependent degradation is a linear increase of the DT50 value from the topsoil surface to a predefined depth z_{ts} , which is set to 50 cm. This value is in line with the assumption of the depth-dependent K_f parameter and was estimated based on the findings of the aforementioned studies. In the subsoil below 50 cm, we apply constant DT50 values (cf. Sect. 3.3.1). The exact DT50 parameterizations of the respective model setups at the different sites are explained in Sect. 3.4.2.1 and 3.4.2.2 and summarized in Tab. 3.2.

Degradation in macropores

The presence of macropores allows pesticides to bypass the topsoil matrix, while they may infiltrate and thus be more persistent in the deeper subsoil matrix where the turnover potential is decreased. As biopores like worm burrows often constitute the major part of macropores in agricultural soils, a number of studies have focused on their key role in pesticide transformation (e.g. Binet et al., 2006; Liu et al., 2010; Tang et al., 2012). These studies consistently revealed an elevated bacterial abundance and activity in the immediate vicinity of worm burrows (Bundt et al., 2001; Bolduan and Zehe, 2006), comparable to the optimum conditions in topsoil. This is attributed to a positive effect of enhanced organic carbon, nutrient, and oxygen supply that may lead to increased adsorption and degradation rates in macropores. Thus, we assume that degradation also takes place in the adsorbing phase of the macropores, which can be quantified with Eq. 3.9. We apply different K_f and DT50 values in the macropores that are in the range of the topsoil values (cf. Tab. 3.2).

3.4 MODEL APPLICATION TESTS

The proposed method to simulate reactive solute transport in a Lagrangian approach is tested by using LAST to simulate irrigation experiments with conservative bromide tracer and the herbicide IPU as a representative reactive substance, at two study sites in the Weiherbach catchment (Zehe and Flühler, 2001a). Here, conservative means that a solute is neither subject to sorption nor to degradation. These two sites are dominated by either matrix flow under well-mixed conditions (site 5) or preferential macropore flow (site 10) on a timescale of 2 d. These experiments are also simulated with the HYDRUS 1-D model. To test the method on simulation periods longer than 2 d, we use data from an additional plot-scale (site P4) irrigation experiment (Klaus et al., 2014) on timescales of 7 and 21 d. Finally, we evaluate the method by simulating the breakthrough and remobilization of the herbicide Flufenacet that was observed in the tile drain of a field site within two irrigation phases: 1 d and 3 weeks after substance application.

3.4.1 Characterization of the irrigation experiments

3.4.1.1 Study area: the Weiherbach catchment

The Weiherbach valley extends over a total area of 6.3 km^2 and is located in the southwest of Germany. The land is used mainly for agriculture. The basic geological formation of the valley is characterized by a Pleistocene loess layer up to 15 m thick, which covers Triassic Muschelkalk marl and Keuper sandstone. At the foot of hills, the hillslopes show a typical loess catena with erosion-derived Colluvic Regosols, while at the top and in the middle parts of hills, mainly Calcaric Regosols or Luvisols are present. More detailed information on the Weiherbach catchment is provided in Plate and Zehe (2008).

3.4.1.2 Pesticides Isoproturon (IPU) and Flufenacet (FLU)

IPU is an herbicide which is commonly applied in crops to control annual grasses and weeds. IPU has a moderate water solubility of 70.2 mg L^{-1} and is regarded as non-persistent (mean DT₅₀ in field: 23 d) and moderately mobile (mean $K_f = 2.83$) in soils (see also typical K_f and DT₅₀ value ranges in Tab. 3.2). IPU is ranked as carcinogenic, and its turnover in soils forms, mainly, the metabolite desmethylisoproturon (Lewis et al., 2016).

FLU is an herbicide that can be applied for a broad spectrum of purposes but is used especially in combination with other herbicides to control grasses and broad-leaved weeds. FLU is regarded as moderately soluble (51 mg L^{-1}) and is not highly volatile (mean $K_f = 4.38$) but may be quite persistent in soils (up to DT₅₀ in field: 68 d) under

certain conditions. FLU is classified as moderately toxic to humans, and its turnover in soils mainly forms the metabolites FOE sulfonic acid, FOE oxalate, and FOE alcohol (Lewis et al., 2016).

3.4.1.3 Plot-scale experiments of Zehe and Flühler (2001a) at the well-mixed site (site 5) and the preferential-flow-dominated site (site 10)

At site 5, the soil moisture and soil properties were initially measured on a defined plot area of 1.4 m × 1.4 m. Before the irrigation, 0.5 g of IPU was applied, distributed evenly, on the surface of the plot area. After 1 d, the IPU loaded plot area was irrigated by a rainfall event of 10 mm h⁻¹ of water for 130 min with 0.165 g L⁻¹ of bromide. After another day, soil samples were taken along a vertical soil profile of 1 m × 1 m in a grid of 0.1 m × 0.1 m. Thus, 10 soil samples were collected in each 10 cm depth interval down to a total depth of 1 m. In subsequent lab analyses, the IPU and bromide concentrations of all samples were measured. The soil at site 5 is a Calcaric Regosol (WRB, 2014), and flow patterns reveal a dominance of well-mixed matrix flow without considerable influence of macropore flows. This is the reason for using site 5 to evaluate our reactive solute transport approach under well-mixed flow conditions. Tab. 3.1 provides all experimental data.

The experiment at site 10 was conducted similarly with the initial application of 1.0 g of IPU on the soil plot and 1 d later a block rainfall of 11 mm h⁻¹ for 138 min. The soil at site 10 can be classified as Colluvic Regosol (WRB, 2014) and shows numerous worm burrows that can facilitate preferential flow. Hence, we select study site 10 for the evaluation of our reactive solute transport approach during preferential flow conditions. The density and depth of the worm burrow systems were examined extensively at this study site. Horizontal layers in different depths of the vertical soil profile were excavated (cf. Zehe and Blöschl, 2004; van Schaik et al., 2013), and in each layer the number of macropores was counted, and their diameters and depths were measured. These detailed measurements provided an extensive dataset of the macropore network. Tab. 3.1 again contains all experimental data.

3.4.1.4 Plot- and field-scale experiments of Klaus et al. (2014)

Klaus et al. (2014) conducted irrigation experiments in the Weiherbach catchment to corroborate the importance of macropore connectivity to tile drains for tracer and pesticide leaching into surface waters. A series of three irrigation experiments with bromide tracer, IPU, and FLU were performed on a 20 m × 20 m field site, which also included the sampling of these substances in different plot-scale soil profiles. We focus first on the plot-scale experiment in which the field site was

irrigated in three individual blocks with a total precipitation sum of 34 mm over 220 min. Additionally, a total of 1600 g of bromide was applied on the field site. We concentrate on site P₄ where soil samples were collected in a 0.1 m × 0.1 m grid down to a depth of 1 m after 7 d and their corresponding bromide concentrations measured. Patterns of worm burrows in the first 15 cm of the soil were also examined (Tab. 3.3). The present soil is a Colluvisol (WRB, 2014), with a strong gleyic horizon present in a depth between 0.4 and 0.7 m, which causes a decreasing soil hydraulic conductivity gradient with depth that leads to almost stagnant flow conditions in the subsoil (Klaus et al., 2013). In general, the experiment design, soil sampling, and data collection are similar to the experiments of (Zehe and Flühler, 2001a). Initial soil water contents and all further experiment parameters as well as the soil properties at the field site are listed in Tab. 3.3.

Second, we focus on two other irrigation experiments of Klaus et al. (2014) on the field scale in which FLU concentrations were measured at the outlet of a tile-drain tube. The tube drained the entire field site and was located 1 – 1.2 m below the surface. Before irrigation, a total of 40 g FLU was applied on the surface of the 400 m² field site. In a first irrigation phase, the field site was irrigated in three individual blocks with a total precipitation of 41 mm over 215 min, and simultaneously, water samples were taken at the outlet of the tile-drain tube. These samples were analysed for FLU as explained in Klaus et al. (2014). After a period of 3 weeks, in which the field site remained untouched without further irrigation and FLU application, the field site was then again irrigated in two individual blocks with a total precipitation of 40 mm over 180 min and the FLU concentration in the tile-drain outflow measured. The objective was to examine the breakthrough of remobilized FLU that was previously adsorbed in soil.

The soil of the field site is again a Colluvisol (WRB, 2014). Overall, the soil exhibits two ploughed layers between 0–10 and 10–35 cm above a third, unaffected Colluvisol layer (Klaus and Zehe, 2010). Klaus and Zehe (2010) also found that 10 macropores/m² reaching into the depths of the tile-drain tube is a good estimate for simulations at this study site. Initial soil water contents and all further experimental parameters are listed in Tab. 3.4.

3.4.2 Model setups

To compare our 1-D simulation results to the observed 2-D concentration data of the plot-scale experiments, the latter are averaged laterally in each of the 10 cm depth intervals. Note that the corresponding observations provide solute concentration per dry mass of the soil, while the LAST-Model simulates concentrations in the water phase and

adsorbed solute masses in the soil solid phase, respectively. We thus compare simulated and observed solute masses and not concentrations in the respective depths. Note that the experimental parameters in Tab. 3.1, 3.3, 3.4 are measured data from the above-described experiments and can be used directly to parameterize the LAST-Model without fitting. In Sternagel et al. (2019), we explain in detail how the observed data are processed, particularly for the macropore domain, and explain the model sensitivity to the uncertainty range of observed data (e.g. to the saturated hydraulic conductivity).

3.4.2.1 Model setups of simulations at the well-mixed plot site (site 5)

LAST-Model setup at the well-mixed site (site 5)

As site 5 is dominated by well-mixed matrix flow, we deactivate the macropore domain of LAST and simulate IPU and bromide transport solely in the matrix domain at this site. Without the influence of macropores, we assume here only small penetration depths of solutes through the first top centimetres of the soil, in line with previous simulations at other well-mixed sites in the Weiherbach catchment (Sternagel et al., 2019). This means that solutes may remain in the upper part of the topsoil, so that a depth-dependent parameterization of sorption and degradation (cf. Sect. 3.3.1, 3.3.2) appears, as a first guess, not necessary at this site. Thus, we apply constant values of K_f and DT50 (Tab. 3.2) and use mean values under field conditions for IPU from the Pesticide Properties Database (PPDB) (Lewis et al., 2016). Consistent with the experiments, we use a matrix discretization of 0.1 m. Initially, the soil domain contains 2 million water particles but no solute masses. All further experiment and simulation parameters are shown in Tab. 3.1.

HYDRUS 1-D setup at the well-mixed site (site 5)

The simulation with HYDRUS 1-D at the well-mixed site (site 5) is conducted with a single porosity model (van Genuchten–Mualem) and an equilibrium model for water flow and solute transport, respectively, with the Freundlich approach for sorption and first-order degradation. At the upper domain boundary, we select atmospheric conditions with a surface layer and variable infiltration intensities. At the lower boundary, we assume free drainage conditions. In general, we use the same soil hydraulic properties, model setups, initial conditions, and reactive transport parameters as for LAST (cf. Tab. 3.1, 3.2).

3.4.2.2 Model setups of simulations at the preferential-flow-dominated plot site (site 10)

LAST-Model setup for simulations at the preferential-flow-dominated site (site 10)

We use an available, extensive macropore dataset to parameterize the macropore domain at site 10. Tab. 3.1 provides the depth distribution of the macropore network, mean macropore diameters, and the distribution factors. The study of Sternagel et al. (2019) explains in detail how the macropore domain of LAST is parameterized based on available field measurements. We vertically discretize the macropores in steps of 0.05 m and assume that they initially contain neither water particles nor solute masses. A maximum of 10,000 possible particles that can be stored in a single macropore, and hence the total possible number of particles in the entire macropore domain, is given by multiplication with the total number of macropores. The studies of Ackermann (1998) and Zehe (1999) provide further descriptions of site 10 and the macropore network.

As the heterogeneous macropore network allows for a rapid bypassing of solutes, we expect a considerable penetration into different soil depths. We use depth-dependent values of K_f and DT50 for IPU in the matrix and in the macropores to account for a depth-dependent retardation and degradation (Tab. 3.2) for the simulations at site 10. Furthermore, we here use different parameterization setups of the reactive transport routine to account for the remarkably variable value ranges of K_f and DT50 reported in various studies (e.g. Bolduan and Zehe, 2006; Rodríguez-Cruz et al., 2006; Bending and Rodríguez-Cruz, 2007; Lewis et al., 2016). To account for the related uncertainty range of the reactive transport behaviour of IPU, we distinguish between two parameter configurations for a rather weak reactive transport of IPU and a strong reactive transport with enhanced retardation and degradation of IPU (Tab. 3.2). To evaluate solely the impact of the K_f value on the model sensitivity, we furthermore perform a simulation at site 10 only with activated sorption and deactivated degradation. Tab. 3.1 provides all relevant simulation and experiment parameters.

HYDRUS 1-D setup at the preferential-flow-dominated site (site 10)

The simulations with HYDRUS 1-D at the preferential-flow-dominated site (site 10) are performed with the same model setups, soil properties, and initial and boundary conditions, as well as reactive transport parameters, as for the simulations with LAST (cf. Tab. 3.1,3.2). In contrast, we select a dual-permeability approach for water flow (Gerke and Genuchten, 1993) and solute transport (physical nonequilibrium) at this site. These approaches distinguish between matrix

and fracture domains for water flow and solute transport. It applies the Richards equation for water flow in each domain, with domain-specific hydraulic properties. The advection–dispersion equation is used to simulate solute transport and mass transfer between both domains, including terms for reactive transport with retardation and degradation (Gerke and Genuchten, 1993). While we apply the same soil hydraulic properties in the matrix (cf. Tab. 3.1) as for the LAST simulations, the macropore domain in HYDRUS gets a faster character with a K_s value of 10^{-3} m s^{-1} . We also select the Freundlich approach for sorption processes and first-order degradation.

3.4.2.3 LAST-Model setup of 7 and 21 d simulations at the plot site (site P4)

We perform simulations for conservative bromide tracer and reactive IPU at site P4 for periods of 7 and 21 d using the parameters in Tab. 3, respectively. Based on examination of the macropore network, we again derive the parameterization of the macropore domain (Tab. 3.3). In line with the LAST-Model setups in Sect. 3.4.2.1 and 3.4.2.2, we apply the same discretization of the matrix dz (0.1 m) and macropore (0.05 m) domain as well as number of particles in both domains (2 million; 10 k per macropore grid element). Additionally, we perform another 7 d simulation for bromide with a finer matrix discretization dz of 0.05 m. Initially, macropores and matrix contain no solute masses, and the macropores also contain no water.

For the simulation of reactive IPU transport, we again apply the weak and strong reactive transport parameterizations with the depth-dependent K_f and DT50 values of the simulations at site 10 (cf. Tab. 3.2). Additionally, we apply here a mean reactive transport parameterization. An evaluation with observed IPU mass profiles is not possible here because robust experimental data are missing. All relevant parameters of the 7 and 21 d simulations at P4 are listed in Tab. 3.3.

3.4.2.4 LAST-Model setup of the FLU breakthrough simulations at the field site

We perform a simulation of FLU concentrations, which migrate from the soil surface into the depth of the tile-drain tube (1 m), over the entire field site, in each of the two irrigation phases. After the first irrigation phase, we assume steady-state flow conditions, as Klaus et al. (2014) found that the flow in the tile-drain tube already approached its initial value after roughly 500 min. This implies hydraulic equilibrium between gravity and capillary forces and thus zero soil water flow in the period of 3 weeks between the first and second irrigation phase. Nevertheless, adsorption and degradation of FLU are still active and simulated using mean K_f and DT50 values in soil (Lewis et al., 2016,

cf. Tab. 3.3) during the 3 weeks until the second irrigation phase starts.

The parameterization of the macropore domain with the number and depth of macropores per square metre follows the recommendations of Klaus and Zehe (2010). In line with the previous LAST-Model setups, we apply the same discretization of the matrix dz (0.1 m) and macropore (0.05 m) domain as well as the number of particles in both domains (2 million; 10 k per macropore grid element). Macropores and matrix again contain no solute masses, and the macropores also contain no water, initially. All further simulation parameters of the FLU breakthrough simulations are listed in Tab. 3.4.

Table 3.1: Parameters of IPU plot-scale experiments and simulations, as well as soil hydraulic parameters according to van Genuchten (1980) and Mualem (1976), at sites 5 and 10, where K_s is the saturated hydraulic conductivity, θ_s the saturated soil water content, θ_r the residual soil water content, α the inverse of an air entry value, n a quantity characterizing pore size distribution, s the storage coefficient, and ρ_b the bulk density. Further, mac. big, mac. med, and mac. sml describe the lengths of big, medium, and small macropores as well as f_{big} , f_{med} , and f_{sml} are the respective distribution factors to split the total number of macropores into these three macropore depths (cf. Sect. 3.2.2.2). For further details on these parameters, see Sternagel et al. (2019).

Parameter	Site 5	Site 10
Experimental parameters		
Irrigation duration (hh:mm)	02:10	02:18
Irrigation intensity ($mm\ h^{-1}$)	10.70	11.00
Applied IPU mass (kg)	5×10^{-4}	1×10^{-3}
Recovery rate (%)	84.4	91
Initial soil moisture in 15 cm (%)	23.7	27.8
Soil type	Calcaric Regosol	Colluvic Regosol
K_s ($m\ s^{-1}$)	1×10^{-6}	1×10^{-6}
θ_s ($m^3\ m^{-3}$)	0.46	0.46
θ_r ($m^3\ m^{-3}$)	0.04	0.04
α (m^{-1})	4.0	3.0
n (-)	1.26	1.25
s (-)	0.38	0.38
ρ_b ($kg\ m^{-3}$)	1300	1500
Number of macropores/ m^2 (-)	-	92
Mean macropore diameter (m)	-	0.005
mac. big (m)	-	0.8
mac. med (m)	-	0.5
mac. sml (m)	-	0.2
f_{big} (-)	-	0.14
f_{med} (-)	-	0.37
f_{sml} (-)	-	0.49
Simulation parameters		
Simulation time t (s)	172,800 (i.e. 2 d)	
Time step Δt (s)	dynamic	
Particle number in matrix (-)	2 million	
Water mass of particle in matrix (kg)	1.9×10^{-4}	2.2×10^{-4}
Particle number in macropore domain (-)	-	920 k
Water mass of particle in macropore domain (kg)	-	1.6×10^{-6}

Table 3.2: Reactive transport parameters of IPU at sites 5, 10, and P4. The upper and lower value limits in the square brackets describe the value ranges of the depth-dependent K_f and DT50 parameters between the soil surface and the starting depth of the subsoil (cf. Fig. 3.3, Sect. 3.3.1.2, 3.3.2.2). At sites 10 and P4, we distinguish between two parameter configurations for a rather weak reactive transport of IPU and a strong reactive transport with enhanced retardation and degradation of IPU. Exclusively at site P4, we additionally apply a mean reactive transport parameter configuration for the 7 and 21 d simulations.

Parameter	Site 5	Site 10 and P4		P4
		weak	strong	mean
K_f for IPU in soil matrix (-) [upper limit; lower limit]	[2.83; 2.83]	[1; 0.26]	[27; 3]	[14; 1.63]
DT50 for IPU in soil matrix (d) [upper limit; lower limit]	[23; 23]	[23; 44]	[3; 12]	[13; 28]
K_f for IPU in macropores (-)	-	5	10	7.5
DT50 for IPU in macropores (d)	-	15.6	10	12.8
beta (-)		0.8		

Table 3.3: Parameters of 7 d bromide experiment at the plot-scale site (site P4) (Klaus et al., 2014) and simulation parameters as well as soil hydraulic parameters according to van Genuchten (1980) and Mualem (1976). For parameter definitions and further details on these parameters, see caption of Tab. 3.1 and (Sternagel et al., 2019). Note that only one macropore depth of 15 cm was observed at this site.

Parameter	P4
Experimental parameters	
Irrigation duration (hh:mm)	03:40
Total irrigation sum (mm)	34.00
Applied bromide mass on 400 m ² field site (kg)	1.6
Recovery rate (%)	ca. 100
Initial soil moisture in 10 cm (%)	24.8
Initial soil moisture in 20 cm (%)	27.1
Initial soil moisture in 30 cm (%)	27.0
Initial soil moisture in 40 cm (%)	28.44
Initial soil moisture in 60 cm (%)	33.11
Initial soil moisture in 100 cm (%)	29.6
Soil type	
Colluvisol	
K_s in topsoil; gleyic horizon (subsoil) ($m s^{-1}$)	1×10^{-5} ; 1×10^{-8}
θ_s in topsoil; gleyic horizon (subsoil) ($m^3 m^{-3}$)	0.5; 0.4
θ_r in topsoil; gleyic horizon (subsoil) ($m^3 m^{-3}$)	0.04; 0.11
α in topsoil; gleyic horizon (subsoil) (m^{-1})	1.9; 3.8
n in topsoil; gleyic horizon (subsoil) (-)	1.25; 1.20
s (-)	0.38
ρ_b ($kg m^{-3}$)	1500
Macropores	
Number of macropores/m ² (-)	68
Mean macropore diameter (m)	0.003
mac. big (m)	0.2
mac. med (m)	-
mac. sml (m)	-
f_{big} (-)	1.0
f_{med} (-)	-
f_{sml} (-)	-
Simulation parameters	
Simulation time t (s)	604,800 (i.e. 7 d)
Time step Δt (s)	dynamic
Particle number in matrix (-)	2 million
Water mass of particle in matrix (kg)	2.3×10^{-4}
Particle number in macropore domain (-)	680 k
Water mass of particle in macropore domain (kg)	1.4×10^{-7}

Table 3.4: Parameters of field-scale FLU breakthrough experiment (Klaus et al., 2014) and simulation parameters as well as soil hydraulic parameters after van Genuchten (1980) and Mualem (1976). For parameter definitions and further details on these parameters, see caption of Tab. 3.1 and (Sternagel et al., 2019). Note that only one macropore depth of 1 m reaching the depth of the tile-drain tube is applied.

Parameter	Field site
Experimental parameters	
Irrigation duration (hh:mm) of 1. and 2. irrigation phase	03:35; 02:00
Total irrigation sum (mm) of 1. and 2. irrigation phase	41.00; 40.00
Applied FLU mass on field site (kg)	0.04
Initial mean soil moisture (%)	28.0
Soil type	
Colluvisol	
K_s in 0–10 cm; 10–35 cm; below 35 cm ($m s^{-1}$)	5×10^{-4} ; 2×10^{-5} ; 5×10^{-5}
θ_s in 0–10 cm; 10–35 cm; below 35 cm ($m^3 m^{-3}$)	0.46; 0.43; 0.4
θ_r in 0–10 cm; 10–35 cm; below 35 cm ($m^3 m^{-3}$)	0.1; 0.11; 0.04
α in 0–10 cm; 10–35 cm; below 35 cm (m^{-1})	2.4; 3.8; 1.9
n in 0–10 cm; 10–35 cm; below 35 cm (-)	1.22; 1.2; 1.25
s (-)	0.38
ρ_b ($kg m^{-3}$)	1500
Number of macropores/ m^2 (-)	10
Mean macropore diameter (m)	0.005
mac. big (m)	1.0
mac. med (m)	-
mac. sml (m)	-
f_{big} (-)	1.0
f_{med} (-)	-
f_{sml} (-)	-
K_f (-) for FLU in soil matrix	4.83
DT50 (d) for FLU in soil matrix	54
K_f (-) for FLU in macropores	4
DT50 (d) for FLU in macropores	19
beta (-)	0.92
Simulation parameters	
Simulation time t (s)	1,814,400 (i.e. 3 weeks)
Time step Δt (s)	dynamic
Particle number in matrix (-)	2 million
Water mass of particle in matrix (kg)	2.9×10^{-4}
Particle number in macropore domain (-)	680 k
Water mass of particle in macropore domain (kg)	1.96×10^{-6}

3.5 RESULTS

In the following sections, we present simulated vertical mass profiles of bromide and IPU at the different plot-scale study sites (sites 5, 10, and P4), as well as breakthrough time series of FLU concentrations at the field site (cf. Sect. 3.4.1).

3.5.1 *Simulation results at the well-mixed plot site (site 5) after 2 d*

3.5.1.1 *IPU transport simulated with LAST*

In Fig. 3.4a, the reference simulation treating IPU as conservative (red profile) overestimates the transport of IPU into soil depths lower than 10 cm, with a maximum penetration depth of 40 cm. This leads in turn to simultaneous underestimation of masses in shallow depths near the soil surface (root mean square error, RMSE: 0.064 g, 12.8 % of applied mass). In the case of the simulation with retardation and no degradation (yellow profile), the simulated mass profile matches the observed profile in the first 10 cm because retardation causes mass accumulation. With additional degradation (light blue profile), the solute masses in the first 10 cm are then slightly reduced. The influence of degradation is relatively small, due to the moderate DT₅₀ value of 23 d and the short simulation period of 2 d, but it is nevertheless detectable. Overall, we find that there are indeed noticeable differences (RMSE difference of 7.3 %) between the IPU profiles of the conservative, reference simulation and the reactive transport simulation with retardation and degradation, which is also in better accord with the observed mass profile, reflected by a smaller RMSE value of 0.027 g (5.5 % of applied mass). At the end of the simulated period of 2 d, a total IPU mass of 0.014 g is degraded, while the observed profile has a mass deficit of 0.078 g corresponding to a recovery rate of 84 %. This observed mass deficit cannot be explained exclusively by degradation. It might be the result of additional mass losses in the experiment execution and lab analyses.

3.5.1.2 *IPU transport simulated with HYDRUS 1-D*

The IPU mass profile simulated with HYDRUS 1-D (Fig. 3.4b), with activated reactive transport, shows similar mass patterns compared to LAST and the observed profile with a RMSE value of 0.036 g (7.3 % of applied mass). While HYDRUS overestimates the IPU masses at the soil surface, considering a stronger retardation compared to the observation and the LAST results, it simulates the observed masses in 10–20 cm soil depth quite well. In these depths, LAST overestimates masses with a maximum penetration depth of 30 cm, which is 10 cm deeper than observed. Overall, the results of HYDRUS and LAST are in comparable agreement with the observed profile. HYDRUS

simulates a total, degraded IPU mass of 0.017 g, which is in the range of the LAST results (cf. Sect. 3.5.1.1). This means that in both models, the total degradation is similar, but the distribution of the remaining IPU masses over the soil profile differs.

3.5.1.3 Bromide transport simulated with LAST

Bromide slightly percolates into greater depths during the short-term irrigation experiment (Fig. 3.4c) compared to the retarded and degraded IPU (cf. Fig. 3.4a). The results generally underline that the Lagrangian approach is able to simulate conservative solute transport under well-mixed conditions, as we have already shown in our previous study (Sternagel et al., 2019). The results further show that the approach is capable of treating both conservative tracers and reactive substances.

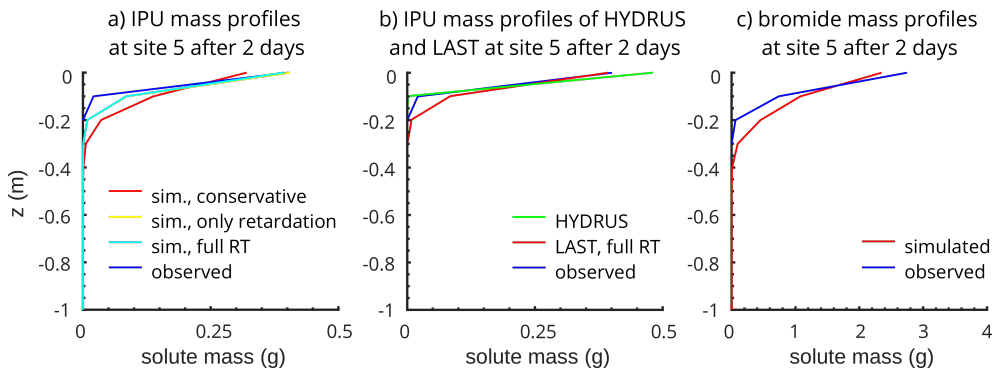


Figure 3.4: (a) LAST-Model results of reactive IPU transport simulations at the well-mixed site (site 5) after 2 d with regarding IPU as conservative without reactive transport which serves as reference (red profile), with activated retardation but without degradation to exclusively show the effect of the sorption processes (yellow profile) and with fully activated reactive transport (light blue profile). (b) Comparison with HYDRUS 1-D results and (c) exemplary results of a conservative simulation with LAST for bromide.

3.5.2 Simulation results at the preferential-flow-dominated plot site (site 10) after 2 d

3.5.2.1 IPU transport simulated with LAST

Fig. 3.5a and b present results of different simulation setups compared to the observed IPU mass profile at site 10 after 2 d. Both figures comprise the observed profile as well as a profile of a reference simulation treating IPU as conservative. Fig. 3.5a focuses on the mass profiles resulting from simulations only with activated retardation, using low and high K_f values. Fig. 3.5b shows results for simulations performed

with full reactive transport subject to retardation and degradation, comparing parameterizations for weak and strong reactive transport. The shaded area between these profiles represents the corresponding uncertainty ranges.

In general, the typical “fingerprint” of preferential flow through macropores is clearly visible in the observed IPU mass profile. The observed mass accumulations and peaks fit well to the observed macropore depth distribution (cf. Tab. 3.1), which implies that water and IPU travelled through the macropores and infiltrated into the matrix in the respective soil depths where the macropores end. The observed mass profile shows a strong accumulation of IPU masses in depths between 70–90 cm, which cannot be explained by the relatively low number of macropores (ca. 13) in this depth. One reason for this could be particle-bound transport of IPU at this study site, as proposed by Zehe and Flühler (2001a). They suggested that IPU is adsorbed to mobile soil particles or colloids at the soil surface, which then travel rapidly through macropores into greater depths at this site. In comparison, the simulated conservative reference profile depicts the observed mass distribution quite well on average, although less well the heterogeneous profile shape with a RMSE value of 0.076 g (7.6 % of applied mass). The mass peaks in the depths of the macropore ends (cf. Tab. 3.1) are relatively weak because solute masses leaving the macropores are not retarded in the matrix but instead flushed out by the water flow into deeper soil depths, resulting in a smoothed mass profile. In the near-surface soil depths between 0–10 cm, the conservative reference simulation clearly overestimates the IPU masses.

The range of simulated mass profiles, corresponding to the weak and strong reactive transport parameterization (Fig. 3.5b), matches the observed profile in terms of both mass amounts and shape, with a RMSE value of 0.038 g (3.8 % of applied mass). Hence, at this site, LAST performs better with activated reactive transport compared to the conservative reference setup. The mass accumulations, which are detectable in those depths where the macropores end, arise from adsorption and retardation of solutes that infiltrated the soil matrix out of the macropores. While the simulation with full reactive transport also overestimates the IPU masses in the upper 10 cm, the simulated and observed mass profiles coincide well in the lower depths. The observed mass peak at 70–90 cm cannot be reproduced completely. Furthermore, the wider ranges between the simulated profiles for weak and strong reactive transport in the topsoil reflect the depth-dependent parameterization of the DT₅₀ values especially. The higher IPU amounts and lower DT₅₀ values in the topsoil cause a faster degradation than in underlying soil depths. In subsoil, degradation is slower and uniform, and due to smaller IPU amounts, there is no

difference between the two parameterizations. The total degraded IPU masses are between 0.026 and 0.131 g for the weak and strong reactive transport simulations, respectively. With an IPU input amount of 1 g, up to 13 % of IPU is degraded in just 2 d. This shows the relevance of the degradation process, even on these short timescales. The relatively high observed IPU mass recovery of 0.908 g (ca. 91 %) implies a possible degraded total mass of 0.092 g, which is consistent with our simulated range.

The simulation only with retardation (Fig. 3.5a) reveals hardly any sensitivity to the variation of K_f values. This implies that the amounts of adsorbed masses are almost equal for different K_f values at the end of the simulation and thus independent of the K_f value. This might be due to nonlinear adsorption, which establishes an equilibrium state between water and the adsorbing phase after a certain time (cf. Sect. 3.3.1). Hence, independent of the magnitude of K_f , no further adsorption occurs unless degradation is activated, which would lead to mass loss in the soil solid phase and a renewed adsorption capacity (cf. Fig. 3.5b). Higher K_f values lead only to a shorter time to reach this equilibrium state; the final adsorbed masses are similar for different K_f values due to the inactivated degradation in this special case.

3.5.2.2 IPU transport simulated with HYDRUS 1-D

In contrast to the findings at site 5, IPU mass profiles simulated with the dual-permeability approach of HYDRUS 1-D (Fig. 3.5c) do not match the observed profile at site 10, resulting in a RMSE value of 0.079 g (7.9 % of applied mass). In the first 35 cm, HYDRUS simulates a strong retardation and overestimation of masses with a maximum penetration depth of only 50 cm. In comparison, simulations with the Lagrangian approach in the LAST-Model match the observed profile better (cf. Sect. 3.5.2.1). However, the total degraded IPU masses of 0.028 and 0.183 g resulting from the weak and strong reactive transport parameterizations simulated with HYDRUS are similar to those resulting from LAST simulations.

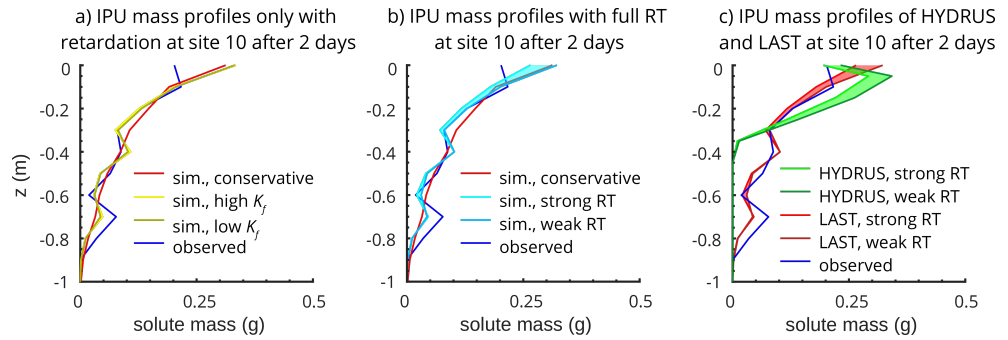


Figure 3.5: LAST-Model results of reactive IPU transport simulations at the preferential-flow-dominated site (site 10) after 2 d. (a) The simulation is performed only with active retardation and with low and high values for K_f . (b) The simulation is performed with activated retardation and degradation. The shaded area between the profiles with weak and strong reactive transport (cf. Tab. 3.2) shows the uncertainty area of the empirical K_f and DT_{50} values. (c) Comparison with HYDRUS 1-D simulation results.

3.5.3 Simulation results of LAST at the plot site (P4)

3.5.3.1 Bromide transport in 7 d

Fig. 3.6a shows the simulated and observed bromide mass profiles at site P4 after 7 d. Note that a model evaluation directly at the surface is not meaningful because the soil sampling in the experiment started at a depth of 5 cm.

The observed mass profile is characterized by two distinct mass peaks. One peak, at 15–30 cm, probably originates from solute masses entering the matrix from the macropores in 15 cm depth, which are subsequently displaced by water movement into this depth range within the 7 d. The second peak in a depth around 60–70 cm likely originates from an accumulation of water and solutes above the less permeable gleyic horizon in this depth. In comparison, the simulated bromide mass profile simulated with a finer discretization dz of 0.1 m (red solid profile) is generally shifted to greater depths, although the shape corresponds quite well to the observed profile. Between 5–30 cm, the simulated masses are underestimated, and conversely, they are overestimated between 30–55 cm depth. Obviously, LAST simulates a solute displacement that is too strong and fast into these deeper soil depths (“deep shift”), compared to the observed mass accumulation (15–30 cm), after solute masses leave the macropores and enter the matrix in 15 cm depth. The simulated mass accumulation in the gley horizon coincides quite well with the observed data but with long tailing. Despite the almost stagnant conditions in the gley horizon, we simulate too strong a displacement of solutes into soil depths even

deeper than 1 m (Fig. 3.6a) with the setup in LAST. This behaviour is also visible in the simulated bromide mass profile with a refined dz of 0.05 m (red dashed line), but the effect is less pronounced as more bromide remains in the upper 30 cm.

3.5.3.2 IPU transport in 7 and 21 d

Fig. 3.6b shows simulated IPU mass profiles after 7 d, for 6.3 g of IPU initially applied to the soil surface. These results provide insights to a possible temporal development of IPU leaching for different reactive transport parameterizations. Note that comparable observed data are unavailable (cf. Sect. 3.4.2.3, Tab. 2.2). The depth transport of IPU is limited compared to bromide and the reference simulation, treating IPU as non-reactive conservative solute (red profile), which reflects IPU retardation and degradation in the topsoil. However, we observe two clear mass peaks at the end of the 15 cm deep macropores and above the gley horizon, as for bromide. In topsoil, the range between the two profiles simulated with a weak and strong reactive transport parameterization is largest. This is caused by the enhanced retardation and degradation potential and the high amount of IPU in the topsoil. The decreased potential for sorption and degradation in the subsoil leads to negligible differences between the profiles in greater soil depths. In total, the degraded IPU masses for the two parameterizations lie between 0.514 and 2.618 g.

After 21 d, the resulting IPU mass profiles show remarkable differences compared to the profiles after 7 d (Fig. 3.6c). We observe a deeper penetration and greater range of profiles simulated with the weak and strong RT parameterization in subsoil. The mass peaks are barely detectable and mostly smoothed out along the 15 cm deep macropores and in the depth of the gley horizon. The total degraded IPU masses for the strong and weak reactive transport parameterizations range between 1.345 and 4.625 g. Furthermore, despite applying mean reactive transport parameters, the resulting IPU mass profile (black profile) is not centred in the light blue shaded profile range due to the non-linear character of sorption and degradation.

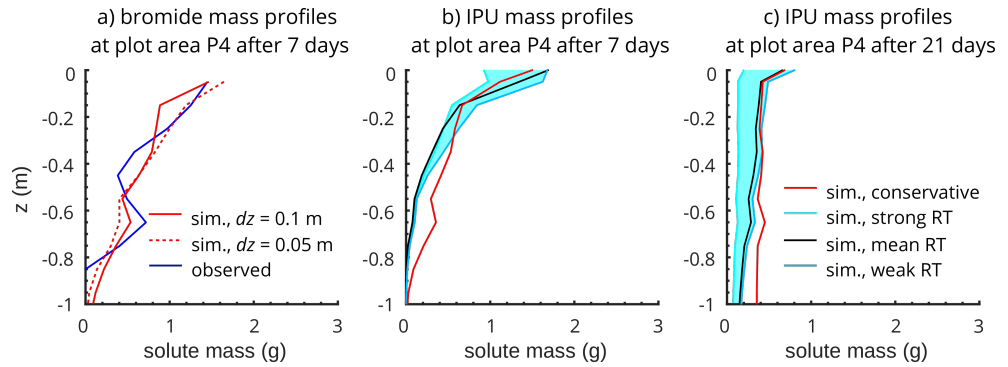


Figure 3.6: (a) LAST-Model results of 7 d simulation with bromide and different soil domain discretization dz at site P4. Panels (b) and (c) show hypothetical results of a 7 and 21 d simulation with a weak and strong reactive transport configuration for IPU (cf. Tab. 3.2, Sect. 3.4.2.3) at site P4. The bright blue range between the two profiles demonstrates a hypothetical and possible range of IPU mass profiles under the influence of retardation and degradation during 7 and 21 d at this site, respectively. The black profiles additionally show results with a mean reactive transport configuration (cf. Tab. 3.2).

3.5.4 Simulation results of FLU breakthrough on field site

During the first irrigation phase, the simulation shows deficiencies to reproduce the observed temporal dynamics and peaks of FLU concentrations (Fig. 3.7a). The first breakthrough peak, probably originating from FLU bypassing the matrix through macropores, is simulated after 50 min with a subsequently slight decrease. After 100 min, the simulation shows a steady increase of FLU concentrations due to delayed breakthrough of FLU through the soil matrix. The clear underestimation of the second concentration peak after ca. 280 min can be partly explained by the fact that about 20 % of FLU was subject to rapid particle-bound transport (Klaus et al., 2014). This mechanism is not considered in our approach.

The simulation of FLU remobilization during the second irrigation phase reveals similar results. The simulated remobilization is too early (75 min) and followed by a second peak after 175 min. Both peaks originate again from a first breakthrough of FLU through macropores and subsequent leaching through the matrix (Fig. 3.7b). Nevertheless, the results underpin the finding that the presented reactive transport method within the Lagrangian approach is able to reproduce the remobilization of FLU into the tile drain during the second irrigation. This implies that the approach was also capable to estimate properly the adsorption and degradation of FLU during the 3 weeks. Despite the limited match with the observed temporal changes of FLU concentrations, the amount of cumulated FLU masses

is at the end of both irrigation phases in good agreement with the observations (Fig. 3.7c and d).

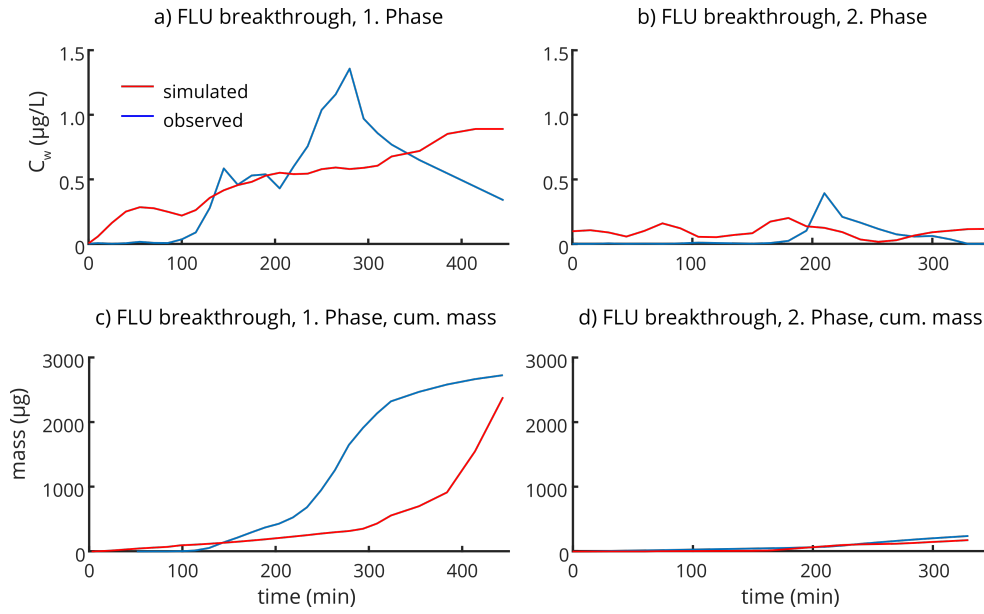


Figure 3.7: LAST-Model results of FLU breakthrough simulations with FLU concentrations C_w in the tile-drain tube of the field site. (a) and (b) show FLU concentration changes over time and (c) and (d) present cumulated FLU masses in the two irrigation phases, respectively (cf. Sect. 3.4.1.4 and 3.4.2.4).

3.6 DISCUSSION

The key innovation of this study is a method to simulate reactive solute transport in the vadose zone within a Lagrangian framework. In this context, we extend the LAST-Model (Sternagel et al., 2019) with the presented method for reactive solute transport to account for non-linear sorption and first-order degradation processes during transport of reactive substances such as pesticides through a partially saturated soil matrix domain and macropores. For the sorption process, we develop an explicit mass transfer approach based on the Freundlich isotherms because the usual method of using a retardation factor (cf. Sect. 3.3.1.1) is not applicable in the particle-based approach of LAST. Model evaluations with data from irrigation experiments, that examined plot-scale leaching of bromide and IPU under different flow conditions on various timescales as well as FLU breakthrough on a field site, corroborate the suitability of the approach and its physically valid implementation. Comparisons to simulations with HYDRUS 1-D reveal furthermore that an explicit representation of macropores and their depth distribution is favourable to predict preferential transport of solutes.

3.6.1 *Sorption and degradation in the Lagrangian framework*

3.6.1.1 *Reactive transport under well-mixed conditions*

The 2 d simulations of IPU transport at the well-mixed site (site 5) corroborate the validity of the Lagrangian approach and the proposed method for sorption and degradation, implemented into the Lagrangian framework of LAST (Fig. 3.4a). Adsorption causes an expected accumulation of IPU in topsoil layers (0–10 cm) and, consequently, reduced percolation into greater soil depths. Although degradation only has a small impact at this short timescale, due to the moderate DT_{50} value of 23 d, we nevertheless observe a total degradation of 0.014 g IPU in 2 d that occurs especially in the shallow soil areas where IPU accumulates. The mass profile simulated with retardation and degradation is more consistent with the observations than the reference simulation treating IPU as a conservative solute. Such a fast reaction and degradation of IPU in the topsoil can be explained by its general non-persistent and moderately mobile character, as well as an obviously very short duration of a lag phase near the soil surface, which was also discovered by several field studies (e.g. Bending et al., 2001, 2003; Rodríguez-Cruz et al., 2006). The simulated mass profiles of the benchmark simulations with the commonly used HYDRUS 1-D model are also in accord with the observations and corroborate our results; in particular, the total degraded masses are in a similar range (Fig. 3.4c, Sect. 3.5.1). This suggests that the developed

reactive transport method in our Lagrangian approach performs similarly to that implemented in HYDRUS 1-D at this well-mixed site (site 5). This finding is in line with our previous study, which revealed that both approaches yielded similar simulations of conservative tracer transport at matrix-flow-dominated sites (cf. Sternagel et al., 2019).

3.6.1.2 *Impact of the macropore domain on reactive transport under preferential flow conditions*

The simulation results at the preferential-flow-dominated site (site 10) show that the Lagrangian approach is capable of reproducing the observed heterogeneous IPU mass profile. The implemented depth-dependent sorption and degradation processes are particularly helpful in this context (cf. Fig. 3.5). However, in the entire context of this study, it should be recognized that mean values of K_f and DT50 (cf. Tab. 3.2, Sect. 3.4.2.1) from the PPDB were determined empirically at other field sites. Measurements of these variables are laborious and not straightforward, as controls on sorption and degradation vary in space and time (Dechesne et al., 2014). The use of literature values for these parameters introduces considerable uncertainty into pesticide fate modelling (Dubus et al., 2003). We explore this uncertainty by varying the K_f and DT50 values for IPU at site 10 in the ranges provided by the PPDB and further literature (cf. Tab. 3.2, Sect. 3.4.2.2).

The results corroborate the importance of a structural representation of macropores and their depth distribution, as implemented in the LAST-Model, consistent with the results of Sternagel et al. (2019). This is also reflected by the fact that the simulated IPU masses in the topsoil between 10–30 cm, and particularly the mass accumulations at the depths where macropores end (cf. Tab. 3.1), match the observations, compared to the reference simulation treating IPU as conservative tracer and to simulations with HYDRUS 1-D. We conclude that an explicit representation of the macropore system with its connectivity, diameter, and depth distribution, and treatment of macropore flow and exchange with the matrix, is crucial to reproduce solute bypassing of the topsoil matrix and subsequent infiltration into the subsoil matrix.

HYDRUS 1-D does not match the heterogeneous shape of the observed mass profile at site 10, despite the use of a dual-permeability approach and the same parameterization as LAST. HYDRUS 1-D barely accounts for IPU bypassing and breakthrough to greater depths, and it overestimates retardation in topsoil, which results in a high mass accumulation in the first 10 cm of soil. The total degraded IPU masses are similar in both models and in accord with the observed data, as both models rely on first-order degradation (Gerke and Genuchten, 1993). These results hence corroborate the findings of Sternagel et al.

(2019), who concluded that HYDRUS is effective under well-mixed conditions but is limited in terms of simulating preferential flow and partial mixing between matrix and macropore flow regimes (e.g. Beven and Germann, 1982; Šimůnek et al., 2003; Beven and Germann, 2013; Sternagel et al., 2019). We propose that incorporating a similarly structured macropore domain into HYDRUS would likely improve simulations under such conditions.

However, all simulated IPU mass profiles at site 10 overestimate the observed masses within the upper 10 cm of the soil. This may be due to an additional photochemical degradation at the soil surface, surface losses due to volatilization, or even plant uptake (Fomsgaard, 1995). Such processes are difficult to detect and parameterize. A possible reason for the mismatch of the observed and simulated mass profiles in 70 cm soil depth at site 10 could be a facilitated pesticide displacement due to particle-bound transport (Villholth et al., 2000; De Jonge et al., 2004).

3.6.1.3 Sensitivity to variations of sorption and degradation parameters

The ranges of the K_f and DT50 values for the case of a weak and strong reactive transport parameterization cause differences in the resulting mass profiles (cf. shaded areas in Fig. 3.5). These differences are generally stronger in topsoil and gradually decrease with depth. This is because sorption and degradation rates are (i) due to the higher IPU masses, larger in topsoil than in the subsoil, and (ii) due to the depthdependent parameterization (cf. Sect. 3.3). The results of the simulation with only sorption, and no degradation (Fig. 3.5a), suggest a moderate to low model sensitivity to the K_f parameter. This may be due to the establishment of an equilibrium state between water and soil solid phase during the simulation time of 2 d. In LAST, the amount of adsorbed masses depends mainly on the substance concentration in water and the soil solid phase. As long as the solute concentration in the water phase is higher than in the solid phase, solutes are adsorbed until an equilibrium concentration between both phases is achieved (cf. Sect. 3.3.1). This means that sorption is also dependent on factors that can disturb this equilibrium state, to enable further sorption. One such factor could be solute mass loss in the soil solid phase due to degradation, which, if not accounted for as in this special case, leads to a stable equilibrium state once it is achieved. Thus, at the end of the simulations with different parameterizations, the amount of solute masses and their distribution are almost always equal, independent of the K_f value. The magnitude of the K_f value alone only determines how fast the equilibrium state arises. For the simulation with small K_f values, an equilibrium state in all soil depths is reached approximately 1 d after pesticide application, while only about 144 min is required for the simulation with the high K_f values.

Simulations with both retardation and degradation (Fig. 3.5b) reveal that degradation is dependent on sorption and the K_f value. This is because we assume that degradation only occurs as long as solutes are adsorbed in the solid phase. This shows the general mutual dependence of sorption and degradation processes.

3.6.2 Indicators for solute over-mixing from the 7 d plot-scale simulations

Despite a reasonably good match of simulated and observed bromide mass profiles after 7 d (Fig. 3.6a), we find indications that an over-mixing of solutes (cf. Sect. 3.2.2.2) could occur in LAST over longer timescales. While the described deep shift and accumulation of bromide masses in soil depths between 30–55 cm (cf. Sect. 3.5.3.1) could reflect the uncertainty of soil hydraulic properties like the saturated hydraulic conductivity K_s , the long mass tail underneath the mass accumulation in the gleyic subsoil around 70 cm depth probably results from artificial over-mixing. Note that the low-permeable gley horizon in this depth has a K_s value of the order of 10^{-8} m s^{-1} , which implies highly stagnant conditions and thus strongly reduced advective particle movement. Nevertheless, particle diffusion (driven by the random walk; Eq. 3.5) still occurs due to the particle density and thus water content gradient in this depth originating from the particle accumulation above the gley horizon. Particle diffusion entails diffusive transport of solute masses into deeper soil depths. However, this mass transport might be too strong in our model, as the perfect mixing of solute masses between all water particles in a grid element (Sternagel et al., 2019) leads to small, systematic errors in each time step. These errors accumulate on the 7 d scale and result in over-predictions of the displaced solute masses transported by the diffusing water particles (Green et al., 2002). In particular, the subsequent infiltration of pure water particles with zero solute concentration has the potential to “flush out” solutes, leading to the clear tailing of bromide masses even deeper than 1 m (Fig. 3.6a). Also, the second simulation with a refined soil domain discretization dz of 0.05 m entails this solute displacement that is too strong, which shows that over-mixing cannot be simply avoided in our model by using a finer vertical Euler grid discretization as sometimes suggested (e.g. Boso et al., 2013). An even finer discretization would lead to huge, excessive simulation times because the finer soil discretization has the consequence that also the time steps become smaller to fulfil the Courant criterion, and a much higher number of water particles would be needed. Without a higher particle number, there would be too few particles in the single soil layers to distribute them to the bins properly and to ensure a numerically and statistically valid random walk.

We argue that in natural soils, solutes spread diffusively across water stored in different pore sizes (Kutílek and Nielsen, 1994). Hence, diffusive movement into and out of these pores, as well as their entrapment, depends strongly on the pore size. This implies a timescale for solute mixing among waters in different pore sizes and a flushing-out process that is significantly larger than assumed in our perfectly mixed approach.

The results of the 7 and 21 d simulation with exactly the same model setup but with activated reactive transport for IPU does not show any indication for over-mixing (Fig. 3.6b). This is probably due to the retardation and degradation processes that hinder, or mask, a possible over-mixing as solute masses are adsorbed to the soil solid phase and degraded. Based on the previous findings, we can only assume that the resulting 7 and 21 d IPU mass profiles are also deep-shifted due to over-mixing; but comparable data are required for analysis, especially on larger timescales of several weeks.

3.6.3 *Comparison of plot-scale simulations over different periods and simulation of FLU breakthrough on the field site*

Comparing the plot-scale mass profiles of the 2, 7, and 21 d periods reveals remarkable differences. Regarding bromide transport, the longer drainage phase after irrigation during the 7 d period implies that water and dissolved bromide have more time to redistribute and diffuse through the soil, compared to the 2 d period. This is reflected in the mass accumulation above the gley horizon observed in the plot-scale experiments at site P4 (cf. Fig. 3.5a). Furthermore, as mentioned in Sect. 3.4.2.2, IPU can indeed exhibit DT₅₀ values of just a couple of days in natural soils, which is surely relevant when comparing periods of 2, 7, and 21 d. This is reflected in the higher relative IPU degradation amount of 41.5 % in the 7 d period (cf. Fig. 3.6b) and 73.3 % in the 21 d period (cf. Fig 3.5c) compared to just 13 % in the 2 d period (cf. Fig 3.4b) for the strong reactive transport parameterization (cf. Tab. 2.2). Bending and Rodriguez-Cruz (2007) found in their experiments a remaining mean IPU mass, relative to input amount, of around 65 % in soil samples between 0–80 cm depth after 20 d. The 21 d simulations for IPU (Fig. 3.6c) result in relative, remaining IPU masses between approximately 30 %–90 % in the depth 0–80 cm for the strong and weak RT parameterization, respectively. Additionally, Bending et al. (2003) found in further experiments a remaining mean IPU mass of around 39 %–55 % of input mass in the first 15 cm of soil at four sites after 21 d. LAST in turn simulates relative, remaining IPU masses between 31 %–94 % in the depth 0–15 cm for the strong and mean RT parameterization, respectively. Hence, the 21 d simulations of IPU transport produce relative, remaining IPU

mass ranges in different soil depths, which seem to be reasonable as they include these observed results.

The results of the FLU breakthrough simulations reveal the general difficulty of simulating the temporal dynamics of the breakthrough curve observed in the tile drain (cf. Fig. 3.7a and b). This confirms that the use of one single parameter configuration in this study (cf. Tab. 3.4) for the simulation of FLU breakthrough on the entire field site is too simple to capture the obviously much higher spatial heterogeneity of the 400 m^2 field. This is in line with experimental findings of Klaus et al. (2014), who reported a strongly variable transport within five distributed soil profiles, which they have examined on this field. Nevertheless, the selected average parameterization of K_f and DT50 (cf. Sect. 3.4.2.4, Tab. 3.4) allows for reasonable simulation of (i) adsorption of FLU, especially during the first, rainfall-driven phase when water with FLU infiltrates and redistributes, as well as (ii) degradation of FLU, particularly during the period of 3 weeks between the two irrigation phases. This is reflected in the remobilization of FLU in the second irrigation phase. As LAST was previously able to calculate adsorption and degradation of FLU to a suitable magnitude, the remobilized, cumulative FLU masses are in turn in the range of observations in the second irrigation phase (cf. Fig. 3.7d). The steady-state assumption after the first irrigation phase (cf. Sect. 3.4.2.4) is in line with the observation of Klaus et al. (2014) that the initial background runoff in the tile-drain tube is approximately regained after 500 min.

We thus conclude that the reactive transport method implemented in LAST, with the simple parameter configuration, is sufficient to reproduce FLU concentrations and masses that leached into the tile drain and the observed remobilization during the second irrigation phase, 3 weeks after FLU application. Klaus and Zehe (2011) obtained similar results by using the 2-D model CATFLOW to simulate observed breakthrough of bromide and IPU into a tile drain at a nearby site in the Weiherbach catchment.

3.6.4 *General reflections on Lagrangian models for solute transport*

In line with other Lagrangian models using particle tracking for solute transport (e.g. Delay and Bodin, 2001; Berkowitz et al., 2006), our approach shares common assumptions and characteristics. Either particles represent solutes or, as in LAST, water parcels, which carry solute masses through the soil domain; and simultaneously, the particles are not independent but interact with each other as well as with the soil domain by sorption and degradation.

However, LAST has important differences compared to some other particle-based models (e.g. Engdahl et al., 2017, 2019; Schmidt et al., 2019), which have been published recently as an alternative to the common solute transport approaches discussed in the introduction. These models calculate mass transfers between particles of different substance species to represent mainly chemical reactions, while our Lagrangian approach calculates the mass transfer of a single substance species among water particles, as well as between water particles and the adsorbing soil phase to represent solute mixing and chemical sorption, respectively. However, by just comparing the implementation of mass transfers in the other models and LAST, regardless of the different application purposes, there is an important difference. These other particle-based models do not use a spatial discretization of the soil domain (Euler grid) to determine the spatial proximity or affiliation of particles and to describe mass transfers between them. Instead, they use a co-location probability approach, which describes solute particle interactions like mass transfer based on a reaction probability dependent on the distance between particle pairs. This approach has advantages in simulating transport and reactions of multiple substances on larger spatial scales of geochemical systems like aquifers, compared to the use of an Euler grid. It also offers advantages to overcome the described artificial over-mixing problem of Eulerian control volumes (cf. Sects. 3.1, 3.6.2). However, this approach also has drawbacks. For example, one drawback of the miRPT algorithm of Schmidt et al., 2019 is related to its transfer process of solutes. In this process, all eligible solute masses must ultimately be transferred from mobile particles (i.e. water phase) to immobile particles (i.e. soil solid phase) to calculate degradation. Subsequently, the residual, non-degraded masses are again transferred back to the water phase for further transport. This implies that masses move between the phases without being subject to degradation or adsorption, which is computationally less efficient because a sufficient spatial distribution and a large number of immobile particles is necessary. In both approaches, miRPT and LAST, solute reactions like degradation are calculated only for the immobile particles. However, due to the use of a spatially discretized soil domain, the reactive solute transport method in LAST is, in contrast, able to perform specific calculations for the partial mass transfer between water and soil solid phase. This is more efficient for transport simulations at the 1-D plot scale and is less time-consuming and computationally intensive than the approach of the miRPT algorithm. Furthermore, these Lagrangian particle tracking approaches ultimately require a spatial discretization to calculate solute concentrations, which they achieve by grouping adjacent particles within a specifically defined radius. This approach is thus similar to soil domain discretization of Eulerian methods, which justifies the Euler grid in LAST.

In general, the extended LAST-Model with an accounting for reactive solute transport requires only a moderate increase in simulation times compared to the originally published model version Sternagel et al. (2019). A total simulation time of only 20 to 30 min on a moderately powerful PC (Intel Core i7, 3400 MHz, 32GB RAM) is required for simulations at the heterogeneous site 10 over 2 d, which we consider reasonable relative to the improved model functionality and physical soundness.

3.7 CONCLUSIONS AND OUTLOOK

Overall, the main findings of this study are as follows:

- Simulation results demonstrate the feasibility to simulate reactive transport of solutes, through partially saturated soils, within a Lagrangian model framework (cf. Sect. 3.6.1.1).
- Comparisons to results of HYDRUS 1-D underline that the structural macropore domain is an asset of LAST, which enables an accounting of preferential bypassing and re-infiltration of solutes (cf. Sect. 3.6.1.2). This is also crucial for predicting preferential leaching of reactive substances under the influence of the effects of sorption and degradation.
- LAST shares common assumptions with other alternative particle-based models but has beneficial characteristics for the simulation of reactive solute transport in partially saturated soil plots (cf. Sect. 3.6.4).
- The 7 d plot-scale simulations show that, while the current formulation yields reasonably good results for bromide transport, some over-mixing of solutes via diffusion is present (cf. Sect. 3.6.2).
- The 21 d plot-scale simulations reveal a reasonable behaviour of reactive IPU transport on larger timescales, also quantitatively compared to results of experiments (cf. Sect. 3.6.3).
- FLU breakthrough simulations prove the ability of the Lagrangian approach to estimate the remobilization of adsorbed reactive substances on a field site in a second irrigation phase 3 weeks after application (cf. Sect. 3.6.3).

Taken together, these findings verify the relevance and innovation of the presented reactive solute transport method in a Lagrangian approach. To the best of our knowledge, no other particle-based Lagrangian framework has applied reactive transport in this way before to simulate sorption and degradation processes at the transport of reactive substances through partially saturated soil plots, even under preferential flow conditions, as well as the breakthrough and remobilization of pesticides on a field site.

In future work, we intend to address possible improvements to the LAST formulation, to better quantify solute transport over longer timescales. One option would be to perform long-term soil column experiments to examine how tracers and pesticides diffusively enter and leave different pore sizes. Based on such experiment results, one could improve the solute transport routine to better account for mixing

between water particles that are stored in pores of different size. The Lagrangian approach offers promising opportunities in this regard, as it distinguishes particle movements in different velocity bins, which represent water in different pore sizes (cf. Sect. 3.2). In this way, it may be possible to simulate, in each time step and grid element, the solute mass exchange between water particles using a specific diffusive transfer rate that is dependent on the pore size or bin in which the particles are stored. With this approach, we would overcome the perfect mixing assumption and may apply pore-size-specific sorption with a bin-dependent gradient of K_f values.

Part IV

STEPPING BEYOND PERFECTLY MIXED CONDITIONS IN SOIL HYDROLOGICAL MODELLING USING A LAGRANGIAN APPROACH

This study is published in the scientific journal Hydrology and Earth System Science (HESS). The remainder of part IV is a reprint of:

Sternagel, A., R. Loritz, B. Berkowitz, and E. Zehe (2022). "Stepping beyond perfectly mixed conditions in soil hydrological modelling using a Lagrangian approach." In: Hydrology and Earth System Sciences 26, pp.1615–1629. <https://doi.org/10.5194/hess-26-1615-2022>.

STEPPING BEYOND PERFECTLY MIXED CONDITIONS IN SOIL HYDROLOGICAL MODELLING USING A LAGRANGIAN APPROACH

ABSTRACT

A recent experiment of Bowers et al. (2020) revealed that diffusive mixing of water isotopes ($\delta^2\text{H}$ and $\delta^{18}\text{O}$) over a fully saturated soil sample of a few centimetres in length required several days to equilibrate completely. In this study, we present an approach to simulate such time-delayed diffusive mixing processes, on the pore scale, beyond instantaneously and perfectly mixed conditions. The diffusive pore mixing (DIPMI) approach is based on a Lagrangian perspective on water particles moving by diffusion over the pore space of a soil volume and carrying concentrations of solutes or isotopes. The idea of DIPMI is to account for the self-diffusion of water particles across a characteristic length scale of the pore space using pore-size-dependent diffusion coefficients. The model parameters can be derived from the soil-specific water retention curve, and no further calibration is needed. We test our DIPMI approach by simulating diffusive mixing of water isotopes over the pore space of a saturated soil volume using the experimental data of Bowers et al. (2020). Simulation results show the feasibility of the DIPMI approach for reproducing the measured mixing times and concentrations of isotopes at different tensions over the pore space. This result corroborates the finding that diffusive mixing in soils depends on the pore size distribution and the specific soil water retention properties. Additionally, we perform a virtual experiment with the DIPMI approach by simulating mixing and leaching processes of a solute in a vertical, saturated soil column and compare the results against simulations with the common perfect mixing assumption. The results of this virtual experiment reveal that the frequently observed steep rise and long tailing of breakthrough curves, which are typically associated with non-uniform transport in heterogeneous soils, may also occur in homogeneous media as a result of imperfect subscale mixing in a macroscopically homogeneous soil matrix.

4.1 INTRODUCTION

Water isotopes are widely used as tracers to investigate a variety of hydrological processes (Sprenger et al., 2016). While they were originally used to separate pre-event and event water contributions to storm runoff (Bonell et al., 1990; Sklash et al., 1996), they are now more frequently considered as a continuous source of information to infer the travel time distributions of water through hydrological systems (e.g. McGlynn et al., 2003; McGlynn and Seibert, 2003; Weiler et al., 2003; Klaus and McDonnell, 2013). Early analyses often relied on time-invariant transfer functions, whereas some of the more recent approaches are time-dependent and, for example, use an age-ranked storage as a “state” variable in combination with StorAge Selection (SAS) functions for streamflow and evapotranspiration to infer their respective travel time distributions (Harman, 2015; Rodriguez and Klaus, 2019; Rodriguez et al., 2021). This inference of transit times from water isotopes commonly implies a distinct relation between water age and its isotopic composition.

However, recent laboratory and field experiments suggest that this relation and the fate of water isotopes in the soil-plant-atmosphere system may in fact be more complex than frequently assumed. Mennekes et al. (2021), for example, used in situ probes to measure isotopic signatures of water in soil and tree xylem, during tracer irrigation experiments on the plot scale, and discussed that the travel times of water fractions in soils and plants may be distinctly different. This is in line with the findings of Benettin et al. (2021), who performed lysimeter experiments with isotopic-labelled waters to not only close, but also trace, all fluxes in the water balance. They found that the isotopic composition of transpiration fluxes was significantly different compared to breakthrough fluxes in soil drainage. On the pore scale, Orłowski and Breuer (2020) investigated how the isotopic composition of water depends on the retention characteristic of a soil. Their experimental results highlight “a need to better characterize processes that govern isotope fractionation with respect to soil water retention characteristics” because they found fractionation of $\delta^2\text{H}$ and $\delta^{18}\text{O}$ isotopes during their diffusive movement over different pore sizes, especially under high tensions in small pores. In this context, Bowers et al. (2020) performed an experiment using a combination of extraction methods to sample isotopically defined water fractions from a saturated soil sample over the complete water retention curve to explore how fast water isotopes ($\delta^2\text{H}$ and $\delta^{18}\text{O}$) mix diffusively over the entire pore size distribution. They showed that mixing and fractionation processes of water isotopes depend on different tensions at which water is held in pores of different size. The most interesting insight of the experiment was that the isotope tracer required up to

3-4 d until it was distributed uniformly over the entire pore space, even though the studied soil sample was only a few centimetres in length.

In particular, the experimental findings of Bowers et al. (2020) suggest that ignoring self-diffusion processes of water isotopes within the soil pore space can result in incorrect estimates of water ages and travel times, which emphasizes the requirement for including these pore-scale processes into soil hydrological models. Common soil hydrological models average over pore-size-dependent differences in the flow field and concentration gradients in control volumes (Berkowitz et al., 2016) to describe diffusive mixing of water and solutes. This implies that incoming “new” event water and “old” pockets of pre-event water in soil mix perfectly and instantaneously over the subscale pore size distribution in a single time step. This common perfect mixing assumption is, thus, not in line with the recent experimental findings (e.g. Bowers et al., 2020; Orłowski and Breuer, 2020). Further studies also have shown that these different pockets of water may indeed co-exist, even in close spatial distances, without perfect mixing and that water and solutes repeatedly travel through the same pathways (memory effect), even after several infiltration cycles of new precipitation (Gouet-Kaplan and Berkowitz, 2011; Kapetas et al., 2014). In this way, the establishment of stable water pockets in soils is possible, which may comprise significantly different isotopic and chemical compositions depending on the properties of infiltrating water. This imperfect mixing of water and solutes in the pore space is frequently discussed rather in the context of rapid preferential flow in macroporous structures (Beven and Germann, 1982; Beven and Germann, 2013), which is also commonly assumed to be the main reason for the characteristic steep rise and long tailing of corresponding breakthrough curves (e.g. Berkowitz et al., 2006; Edery et al., 2014). Based on the findings of Bowers et al. (2020), we hypothesize that imperfect mixing of water and solutes over the pore sizes of a macroscopically homogeneous and saturated soil matrix will also yield such typical shapes of breakthrough curves, even without the presence of macroporous soil structures.

To account for subscale diffusive mixing of solutes or water isotopes over pore sizes, in line with the findings of Bowers et al. (2020), we propose that the recent particle-based Lagrangian approaches (e.g. Berkowitz et al., 2006; Zehe and Jackisch, 2016; Jackisch and Zehe, 2018; Engdahl et al., 2017; Engdahl et al., 2019; Schmidt et al., 2019) offer a series of new possibilities in this regard. Zehe and Jackisch (2016) showed that the conceptualization of fluid flow in partially saturated soils as a Lagrangian advective-diffusive random walk of water particles is feasible for successfully reproducing observed soil water

dynamics and distinguishing explicitly pre-event and event waters. The key was to account for a variable, pore-size-dependent mobility of water particles, which was achieved by discretizing the pore space into pores of different sizes with specific hydraulic conductivities and water diffusivities (cf. Sect. 4.2.1). In follow-up studies (Sternagel et al., 2019; Sternagel et al., 2021), we extended this model approach and developed the Lagrangian Soil Water and Solute Transport (LAST) Model for simulations of (reactive) solute transport combined with water motion in heterogeneous, partially saturated 1-D soil domains. These former versions of the LAST-Model, however, assumed instantaneous, perfect mixing of solutes among water particles in a control volume, which implied that the model may have smoothed out concentration gradients too quickly (Sternagel et al., 2021).

In this study, we eliminate this perfect mixing assumption and introduce the diffusive pore mixing (DIPMI) approach to provide a Lagrangian method to improve our ability to describe diffusive mixing processes on the pore scale. The idea of DIPMI is to account for the self-diffusion of water particles across a characteristic length scale of the pore space using pore-size-dependent diffusion coefficients. Its model parameters can be derived from the soil-specific water retention curve, and no further calibration is needed. We initially test the DIPMI approach by simulating the experiment of Bowers et al. (2020), using the respective dataset. Furthermore, we implement the DIPMI approach into our LAST-Model framework and perform a virtual experiment to test our hypothesis. To this end, we simulate diffusive mixing and the breakthrough of a representative solute in a vertical 1-D soil column during a steady-state saturated flow and compare the results to simulations using the perfect mixing assumption.

4.2 LAGRANGIAN APPROACH FOR SOIL HYDROLOGICAL AND SUBSCALE DIFFUSION PROCESSES

4.2.1 *Underlying concept of the LAST-Model*

The Lagrangian perspective describes a mobile observer travelling along the trajectory of a fluid particle through a system (Currie, 2002). As mentioned above, we have applied the Lagrangian perspective before in our LAST-Model (Sternagel et al., 2019; Sternagel et al., 2021) to describe vertical displacement of water particles with related (reactive) solute transport in interacting domains of soil matrix and macropores. Water particles are defined discretely by constant water mass and volume. They additionally carry time-dependent information about, for example, their vertical position in both domains and solute concentrations. The two flow domains of soil matrix and macropores are vertically subdivided into layers. This vertical discretization is required to quantify and translate the number of water particles, in combination with the water particle mass and density, into a soil water content per vertical soil layer. The soil water content in turn corresponds to the sum of volume fractions of soil water, which are stored in soil pores of different sizes. Water particles travel at different velocities in these pore fractions that are characterized by the shape of the water diffusivity and hydraulic conductivity curve. These curves are partitioned into a certain number of pore size classes or bins (“binning”) between the residual and saturated water content. Depending on the pore size class/bin in which a water particle is located, it experiences different displacements in the vertical direction by means of pore-size-specific advection and diffusivity, i.e. water particles in smaller pores experience a smaller vertical displacement step than in coarser pores. Hence, this approach accounts for the combined effects of gravity and capillarity on water flow in partially saturated soils, as well as the subscale variability in flow velocities across different pore sizes (Zehe and Jackisch, 2016). However, in former versions of LAST (Sternagel et al., 2019; Sternagel et al., 2021), we assumed that the timescale for diffusive mixing is smaller than the simulation time step and hence, solutes perfectly and instantaneously mix over all pore size classes/bins in a soil layer. Thus, after the non-uniform, vertical movement of particles, solute concentrations were averaged over all present water particles within a vertical soil layer per time step (perfect mixing assumption). Furthermore, the LAST-Model allows for the simulation of sorption and degradation processes during the transport of reactive substances. Non-linear adsorption and desorption processes are realized by an explicit transfer of dissolved solute mass between water particles and surrounding sorption sites of the soil phase in a certain depth. Adsorbed solute masses are then degraded by means of first-order kinetics.

Previous test simulations revealed that the LAST-Model effectively describes solute concentration profiles and leaching behaviours of both conservative tracers and reactive substances, on the plot and field scale under various flow conditions. In particular, the structural macropore domain of LAST is an asset in the capturing of the typical pattern of preferential bypassing of solutes in macroporous soils. Despite these promising results, we also showed that our former assumption of perfect mixing of solutes within a vertical soil layer was a strong simplification that could lead to smoothing of pore-size-dependent differences in the flow field and concentration gradients, called over-mixing (Sternagel et al., 2021).

4.2.2 *The DIPMI approach: concept to represent subscale diffusion in a Lagrangian model*

In this study, we step beyond the use of the perfect mixing assumption by developing a Lagrangian approach to simulate self-diffusive mixing of water and solutes over the pore space. We explain this diffusive pore mixing (DIPMI) approach based on the schematic sketch in Fig. 4.1.

The rectangle in the left box at to schematically illustrates a control volume with height dz (e.g. a soil layer) of a 1-D vertical soil profile with total depth z . The width of this rectangle illustrates the entire subscale extent of pore space L_D in which fluid particles can move by self-diffusion. L_D represents a characteristic flow length in the pore space, which is related to tortuosity of flow paths, the subscale distribution of pore sizes and thus, to the soil-specific water retention curve (see right box at t_0). The extent of pore space L_D and the soil water retention curve are subdivided equally into a certain number N of bins i , which represents water storage in different pore size classes with corresponding matric potentials ψ . N generally depends on soil-specific properties (Talbot and Ogden, 2008; Ogden et al., 2017), and we assign $N = 200$. This value of N is in line with Talbot and Ogden (2008), who used a comparable method and suggested that the soil moisture domain of most soil types can be discretized sufficiently by 200 bins. Furthermore, Zehe and Jackisch (2016), who used a similar Lagrangian approach to simulate soil water dynamics, performed an analysis of the sensitivity of N and found that $N > 50$ is favourable for producing good simulation results compared to a Richards solver.

Based on the Young-Laplace equation and the subdivided (“binned”) soil water retention curve, we can determine the total subscale extent of the pore space L_D (L) by the integral (Eq. 4.2) over the correspond-

ing distribution of pore radii r_i (Eq. 4.1), as follows:

$$r_i = \frac{-2 \cdot \sigma}{g \cdot \rho \cdot \psi(i)}, \quad (4.1)$$

$$L_D = \int_{i=1}^N r_i, \quad (4.2)$$

where r_i (L) is the radius of a pore size class, σ (F L⁻¹) the surface tension of fluid, g (L T⁻²) the gravitational acceleration of the Earth, ρ (M L⁻³) the fluid density, $\psi(i)$ (L) the matric potential of a pore size class/bin, derived from the soil water retention curve. Hence, the Young-Laplace equation represents a connection between measurable matric potentials and corresponding pore radii of each pore size class.

Each bin is defined by a constant width $\delta L_D = L_D \cdot N^{-1}$ (L) and a corresponding location within L_D . In our example, each bin is saturated by fluid particles carrying two different isotopic signatures (illustrated by the green and dark yellow particles). These fluid particles have a position within L_D and accordingly, they are located within a certain bin ($i = 1 \dots N$). This means that, at t_0 , the pore space is filled by fluid particles with different isotopic signatures: coarse and medium pore size classes/bins (on the left) are filled by particles with one isotopic signature (green particles), while small pore size classes/bins (on the right) are filled by particles with another isotopic signature (dark yellow particles). Hence, fluid particles with different isotopic signatures are distinctly unmixed in the pore space before self-diffusive mixing starts at t_1 .

At t_1 , self-diffusive mixing of particles with different isotopic signatures begins. For each particle, a displacement step Δd_{LD} (L) along L_D is calculated using a random walk equation (Eq. 4.3), which is then subtracted from the current position of the particle.

$$\Delta d_{LD} = Z \sqrt{2 \cdot D(i) \cdot dt} - \left(\frac{\delta D(i)}{\delta L_D} \right), \quad (4.3)$$

where Z [-1,1] is a random number drawn from a standard normal distribution, $D(i)$ (L² T⁻¹) the diffusion coefficient in a certain bin or pore size class and dt (T) the time step. The last term $\frac{\delta D(i)}{\delta L_D}$ is a correction term to avoid artefacts in case of spatially variable diffusion coefficients (see explanation below).

The random number between -1 and 1 enables the displacement of particles in the positive as well as in the negative direction along

L_D , representing the undirected process of molecular self-diffusion due to Brownian motion. In this diffusion process, particles are not displaced by the same diffusion coefficient D . Depending on the bin or pore size class in which a particle is located, it experiences a specific diffusivity. Each bin/pore size class has its own $D(i)$ value, which is determined by its proportion on the total soil porosity (proportion factor), multiplied with the molecular diffusion coefficient of free water = $2.272 \times 10^{-9} \text{ m}^2 \text{ s}^{-1}$ (after Mills, 1973) (Eq. 4.4), as follows:

$$D(i) = 2.272 \times 10^{-9} \cdot \left(\frac{\theta(i) - \theta_r}{\phi} \right), \quad (4.4)$$

where the proportion factor comprises the respective water content of a specific bin $\theta(i)$ (-) according to the binning of the water retention curve (cf. Fig. 4.1), the residual water content θ_r (-) and the total soil porosity ϕ (-).

In this way, larger pores/bins have higher D values and thus, particles experience a larger diffusive displacement in these pores/bins, while particles in smaller pores/bins with lower D values experience a smaller diffusive displacement. This reflects the decline of the free path length for Brownian motions in smaller pores. With this approach of variable, pore-size-dependent diffusion coefficients, we account for the general controls on the diffusion rate in soil solution, e.g. the diffusion coefficient of a certain fluid or substance, pore size or water content and tortuosity of flow paths (Chou et al., 2012). With these variable diffusivities in pore size classes, we add a correction term $\frac{\delta D(i)}{\delta L_D}$ (Zehe and Jackisch, 2016) to the random walk equation (Eq. 4.3) to avoid artificial particle accumulation in the smallest pores/bins, as stated by Uffink (1990). The random number Z in Eq. 4.3 is either positive or negative and determines in this way in which direction a fluid particle is displaced along L_D , i.e. if it moves diffusively in the direction of smaller or coarser pore size classes/bins (minus-sign: in direction of coarse pores, plus-sign: in direction of small pores). At the same time, the correction term has a constant negative-sign and thus, the diffusive displacement steps Δd_{LD} of particles in the direction of coarse pores are enhanced, while they are diminished in the direction of smaller pores. In this way, calculated displacement step lengths of particles are corrected with different strength. The overall, greater displacement lengths of particles in coarser pores (due to higher D values) in the direction of smaller pores are balanced and, consequently, artificial particle accumulations in the smallest pores are prevented. According to its displacement step, a particle is assigned a new position within L_D , and if $\Delta d_{LD} > \delta L_D$, the particle is also assigned a new bin number. At the left and right boundary of the entire pore space L_D , particles are reflected into the pore space to

avoid particle accumulation at the boundaries.

Finally, after a certain mixing time t_2 , the pore space L_D in our example has reached a final equilibrium state with an uniform isotopic signature in all bins. The subscale separation (“binning”) of the pore space allows for the calculation of mixing concentrations in single bins or tension areas (i.e. certain number of adjacent bins/pore size classes within defined ranges of matric potentials).

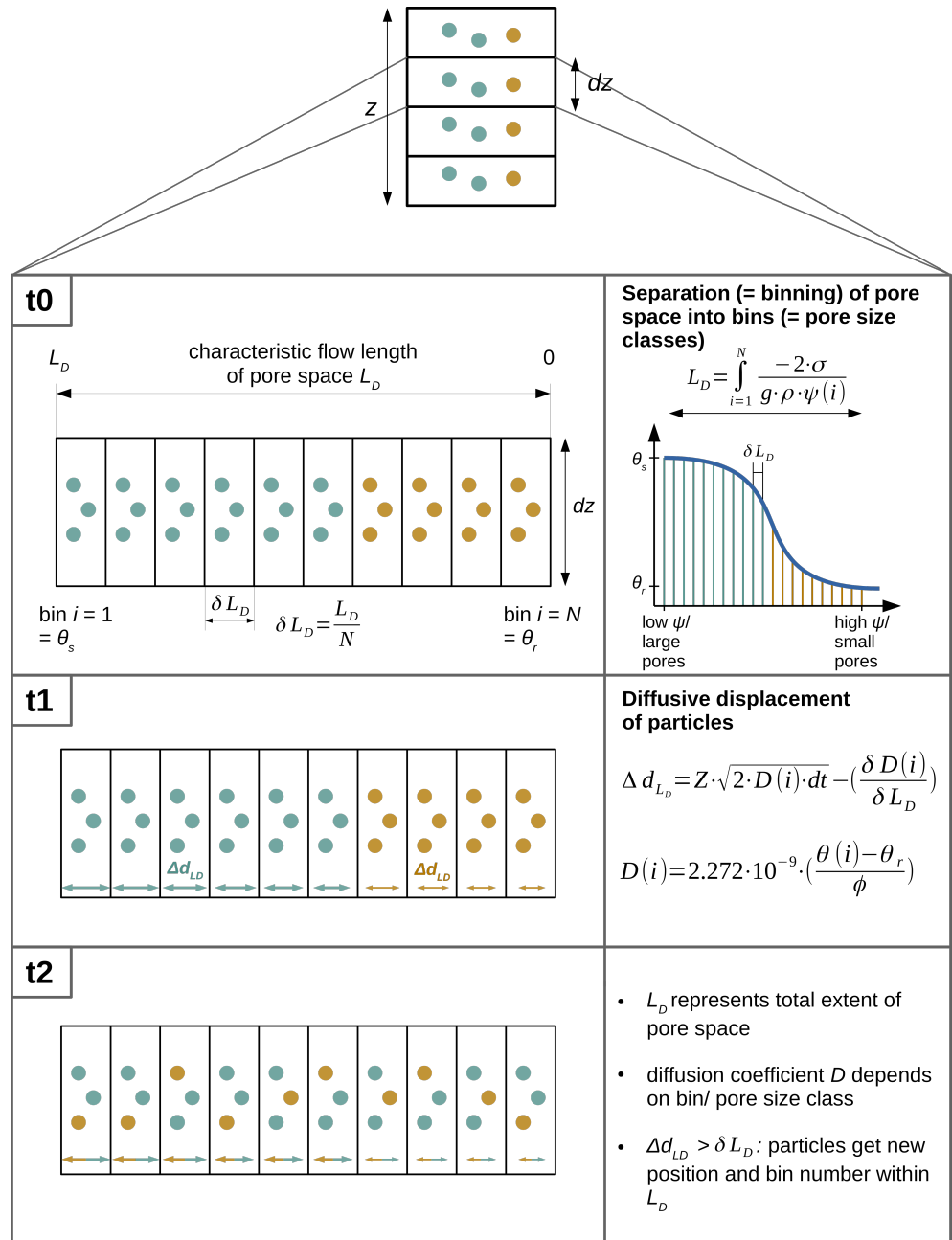


Figure 4.1: Schematic sketch of the diffusive pore mixing (DIPMI) approach. See descriptions of Eqs. 4.1-4.4 in Sect. 4.2.2 for further information on the parameters.

4.3 TESTING THE DIPMI APPROACH

We test our DIPMI approach by simulating the experiment of Bowers et al. (2020) with diffusive mixing of water isotopes over the pore space of a fully saturated soil volume. Furthermore, we perform a virtual experiment by simulating mixing and leaching processes of a representative solute in a vertical, saturated soil column, and compare results of the DIPMI approach against simulations that employ the common perfect mixing assumption.

4.3.1 *Simulating the experiment of Bowers et al. (2020)*

4.3.1.1 *Original experiment*

Bowers et al. (2020) used a combination of extraction methods to quantify time-dependent mixing of different water isotopes ($\delta^2\text{H}$ and $\delta^{18}\text{O}$) held at different tensions in fully saturated soil samples over the entire water retention curve. Their objective was to analyse how separate soil water fractions, stored in different pore sizes, interact by self-diffusion. They took oven-dried, homogenized soil samples (18-30 g) of a sandy loam (cf. Tab. 4.1) and initially wetted them with isotopically light water ($\delta^2\text{H} = -130 \text{ ‰}$ and $\delta^{18}\text{O} = -17.6 \text{ ‰}$) to a relative saturation of about 16-17 %. This water fraction represented an initial water content stored at high matric potentials in the smallest pores. The remaining free pore space was then completely saturated with isotopically heavy water ($\delta^2\text{H} = -44 \text{ ‰}$ and $\delta^{18}\text{O} = -7.8 \text{ ‰}$) representing new incoming water. Soil samples were then placed into horizontal cylinders and different equilibration time periods of 0 h, 8 h, 1 d, 3 d and 7 d were applied to enable mixing of the two isotopically distinct waters over the pore space by pure self-diffusion (no advection). After each time period, soil water samples were sequentially extracted from the soil samples at three subsequent tensions: (i) centrifugation at $\sim < 0.016 \text{ MPa}$ for waters in low-tension areas, (ii) centrifugation at $\sim 0.016 - 1.14 \text{ MPa}$ for waters in mid-tension areas, and finally (iii) cryogenic vacuum distillation (CVD) at 100 MPa to capture residual waters in high-tension areas ($\sim > 1.14 \text{ MPa}$). Isotopic compositions of extracted water samples were then analysed to assess differences between the diffusive mixing behaviour in the three tension areas over 7 d. All experimental data with detailed information about soil hydraulic properties of the sandy loam are freely accessible via an Open Science Framework (Bowers and Mercer, 2020).

4.3.1.2 *Simulation with the DIPMI approach*

For our simulations with the DIPMI approach, we assume a representative, saturated soil layer volume with the same soil hydraulic properties and soil water retention characteristics as the sandy loam

used by Bowers et al. (2020). From the given soil water retention curve in the study of Bowers et al. (2020), it is possible to infer the pore diameters corresponding to the respective matric potential ranges of the sandy loam (cf. Eq. 4.1, Sect. 4.2.2). The representative soil layer is defined only by the extent of the pore space L_D (cf. Sect. 4.2) and has no vertical extent, as we simulate pure diffusion over the pore space without any vertical displacement of particles in this case. For saturation of the pore space, we generally use the same saturation procedure but we do not use the pure isotopically light and heavy waters as in the experiments (cf. Sect. 4.3.1.1). Instead, we use the upper and lower standard deviation (SD) values of isotopic concentrations, which Bowers et al. (2020) measured after the first extraction time at 0 h. This is necessary to enable an equal initial condition of isotopic concentrations in simulations compared to observation; we thus perform simulations with differing initial isotopic values for light and heavy water (cf. Tab. 4.1). First, we use the upper SD values for light water ($\delta^2\text{H} = -79 \text{ ‰}$ and $\delta^{18}\text{O} = -9.3 \text{ ‰}$) and heavy water ($\delta^2\text{H} = -46 \text{ ‰}$ and $\delta^{18}\text{O} = -7.2 \text{ ‰}$). Second, we use the lower SD values for light water ($\delta^2\text{H} = -99 \text{ ‰}$ and $\delta^{18}\text{O} = -12.3 \text{ ‰}$) and heavy water ($\delta^2\text{H} = -48 \text{ ‰}$ and $\delta^{18}\text{O} = -7.8 \text{ ‰}$). After both simulation runs, isotopic concentrations are averaged over the respective tension areas at each time point, resulting in the mean and SD values of our simulations (cf. 4.2). We use given experimental data of the soil water retention curve and Eqs. 4.1 and 4.2 to quantify the total extent of pore space L_D of the soil volume by $21,000 \text{ }\mu\text{m}$ and subdivide it into 200 bins or pore size classes (cf. Sect. 4.2.2). Additionally, we repeat the simulations with the (i) constant diffusivity D of $2.272 \times 10^{-9} \text{ m}^2 \text{ s}^{-1}$ (diffusion coefficient of free water) in all bins, and (ii) linear pore-size-distributed diffusivities D over all bins calculated by Eq. 4.4 (cf. Sect. 4.2.2). Pore-size-distributed D values thus range from $\sim 1.9 \times 10^{-9} \text{ m}^2 \text{ s}^{-1}$ in bin 1 (i.e. largest pore in low-tension area) to $\sim 9.0 \times 10^{-9} \text{ m}^2 \text{ s}^{-1}$ in bin 200 (i.e. smallest pore in high-tension area). We do not distinguish between specific diffusion coefficients for $\delta^2\text{H}$ and $\delta^{18}\text{O}$, as Hasegawa et al. (2021) recently found generally equal diffusion properties of both isotopes in artificial and natural porous media.

We use a total of 10^5 particles, which corresponds to 500 particles per bin at full saturation. A high number of particles is needed to enable a stochastically valid random walk process (cf. Eq. 4.3) (Zehe and Jackisch, 2016). Initially, all particles are distributed randomly over all bins in L_D and thus, each particle is assigned an exact position and bin number within the pore space prior to the start of the mixing process. To saturate the pore space with the two isotopically distinct waters, we further initially define the particles in each bin that contain the isotopically light or heavy water concentrations. According to

the binning of the water retention curve (cf. Sect. 4.2.2), we identify that the bins 168-200 correspond to a relative saturation of 16-17 % (cf. Sect. 4.3.1.1). Thus, these bins are filled with particles carrying the light water concentration mimicking the initial water content stored at high matric potentials in the smallest pores. The residual bins 1-167 are filled accordingly with particles carrying the heavy water concentration representing new input water. Furthermore, we also link the three tension areas to bin numbers, with bins 1-143 as low-tension area, bins 144-177 as mid-tension area and bins 178-200 as high-tension area. Isotopic concentrations in these tension areas are calculated by averaging concentrations of all particles present in the corresponding bin numbers.

Table 4.1: Experimental and simulation parameters as well as soil hydraulic parameters (van Genuchten, 1980; Mualem, 1976) of sandy loam, where θ_s is the saturated soil water content, θ_r the residual soil water content, α the inverse of an air entry value, n a quantity characterizing pore size distribution.

Parameter	Value
Soil type	Sandy loam
θ_s ($m^3 m^{-3}$)	0.41
θ_r ($m^3 m^{-3}$)	0.065
α (m^{-1})	7.5
n (-)	1.89
Clay (%)	9
Silt (%)	32
Sand (%)	59
δ^2H (‰) of light water at $t = 0$ h	-89 ± 10
$\delta^{18}O$ (‰) of light water at $t = 0$ h	-10.8 ± 1.5
δ^2H (‰) of heavy water at $t = 0$ h	-47 ± 1
$\delta^{18}O$ (‰) of heavy water at $t = 0$ h	-7.5 ± 0.3
Low-tension area range (MPa)	$\sim < 0.016$ (bins 1-143, L_D : 21,000-5,985 μm)
Mid-tension area range (MPa)	$\sim 0.016 - 1.14$ (bins 144-177, L_D : 5,880-2,415 μm)
High-tension area range (MPa)	$\sim > 1.14$ (bins 178-200, L_D : 2,310-0 μm)
Simulation time step (s)	600
Total number of particles	10^5
Total number of bins	200
L_D (μm)	21,000
δL_D (μm)	105

4.3.2 *Setup of virtual experiment: simulating diffusive pore mixing and leaching of solute during steady state, saturated flow in a soil column*

The virtual experiment serves as an additional evaluation of the capability of the DIPMI approach to simulate pore-scale mixing in a more complex setting. We use the term virtual to emphasize that these numerical simulations do not rely on real, existing experiments, which is in contrast to the experiments of Bowers et al. (2020) in the first part of this study.

For the virtual experiment, we assume a vertical 1-D soil column of length $z = 1.0$ m, which is subdivided into vertical layers of $dz = 0.1$ m length (cf. top of Fig. 4.1). The (fully water-saturated) soil column contains the same, macroscopically homogeneous sandy loam with a saturated hydraulic conductivity K_s of 10^{-6} m s^{-1} , and has all other hydraulic properties and the definition of the three tension areas in each soil layer, as used in the experiment of Bowers et al. (2020). All other experimental and simulation parameters are also the same (cf. Tab. 4.1). Water particles initially located in the pore space of the surface soil layer (0-0.1 m) carry a concentration $C = 100$ M L^{-3} of a representative conservative solute, while water particles in the other (lower) soil layers carry a zero solute concentration. The soil column is then irrigated by pure water without any solute. A steady-state flow through the soil domain is established for 7 days driven by a free drainage condition at the bottom boundary, neglecting any evaporation effects at the soil-atmosphere interface. For the virtual experiment, the vertical displacement routine of LAST is used, assuming pure matrix flow without the influence of macropores or reactive transport processes (cf. Sect. 4.2.1, Zehe and Jackisch, 2016; Sternagel et al., 2019; Sternagel et al., 2021). It calculates a vertical displacement step, by means of advection and dispersion, for each fluid particle in all soil layers, starting from the bottom to the surface layer. Thus, a certain number of particles initially leaves the soil domain via the bottom boundary and to maintain the saturation state, missing numbers of particles in soil layers are gradually refilled by particles from overlying layers until the soil domain is, at the top, finally re-saturated by adding new event particles to the surface soil layer (steady state). The length of a vertical displacement step is therefore also dependent on the bin/pore size (cf. Sect. 4.2.1). Particles in coarse pores experience a larger vertical displacement than particles in smaller pores due to higher advective velocities and diminished capillary effects. Hence, particles in coarse pores/bins are more likely to travel into the next underlying soil layer.

We simulate this virtual experiment setup with our LAST-Model with (i) the DIPMI approach, with constant and pore-size-distributed

diffusivities D (cf. Sect. 4.2.2) over bins, respectively, and (ii) the common perfect mixing assumption used in the former versions of LAST (cf. Sect. 4.2.1, Sternagel et al., 2019; Sternagel et al., 2021).

4.4 RESULTS AND DISCUSSION

In Sects. 4.4.1 and 4.4.2, we present and discuss the results of the DIPMI simulations of the experiment of Bowers et al. (2020), followed by the presentation and discussion of the results of the virtual experiment in Sects. 4.4.3 and 4.4.4.

4.4.1 DIPMI simulations of the experiment of Bowers et al. (2020)

Tab. 4.2 contains the mean and standard deviation of isotopic concentrations in each tension area and time point for each simulation with constant and pore-size-distributed D values, respectively. Values highlighted in bold are within the measured standard deviation range of the experimental values of Bowers et al. (2020), which are additionally given. It is obvious that most of the simulated isotopic values are in accordance with the observation. Deviations mainly occur in the high-tension area after 8 h, as simulations over-predict the degree of mixing (i.e. mixing is too fast) in this high-tension area. All three tension areas require different times to reach a mean equilibrium concentration δ_e of around -54 ‰ for $\delta^2\text{H}$ and -8.0 ‰ for $\delta^{18}\text{O}$. These equilibrium concentrations are reached in the simulation with pore-size-distributed D values after (i) 8 h to 1 d in the low-tension area, (ii) \sim 1 d in the mid-tension area, and (iii) 3 d in the high-tension area. Thus, our DIPMI approach simulates complete isotope mixing somewhat faster than Bowers et al. (2020), who found that complete mixing is achieved after around 4 d. However, mixing times and isotopic concentrations of our simulations, with pore-size-distributed D values in particular, are generally consistent with the measured values. Comparing results of simulations with constant and pore-size-distributed D values reveal differences in the mid- and, especially, high-tension areas, while isotopic concentrations in the low-tension area are quite similar. All tension areas reach the equilibrium state already between 8 h and 1 d when simulating with constant D values in all bins.

Table 4.2: Mean and standard deviation of isotopic concentrations in each tension area and time point for simulation with constant (const.) and pore-size-distributed (distr.) D values, respectively. Bold values are within the standard deviation range of the measured values of Bowers et al. (2020).

Tension area	Time point	Mean $\delta^2\text{H}$ (‰)			Mean $\delta^{18}\text{O}$ (‰)		
		const. D	distr. D	Bowers	const. D	distr. D	Bowers
Low tension $\sim < 0.016$ MPa	0 h	-47 ± 1	-47 ± 1	-47 ± 1	-7.5 ± 0.3	-7.5 ± 0.3	-7.5 ± 0.3
	8 h	-53 ± 2	-50 ± 2	-53 ± 1	-8.0 ± 0.5	-7.7 ± 0.4	-7.8 ± 0.2
	1 d	-54 ± 3	-53 ± 3	-56 ± 1	-8.0 ± 0.5	-8.0 ± 0.5	-8.0 ± 0.2
	3 d	-54 ± 3	-54 ± 3	-56 ± 1	-8.0 ± 0.5	-8.0 ± 0.5	-7.8 ± 0
	7 d	-54 ± 3	-54 ± 3	-55 ± 1	-8.0 ± 0.5	-8.0 ± 0.5	-7.3 ± 0.3
Mid tension $\sim 0.016 - 1.14$ MPa	0 h	-59 ± 4	-59 ± 4	-65 ± 4	-8.5 ± 0.7	-8.5 ± 0.7	-9.2 ± 0.6
	8 h	-56 ± 4	-61 ± 4	-63 ± 5	-8.3 ± 0.5	-8.6 ± 0.7	-8.6 ± 0.4
	1 d	-55 ± 3	-57 ± 3	-60 ± 0	-8.1 ± 0.5	-8.3 ± 0.5	-8.3 ± 0.2
	3 d	-54 ± 2	-55 ± 3	-57 ± 1	-8.0 ± 0.5	-8.1 ± 0.6	-7.9 ± 0.2
	7 d	-54 ± 2	-54 ± 2	-55 ± 0	-8.0 ± 0.5	-8.1 ± 0.6	-7.0 ± 0.2
High tension $\sim > 1.14$ MPa	0 h	-89 ± 10	-89 ± 10	-89 ± 10	-10.8 ± 1.5	-10.8 ± 1.5	-10.8 ± 1.5
	8 h	-57 ± 3	-71 ± 6	-79 ± 3	-8.3 ± 0.5	-9.4 ± 1.0	-9.5 ± 0.4
	1 d	-55 ± 3	-60 ± 4	-72 ± 4	-8.1 ± 0.5	-8.5 ± 0.7	-8.4 ± 0.2
	3 d	-54 ± 3	-55 ± 3	-65 ± 2	-8.0 ± 0.5	-8.1 ± 0.5	-7.6 ± 0.6
	7 d	-54 ± 3	-54 ± 3	-62 ± 2	-8.0 ± 0.5	-8.1 ± 0.5	-6.5 ± 0.5

Additionally, Fig. 4.2 shows the isotopic concentrations, simulated with pore-size-distributed D values and the observations, for each tension area and time point in a dual-isotope space. The isotopic concentrations in the three tension areas gradually converge towards the mean equilibrium concentrations over time. Simulated concentrations in low- and mid-tension areas are in accordance with the observations, indicated by the overlapping of simulated and measured standard deviation ranges. An exception is the high-tension area, where measured isotopic concentrations of especially $\delta^2\text{H}$ have lower values compared to our simulations after 8 h; these findings show that the actual mixing process in the smallest pores is delayed. Furthermore, there are also differences between the two isotope species. For $\delta^{18}\text{O}$, simulated concentrations are consistent with the observations in all tension areas over the entire period, except the 7 d concentrations in the mid- and high-tension areas. However, these measured concentration values were unexpectedly high in the experiments of Bowers et al. (2020) as further discussed in Sect. 4.2.2. The value range of $\delta^{18}\text{O}$ is also generally larger compared to $\delta^2\text{H}$.

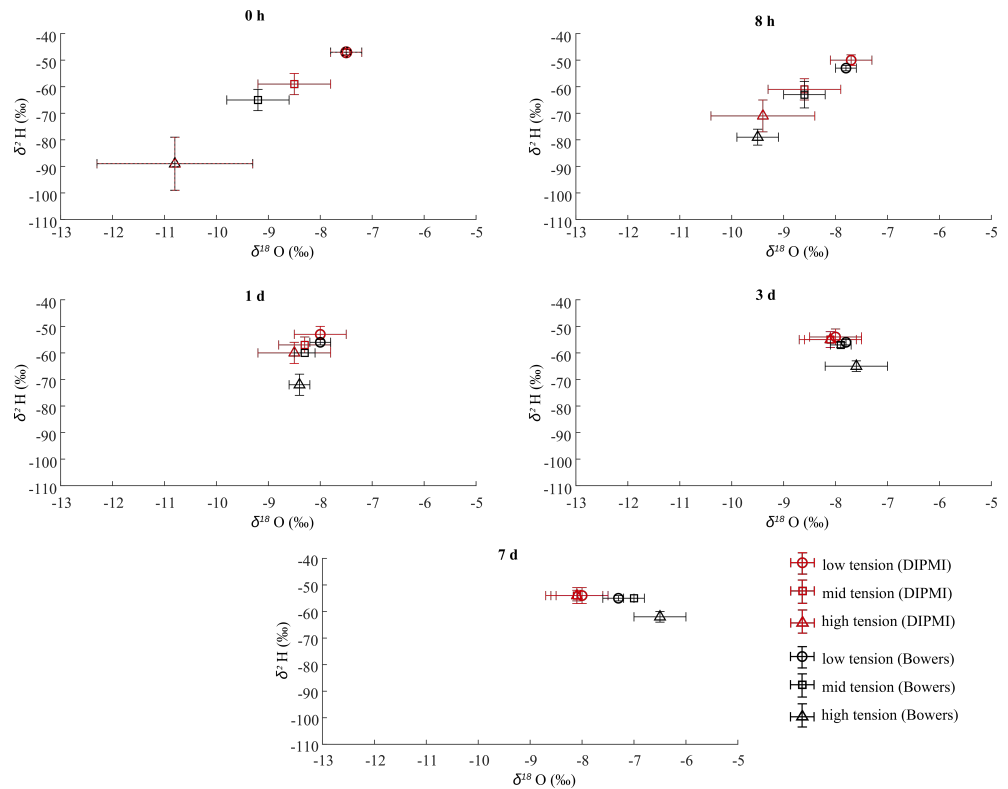


Figure 4.2: Isotopic concentrations in dual-isotope space for each tension area and time point, simulated (red) by the DIPMI approach with pore-size-distributed D values and measured (black) by Bowers et al. (2020). Note that at $t = 0$ h the simulated and measured isotopic values in the low- and high-tension areas are identical.

4.4.2 Analysis of simulations of the experiment of Bowers et al. (2020)

The simulation results (cf. Sect. 4.4.1) indicate that our diffusive pore mixing (DIPMI) approach is capable of reproducing the experiment of Bowers et al. (2020). The results in Sect. 4.4.1 show that our approach is suitable for (i) simulating the measured mixing time (~ 3 d) required to reach an equilibrium concentration δ_e in the entire pore space and (ii) resolving most of the isotopic concentrations in all tension areas with time (cf. Sect. 4.4.1, Tab. 4.2 and Fig. 4.2).

In general, the concept of DIPMI is consistent with other studies, which usually observe a lag time in isotopic mixing of waters stored initially in different pore sizes (e.g. Adams et al., 2020; Bowers et al., 2020; Orłowski and Breuer, 2020), proving that diffusive mixing over an entire pore space is far from being a perfect, instantaneous process, even on the (small) scale of a few centimetre long soil sample. A realistic description of diffusive mixing processes is especially crucial for interpreting studies examining origins of plant water (e.g. Sprenger et al., 2016; Penna et al., 2020), water ages (e.g. Hrachowitz et al.,

2013; Sprenger et al., 2019), travel times (e.g. Klaus et al., 2015; van der Velde et al., 2014) or even groundwater (e.g. Berkowitz et al., 2016).

Our calculated extent of $L_D = 21,000 \mu\text{m}$ (cf. Eqs. 4.1 and 4.2) appears to feasibly resolve the internal pore space of the sandy loam soil volume used in the experiment of Bowers et al. (2020). The distributed, bin-dependent diffusivities D (cf. Eq. 4.4) facilitate a realistic simulation of measured isotopic concentrations, which is superior to simulations with constant D values (cf. Tab. 4.2). The latter results in an over-prediction of the degree of mixing, which reaches the equilibrium state almost simultaneously in all tension areas after just 8 h to 1 d. A constant diffusivity of $2.272 \times 10^{-9} \text{ m}^2 \text{ s}^{-1}$ seems feasible only in coarser pores. The smaller a pore size class, the greater the capillary forces and friction caused by interactions between solid surfaces and the thin water layers directly adjacent to them. Both, capillary forces and friction, decrease significantly water movement in the smallest pores. This effect corroborates our calculation of pore-size-dependent diffusivities. However, D values in the high-tension area are still too high because measured concentrations are not matched to the same extent as for the case in the low- and mid-tension area. This implies that our approach still simulates overly strong mixing in the high-tension area.

The high-tension area of the water retention curve probably bears the highest uncertainty. In this area of the pore space, water is held at tensions $\gg 1.0 \text{ MPa}$ and is usually extracted by cryogenic vacuum distillation (CVD). This method, however, may be prone to producing artefacts when analysing isotopic concentrations of soil and plant water (Orlowski et al., 2013; Adams et al., 2020; Orlowski and Breuer, 2020; Allen and Kirchner, 2021). Beside possible uncertainties in the measurement procedure, specific subscale processes can be the reason for discrepancies between simulation and observation in the high-tension area. Bowers et al. (2020) suggested that interactions/adsorption of water ions with clay minerals within smaller pores can have a significant effect on the mixing behaviour. This might also be the reason for the discrepancies between simulated and measured $\delta^{18}\text{O}$ concentrations in mid- and high-tension areas after 3-7 d, as measured values are higher than expected as stated by Bowers et al. (2020). Such $\delta^{18}\text{O}$ enrichment was also reported in other studies (e.g. Oerter et al., 2014). Orlowski and Breuer (2020) further suggested that isotopic fractionation may occur during diffusive mixing, especially in high-tension areas. Reasons for such isotopic fractionations are difficult to define and in addition to adsorption effects, further subscale processes may play a role, such as adhesion or evaporation effects. Evaporation is often regarded as a main driver for isotopic fractionation, especially at the interface of the soil-atmosphere system

(Sprenger et al., 2016; Sprenger et al., 2018b). However, it may also result in a fractionation effect on the pore scale during the water extraction process in experimental studies when a phase change from liquid to gaseous occurs at the interface of saturated and unsaturated pores, which in turn may lead to vapour-pressure-controlled adsorption of water on soil surfaces (Lin and Horita, 2016; Lin et al., 2018).

Such detailed subscale processes are not incorporated specifically in the current version of our DIPMI approach. We focus on the abstraction of physical properties, which we think generally have the greatest influence on the diffusion process inside of soil domains, e.g. the diffusion coefficient of certain fluid or substance, distinct water pockets in soil pores of different sizes, and tortuosity of flow paths (Chou et al., 2012; Bowers et al., 2020). We lump these physical properties into the two main assets of our DIPMI approach, i.e. (i) the extent and characteristic flow length of the pore space L_D and the (ii) variable diffusivities D in different pore size classes, both of which can be directly derived from the soil water retention curve (cf. Sect. 4.2.2).

The results of Bowers et al. (2020) and our simulations both highlight that mixing processes in soils are by no means instantaneous or perfect, even in very small and fully saturated control volumes. Rather, the diffusive spreading of water depends on the pore size distribution and specific soil water retention properties. With this insight, it is of interest to examine, in the following virtual experiment (Sects. 4.3 and 4.4), how pore-size-dependent and non-instantaneous mixing affect simulations of water flow through a saturated soil column on a larger scale, and to delineate their effects on solute breakthrough and redistribution in soil.

4.4.3 *Simulation of the virtual experiment*

Solute breakthrough curves exhibit a clear difference between simulations with the DIPMI approach and the perfect mixing assumption (Fig. 4.3). Simulation with the perfect mixing assumption results in a breakthrough curve that is shaped like an approximately normal distribution with a concentration peak of 13 M L^{-3} after $\sim 42 \text{ h}$, followed by a sharp decrease converging a zero solute concentration after $\sim 105 \text{ h}$. Thus, all solute stored initially in the surface soil layer is eluted completely from the entire soil column by ~ 2.3 pore volumes, when simulation is performed with the perfect mixing assumption. In contrast, simulation with the DIPMI approach and constant D values results in a breakthrough curve that exhibits a right-skewed distribution. The peak concentration of $\sim 7 \text{ M L}^{-3}$ is reached after around 38 h and is followed by a long tailing of solute breakthrough, which converges the zero concentration only after 7 days, corresponding

to 3.5 pore volumes. Hence, significantly more time is required to elute all solute from the soil column. The simulation with the DIPMI approach and pore-size-distributed D values generally results in a breakthrough curve with a similar shape, as the breakthrough curve with constant D values, with comparable peak concentration and long tailing behaviour. However, it needs a shorter time to peak (~ 22 h) and the solute breakthrough tailing does not converge to zero concentration at all, not even after the simulation period of 7 d. Thus, more than 3.5 pore volumes are needed to leach all solute from soil in the case of pore-size-distributed D values.

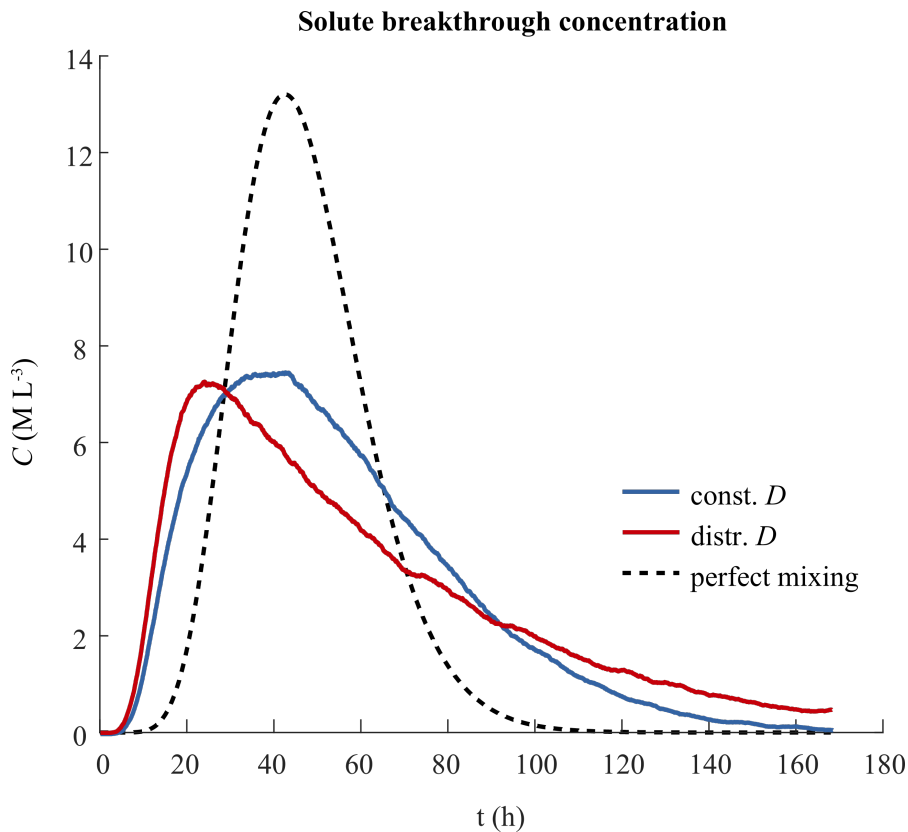


Figure 4.3: Solute breakthrough curves over 7 d, simulated with (i) the DIPMI approach and constant D (const.) values (blue), (ii) DIPMI approach and pore-size-distributed D (distr.) values (red), as well as (iii) the perfect mixing assumption (black).

Fig. 4.4 further shows the mean solute concentrations in the three tension areas per vertical soil layer at different points in time. Comparing the results of simulations with the DIPMI approach (with pore-size-distributed D values) and the perfect mixing assumption generally supports the previous insights of the breakthrough curves.

There is no difference in concentration between tension areas when using the perfect mixing assumption, as this approach averages solute

concentrations over the entire pore space of a soil layer (cf. Sect. 4.2.1). Consequently, solute gradually propagates, in the form of a fast wave, through all soil layers resulting in a complete elution of solute in all soil layers within the first 3-4 days. The results of the simulation with the DIPMI approach and pore-size-distributed D values exhibit a different and more heterogeneous picture (red shaded symbols and lines), especially regarding solute propagation behaviour and concentrations in different tension areas. Due to the imperfect mixing, a large fraction of solute preferentially propagates vertically through the low-tension areas (dark red) of the soil layers. This vertical leaching process is faster than the diffusive mixing over the tension areas within a soil layer, leading to the fast breakthrough of solute during the first 12 h (cf. Fig. 4.3). Hence, only smaller amounts of solute enter the mid- and high-tension areas (light red and orange) in deeper soil layers (0.1-1.0 m). In contrast, the initially solute-filled mid- and high-tension areas in the surface soil layer only release their solute slowly. This mechanism entails a retardation effect, which results in the persistence of solute in soil over the entire period of 7 d and the long breakthrough curve tailing with incomplete elution of solute (cf. Fig. 4.3).

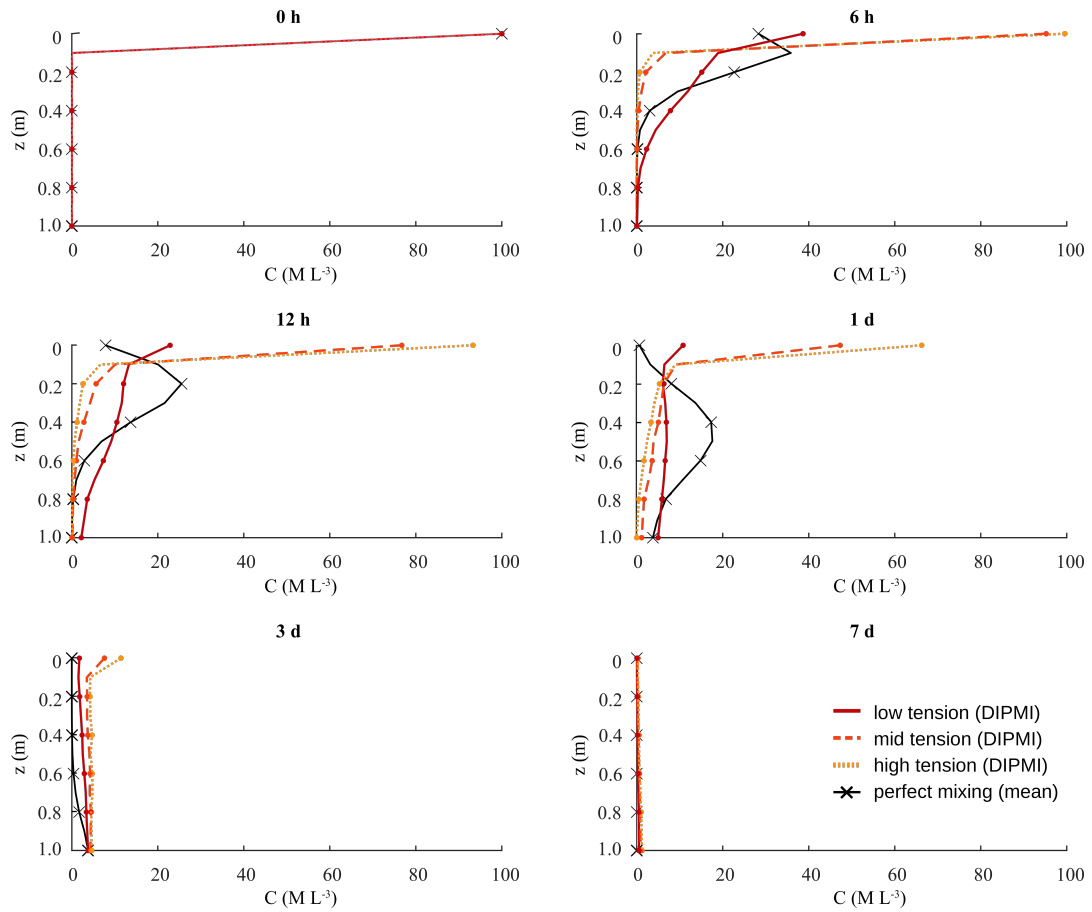


Figure 4.4: Vertical concentration profiles of a solute with mean concentrations in three tension areas over 7 d, simulated by the DIPMI approach with pore-size-distributed D values (red shades) and the perfect mixing assumption (black), respectively. Note that the black line and crosses illustrate the same mean concentration in all three tension areas per soil layer, as the perfect mixing assumption averages out pore-size-dependent differences.

4.4.4 *Analysis of the virtual experiment*

The use of the perfect mixing assumption shows two effects in our virtual experiment: (i) a longer time to first breakthrough and peak (cf. Fig. 4.3) and (ii) a steeper and shorter tailing of solute breakthrough concentration after the peak with a complete leaching of solute within 105 h (cf. Fig. 4.4). These effects can be explained by the fundamental assumption that solutes always perfectly and instantaneously mix over the entire pore space in each soil layer during passage of the soil domain. Consequently, solute spreads uniformly over the pore spaces of initially solute-free soil layers (0.1-1.0 m) before reaching the bottom boundary, which leads to dilution and the delayed breakthrough front arrival. Thereafter, the perfect and instantaneous mixing of pure infiltrating event water with solute-containing, pre-event water causes the rapid and complete elution of all solute, especially out of the surface soil layer, also with a relatively high peak concentration. These dilution and elution effects are characteristic of over-mixing phenomena (e.g. Green et al., 2002; Boso et al., 2013) and may be problematic for assessing the risk of contaminant leaching by potentially giving wrong predictions regarding breakthrough times and persistence in soil, for example.

Using the DIPMI approach with pore-size-distributed D values (cf. Eq. 4.4) for simulation of the virtual experiment bears opposite effects: (i) a faster initial breakthrough (cf. Fig. 4.3) and (ii) a long tailing of solute breakthrough concentration with an incomplete elution of solute (cf. Fig. 4.4). The timescale for diffusive mixing over pore sizes is significantly larger than the timescale for vertical transport of solute. This leads to an early arrival of the breakthrough front, as solute travels downward mainly through the pores of low-tension areas without spreading uniformly over soil layers. The smaller peak concentration and long tailing of the breakthrough curve are, thereafter, caused by a retardation effect of pores in the mid- and high-tension areas. These pores, with smaller diffusivities and higher capillary tensions, bind solute for a longer time (cf. Fig. 4.4) before they are mixed diffusively with pure infiltrating water and leached out. Regarding these effects, it is important to recall that the vertical displacement of fluid particles also depends on the different pore size classes/bins in our LAST-Model (cf. Sect. 4.2.1, Sternagel et al., 2019; Sternagel et al., 2021). Particles in coarse pores of low-tension areas are more mobile and displaced vertically by a higher advective velocity compared to particles in smaller pores. Consequently, water and solute flow mainly through these pores in low-tension areas, with a limited diffusive exchange with smaller pores and thus, the mid- and high-tension areas are essentially bypassed. This behaviour implies that the saturated flow system is dominated by preferential

bypassing flow through the low-tension area.

In the low-tension area, the mean D values of the constant D method ($2.272 \times 10^{-9} \text{ m}^2 \text{ s}^{-1}$) and the pore-size-distributed D method ($1.243 \times 10^{-9} \text{ m}^2 \text{ s}^{-1}$) are (relatively) similar, leading to breakthrough behaviours of both methods that are comparable in an early phase of breakthrough (cf. Fig. 4.3). However, the overall higher and constant D value causes a stronger leaching of retarded solute over time in later phases of breakthrough, especially from mid- and high-tension areas, with a complete elution after the period of 7 d. This implies that during early phases of fast, bulk leaching of solute the influence of pore-size-dependent diffusive mixing is less significant due to preferential bypassing. Nevertheless, pore-size-dependent diffusive mixing becomes highly relevant in later phases of the breakthrough when residual amounts of solute, stored and retarded in small pores, are gradually moved back into coarser pores by diffusive mixing with infiltrating water and hence, remobilized. Note that we perform our simulations in saturated media because in a fully saturated pore space, differences of the diffusivities between the largest, saturated pore size class and the smallest, saturated pore size class are more distinct than in a partially saturated pore space. Thus, simulations under saturated conditions are more suitable for highlighting the influence of diffusive mixing with pore-size-distributed D values, also in comparison to the use of constant D values and the perfect mixing assumption.

The breakthrough curves (cf. Fig. 4.3) also show the sensitivity of the DIPMI approach to variations of the diffusion coefficient value. The simulations are performed with significantly different D values in the setups with distributed (i.e. mean D of $9.7 \times 10^{-10} \text{ m}^2 \text{ s}^{-1}$) and constant (i.e. mean D of $2.272 \times 10^{-9} \text{ m}^2 \text{ s}^{-1}$) D values (i.e. range of 57 %), as well as with the instantaneous, perfect mixing assumption (i.e. infinite D of $10^\infty \text{ m}^2 \text{ s}^{-1}$). We can infer that (i) higher D values result in breakthrough curves with shorter tailings, which gradually approaches the shape of the curve of the perfect mixing assumption, the higher D values are; and (ii) smaller D values result in breakthrough curves with increasingly longer tailings. The latter situation is the case when simulating the diffusive spreading of common solute tracers (e.g. bromide or chloride) in porous media, because diffusion coefficients of the dissolved solute molecules are usually smaller compared to those of pure water or stable water isotopes (Hasegawa et al., 2021).

Overall, the results of the virtual experiment reveal a different behaviour in the solute leaching and redistribution in soil for simulation with the DIPMI approach, compared to simulations that invoke the perfect mixing assumption. In particular, the long tailing of breakthrough curves is in line with common observations of several

studies (e.g. Zinn and Harvey, 2003; Willmann et al., 2008; Edery et al., 2014). Zinn and Harvey (2003) linked the long tailing of breakthrough curves to mass transfer between regions of different mobility, e.g. pore size classes in different tension areas. Edery et al. (2014) also simulated solute breakthrough in saturated, porous media by a Lagrangian particle tracking approach. They showed that the broadness and tailing of breakthrough curves increase with a generally higher heterogeneity of pore space and flow paths. Our subdivision of the pore space into different pore size classes with pore-size-dependent diffusivities in the DIPMI approach is in line with this finding and adds, furthermore, an important aspect to account for imperfect subscale mixing in soil hydrological modelling.

Moreover, our results highlight that these typical shapes of breakthrough curves are not exclusively caused by explicit hydraulic (e.g. macropore flow) or chemical (e.g. adsorption and desorption) heterogeneity in soil, but that early breakthroughs and long tailing may also be a result of imperfect diffusive mixing within the pore space (Willmann et al., 2008), even when the flow domain is fully saturated and its soil properties are macroscopically homogeneous. Hence, we can verify our proposed hypothesis (cf. Sect. 4.1) and state that imperfect mixing across soil pores with different hydraulic properties within the soil matrix may entail an implicit heterogeneity of flow causing typical shapes of breakthrough curves, even in the absence of explicitly defined preferential flow paths.

4.5 CONCLUSIONS AND OUTLOOK

The main findings of this study are as follows:

- Simulation results show the feasibility of the DIPMI approach for reproducing the findings of the experiment of Bowers et al. (2020) by correctly capturing the measured diffusive mixing times and concentrations of water isotopes over the pore space of a fully saturated soil sample (cf. Sects. 4.4.1, 4.4.2).
- A virtual experiment highlights that imperfect mixing in a macroscopically homogeneous soil matrix can produce breakthrough patterns that are usually associated with preferential flow in heterogeneous soil structures such as macropores (cf. Sects. 4.4.1, 4.4.2).
- The DIPMI approach is physically based in the sense that its model parameters can be derived from the soil water retention curve, and no further calibration is needed (cf. Sect. 4.2.2).

In the future, in situ 1-D column experiments are planned to analyse the influence of the microstructure of partially saturated soils on the temporal and spatial mixing of isotopes over the pore space. The experimental results may provide a representative dataset serving as a reference to further extend and test the DIPMI approach, as comparable data on pore-scale mixing processes remain scarce.

Part V

SUMMARY AND DISCUSSION

In the following chapter, I condense the key findings and results I obtained in this thesis. Furthermore, I propose opportunities for further research and discuss the key findings and their general relevance for soil hydrological modelling.

SUMMARY AND DISCUSSION

5.1 CONCLUSIONS AND SUMMARY OF THE KEY FINDINGS

In the previous Sects. 2 – 4, I present the development of the LAST-Model framework. I describe how the model incorporates various soil hydrological processes to simulate preferential transport of (reactive) solutes and subscale diffusive mixing in the pore space. In the Sects. 5.1.1 – 5.1.4, I give a short summary of the key findings of the respective parts of my thesis and draw conclusions from these findings for soil hydrological modelling.

5.1.1 *Part II: Simulating preferential soil water flow and tracer transport using the Lagrangian Soil Water and Solute Transport Model*

The results of Sect. 2 reveal the feasibility of the LAST-Model to simulate well the redistribution of a solute tracer in the subsoil. Results are compared to observations and to simulation results of the HYDRUS 1-D model (based on the Darcy-Richards equation and the ADE). While LAST and HYDRUS perform equally well at sites with homogeneously structured soils (cf. Fig. 2.5), LAST better matches the observed tracer profile at sites with a heterogeneous soil structure and macropores (cf. Fig. 2.6). Solute accumulations in deeper soil layers are captured by the LAST-Model. The structural macropore domain allows for a rapid, matrix-bypassing flow of water and solutes, infiltrating the macropores at the soil surface and re-infiltrating the soil matrix in greater depths. The results of sensitivity analyses underpin the physical validity and robustness of the underlying model concept. They reveal the highest sensitivity of the model towards the soil hydraulic conductivity and to the depth-distribution of the macropore network (cf. Figs. 2.7 and 2.10).

First simulation successes of LAST.

Sensitivity analyses show the physical validity.

The key findings of Sect. 2 are:

- A main asset of LAST is the structural macropore domain with geometrically defined macropores and the explicit, vertically distributed exchange between the soil matrix and the macropore domain.
- The particle-based, Lagrangian approach is a novel concept to simulate water and solute dynamics as a coupled process. It is superior suitable to capture the patterns of preferential flow in comparison to a Darcy-Richards (+ ADE) model.

Structural macropore domain is key.

5.1.2 Part III: Simulation of reactive solute transport in the critical zone: a Lagrangian model for transient flow and preferential transport

Simulation of transport and leaching of reactive solutes.

The results of Sect. 3 highlight that the LAST-Model with the new reactive solute transport routine is capable to match the vertical mass distribution of two herbicides observed in natural soils. In line with the results of Sect. 2, the performances of LAST and the benchmark model HYDRUS 1-D are equal under homogeneous soil conditions (cf. Fig. 3.4). However, LAST reveals again advantages in the prediction of herbicide mass profiles in soils with macropores (cf. Fig. 3.5). A new insight is that LAST performs also well on larger spatial (field site) and temporal (several weeks) scales (cf. Fig. 3.7).

The key findings of Sect. 3 are:

Assets and drawbacks of LAST at simulating (reactive) solute transport.

- The reactive processes of retardation, degradation and remobilization have a significant impact on the preferential bypassing and the depth-accumulation of reactive solute masses. In this context, the Lagrangian approach with the structural macropore domain proves again its suitability for the correct simulation of heterogeneous transport dynamics.
- On larger time scales, simulation results reveal the occurrence of artificial over-mixing effects in the LAST-Model. Reason for that is the assumption of perfect diffusive mixing of solutes between water particles in a control volume. This may lead to the simulation of a too strong mixing and a smoothing of concentration gradients over the vertical soil profile (cf. Sect. 3.6.2; Green et al., 2002).

5.1.3 Part IV: Stepping beyond perfectly mixed conditions in soil hydrological modelling using a Lagrangian approach

DIPMI simulations of isotopic mixing and solute breakthrough.

The results of Sect. 4 highlight that the new routine for the simulation of diffusive pore mixing processes (DIPMI) produces more reasonable mixing behaviours than the previous perfect mixing assumption. The DIPMI approach is capable of reproducing the experimental results of Bowers et al. (2020). It simulates correctly (i) the measured mixing times needed to reach an equilibrium concentration over the pore space of a soil sample, and (ii) the concentrations of $\delta^2\text{H}$ and $\delta^{18}\text{O}$ isotopes in different tension areas (cf. Tab. 4.2 and Fig. 4.2). A virtual experiment reveals that solute breakthrough simulations with DIPMI generate more reliable breakthrough curve (BTC) shapes compared to ones simulated with the perfect mixing assumption.

The key findings of Sect. 4 are:

- The new DIPMI approach properly represents diffusive (imperfect) mixing processes on the pore scale. The approach is physically based as all model parameters can be derived from the soil water retention curve and no further calibration is needed.
- Pore-size-dependent, imperfect mixing of different water fractions over a macroscopically homogeneous soil matrix can cause non-uniform BTC shapes with steep rises and long tailings after peak (cf. Fig. 4.3). These shapes are commonly observed but usually associated with preferential flow in heterogeneous soil structures.

Imperfect mixing in homogeneous soils may have same effect on breakthrough like preferential flow.

5.1.4 What can we learn from these findings?

There are some essential lessons that we can learn from the key findings of this thesis for soil hydrological modelling in general:

- The particle approach allows to describe fluxes in and between the matrix and macropore domain by a consistent combination of physics and stochastic (statistical mechanics).
- A structural, physically defined macropore domain can benefit the simulation of preferential flow patterns. Flow in the macropore domain is driven by advection, independent from the capillary-flow conditions in the soil matrix. In principle, any kind of physical flow law could be applied to describe flow in the macropore domain, e.g. Stokes flow.
- Caution when applying the perfect mixing assumption in a soil hydrological model. Potential over-mixing phenomena must be considered in the model setup. They can be a significant source of simulation uncertainties and errors.
- Subscale pore processes matter. Diffusive mixing in the pore space has a crucial influence on macroscopic leaching behaviours and chemical/isotopic compositions of soil water fractions. This must be taken into account.

Lessons learned from the findings of this thesis.

5.2 OUTLOOK

In the following sections, I propose possibilities for extending the scope of the LAST-Model framework in future research. In Sect. 5.2.1, I discuss how the approach can be used to simulate water ages and related travel time distributions of different water fractions in the subsoil. In Sect. 5.2.2, I present ideas on model extensions for ecohydrological applications, such as simulating evapotranspiration and its associated pore-scale processes (e.g. root water uptake, capillary rise).

5.2.1 *Water ages and travel times*

*Hydrological focus
on water ages and
travel times.*

The quantification of ages and travel times of different water fractions in soils is crucial to assess the generation of runoff fluxes, groundwater recharge and rainfall-runoff responses of hydrological systems. The distribution of different water fractions reaching the outlet of a hydrological system reflects the internal hydraulic properties of the partially saturated soil zone as well as the spatio-temporal heterogeneities of flow paths and velocities. Over the last years, the focus of the hydrological research has been extended from simply quantifying the magnitude of rainfall-runoff responses to analysing the age and travel time distributions (TTD) of water fractions that contribute to runoff and storage in different hydrological compartments.

*Approaches for
describing travel
time distributions.*

Tracer experiments are a common tool to infer information about water ages and TTDs. They are, however, restricted to rather small spatio-temporal scales. For studies on larger scales, experiments need to be supported by the additional use of models. Many of these models comprise different stores to represent the different compartments of a hydrological system (e.g. soil water storage, groundwater aquifers, surface waters), and they are linked by water exchanges. The distribution of water ages and travel times in these linked storage elements can be derived from measured input-output relationships under different assumptions. Common assumptions use (i) steady-state conditions, applying a pre-defined, time-invariant distribution of travel times (McGuire and McDonnell, 2006) or (ii) StoreAge Selection (SAS) functions for time-variant, storage-volume-dependent distributions of travel times (Rinaldo et al., 2015). While these approaches have a more conceptual nature, the more physically based concepts of particle-tracking approaches particularly allow for a linking of TTDs with soil physical processes (e.g. Davies et al., 2013; Engdahl et al., 2016).

*LAST-Model: Age
tagging of particles
for simulating travel
times.*

In the LAST-Model framework, this can be realised by an age-tagging of water particles. In line with the tagging of particles with concentrations (cf. Sects. 2.2 and 4.2), a particle can carry a time through the system. When infiltrating the soil domain, a water particle gets the current simulation time as an age-tag. During its passage through the subsoil, a particle keeps its age-tag unchanged until it breaks through the outlet boundary of the domain. The difference between the individual breakthrough time and age gives the travel time of each particle. In this way, overall TTDs and average ages of different water storage fractions can be determined at each location and time.

The temporal entrapment of water particle fractions inside of local soil water pools, that are hydraulically detached from the main

flow area, can increase overall travel times. Preferential flow processes in contrast can decrease TTDs. To resolve these kinds of subscale processes in more detail, an extension of the LAST-Model framework to 2D would be an innovation step. The implementation of a second flow dimension is theoretically straightforward by assigning each particle a position in horizontal direction and solving the random walk equation a second time for displacements in horizontal direction. However, in practice an extension to 2D has the potential to cause unreasonable simulation times as a much higher number of total particles would be needed to resolve properly the random walk in two dimensions (cf. Jackisch and Zehe, 2018).

2D: Extending the spatial dimension of the LAST-Model.

5.2.2 Root water uptake for evapotranspiration

Evapotranspiration (ET) induces the upward transport of water out of the soil zone via capillary rise and plant root uptake. It is then released, in the form of water vapour, into the atmosphere at the interfaces of soil surfaces (evaporation) and plant surfaces (transpiration) (Dingman, 2015). Simulations of its associated subsoil processes (capillary rise, root water uptake) are an essential part of soil hydrological models. Common model approaches apply rather simple and coarsely resolved representations of these processes. Root water uptake is usually described macroscopically on the scale of a control volume, by adding an extraction/sink term to the Darcy-Richards equation that acts contrary to the main downward flux (Kutilek and Nielsen, 1994; Šimůnek et al., 2008). The extraction term is assumed to be a lumped representation of all microscale processes that are involved in the water uptake by plant roots and which cannot be resolved by these model approaches.

Only macroscopic representation of root water uptake in common models.

The concept of the LAST-Model, with its specific treatment of different pore size classes (cf. Sects. 2.2 and 4.2), allows for the consideration of root water uptake processes on the pore scale. It enables an exact process simulation from which regions and pore sizes plant roots extract water from the soil for transpiration:

Plants have a water potential that is similarly defined as the water potential in soils. Due to this water potential, plant roots have the ability to apply an underpressure to absorb water against gravity and the matric potential of the surrounding soil pores. If the water potential balance between plant roots and soil pores is in equilibrium, no water is extracted by the plant. The transpirational loss of water vapour via the leaf stomata induces a replacement water flux through the entire plant, with water being transferred from the roots to the leaves. Lower plant water contents lead to increased water potentials in the roots and ultimately, to the establishment of a potential gradient

The process of root water uptake on the pore scale.

between roots and soil. Along this gradient, a water flux from the soil into the roots develops, whereby the plant preferably extracts water from those soil pores that have the largest water supply and thus, the smallest matric potentials (energetic optimum). The quantification of this flux can be derived from Sap-flow measurement data or calculated by a mass-transfer equation driven by atmospheric conditions (Dingman, 2015).

Particles and pore sizes benefit the simulation of root water uptake with the LAST-Model.

For a realization in the LAST-Model, water fluxes from soil pores into plant roots are converted into corresponding particle numbers per time step. They are then removed out of these pore size classes that have the lowest matric potential at a given soil water content in a soil layer. The process can be further refined by assuming depth-dependent extraction intensities of plants following a depth-distribution of root densities. Removed particles are in the following not considered anymore for the processes in the soil domain. They are then part of a new flow continuum that describes the plant water flux from the roots to the leaves, where they are finally transpired. For the simulation of this flux, an explicit plant domain can be implemented into the model, which is independent but interacts with the soil domain (similar to the macropore domain). In this way, the entire sequence of the atmosphere-soil-plant interactions could be simulated (rainfall infiltration < leaching < root uptake < plant transport < transpiration).

The root uptake method could be in general extended from water to all kind of substances or information that roots can extract out of the soil solution, e.g. isotopic species, nutrients or even energies. The particle-based concept of LAST makes it possible to connect, and treat simultaneously, any number of information with a water particle.

5.3 DISCUSSION: WHY ARE DARCY-RICHARDS MODELS STILL PREFERABLY USED?

In Sect. 1.2.1, I introduce the limitations of the Darcy-Richards and ADE theory. Throughout the thesis, I present evidences that these common theories struggle to describe preferential flow and transport processes in heterogeneous soils. My findings are in accordance to other studies that provide alternative model concepts (cf. Sect. 1.2.1) and that doubt the applicability of Darcy-Richards models to more natural conditions (in the following, Darcy-Richards models = Darcy-Richards equation + ADE). In light of all these evidences and the existence of promising alternative model concepts, it raises the question: *Why are Darcy-Richards models still preferably used in physically based, soil hydrological modelling?*

Question: Reasons why Darcy-Richards models are still preferably used?

Possible reasons cannot only be found at the Darcy-Richards models

themselves but also at the new, alternative concepts. In the following, I go further into this question and discuss relevant aspects.

Reasons regarding the Darcy-Richards models

One reason is the historical evolution of the underlying Darcy-Richards equation. The experiment of Richards (1931) and the theoretical formulation of the equation have been highly recognized by the hydrological community at that time. In the following decades, the research mainly remained within the Darcy-Richards framework as the focus of soil hydrologists shifted away from questioning theoretical concepts (Beven, 2018). Only by the late 1980s, the topic of subsurface flow started to regain increased attention. An increasing number of experimental studies reported unexpectedly strong leaching of pollutants through soils into water bodies, which could not be predicted by models relying on the Darcy-Richards theory. As a consequence, soil hydrologists intensified the research on preferential flow processes and became aware of the theoretical limitation of the Darcy-Richards equation in these cases (Gish and Shirmohammadi, 1991). However, the quite long time period until this awareness emerged allowed for a strong manifestation of the theory in the minds of several generations of soil hydrologists.

Reason 1: Historical evolution and shifted research focus favoured manifestation of Darcy-Richards theory.

Instead of looking for a novel physical description, it is today tried to adapt and modify the Darcy-Richards + ADE approach to make it applicable to preferential flow. The applicability and functionality of Darcy-Richards models are more favoured than the general correctness of the underlying theory. In this context, dual-domain or dual-permeability models are frequently used. They assume two distinct domains for well-mixed matrix flow and preferential flow, respectively. Both domains are not explicitly defined in a geometrical, physical manner but they are characterized by different soil hydraulic properties. A specific fraction of water is assumed to move at the saturated hydraulic conductivity to represent preferential flow. The bulk fraction of matrix water is, at the same time, either assumed to be immobile or follows a smaller, soil-moisture-dependent conductivity. However, flow in both domains still relies on the Darcy-Richards equation and is hence mainly capillarity controlled. I have shown in this thesis that simulations with such a dual-approach (+ ADE) can account for an overall faster solute leaching, but the detailed heterogeneous patterns of vertical solute mass distributions are represented incompletely (cf. Sects. 2.4.3 and 3.5.2). Nevertheless, dual-models like MACRO (Jarvis and Larsbo, 2012) or HYDRUS (Šimůnek et al., 2008) are extensive and freely accessible model frameworks with user-friendly graphical interfaces. They comprise a broad range of application fields and for parameterization, several degrees of free-

Reason 2: Adapted dual-models are widespread and easy to use but still on the basis of Darcy-Richards theory.

dom allow for a rigorous calibration of model setups. Continuous developments have led to model codes that are performant and well documented. In this way, these dual-models are attractive for a broad range of users in research, economy and administration.

Reason 3: Often necessary to use Darcy-Richards models with simplifications for description of highly complex processes on larger scales.

The subject itself and its scale-dependency are other reasons for the widespread use of the Darcy-Richards models. A complete description of all the complex, interacting physical processes in the partially saturated zone is in fact only hardly realisable. In many cases, this would be also not reasonable as models should be entitled to balance necessary complexity with the highest possible simplicity (Zehe et al., 2014). While a complete process description is maybe useful on smaller plot or pore scales over a few hours to days (Bowers et al., 2020; Orłowski and Breuer, 2020), it is on larger scales (hillslope to catchment, months to years) only feasible in a more qualitative or lumped manner. Many subscale properties lose their importance for model quality or cannot be adequately parameterized on larger temporal and spatial scales (e.g. exact macropore geometries, preferential flow). To maintain efficiency, it is a crucial ability of many Darcy-Richards models (e.g. dual-permeability approaches) to simplify subscale processes for larger scales applications. This is an advantage compared to some alternative model concepts that are restricted to small scale applications as their physical sophistication may hinder an efficient use on larger temporal and spatial scales (e.g. Jackisch and Zehe, 2018).

Reasons regarding the new, alternative model concepts

Reason 4: New model concepts get lost in multitude of publications and stay invisible for community.

Further aspects can be found by focusing on the alternative model approaches and the modern hydrological research landscape in general. In line with almost every research discipline (Ioannidis et al., 2018), in hydrology the tendency is obvious that more and more studies are published in an ever increasing number of scientific journals. For a single researcher, it is nowadays almost impossible to survey completely the vast supply of publications and to identify relevant studies. This tendency leads to the effect that many of the newly proposed model concepts get lost in the multitude of publications. This makes it significantly difficult for them to become visible for a broad community. Without a network or an active promotion, even maybe by using social networks like Researchgate or Twitter, many studies and model concepts do not gain adequate attention. This lack of attention seems to be true even for a model approach of such a famous hydrologist like Peter F. Germann. Despite his great reputation in hydrology, his viscous film flow approach (Germann, 2018) seems to have also only minor impact on the community, which is indicated by relatively low citation numbers of the respective studies compared to his usual outreach. Addor and Melsen (2019) further argue that "the

legacy, rather than the adequacy, drives the selection of hydrological models". They found evidences for regional preferences in the model selection. Hydrologists obviously tend to use preferably models from their own affiliation, which they are experienced with, although external models may be more adequate in specific cases.

The lack of freely accessible digital materials (model codes, data, guidelines) complicates the public distribution of models. These additional materials are still not standardly provided with a model publication but often only available upon request. This reduces the chances that a model is ever used, or published results can be validated and reproduced by a third-party. If model codes are accessible, a proper organisation and documentation of the codes play further a decisive role whether a model is used or not. Especially for physical models, comprising a number of complex mathematical formulations and several degrees of freedom, the provision of a tutorial or manual may be inevitable for the application of new users. In this context, Stagge et al. (2019) developed a survey tool to check the availability of digital materials of published studies and the reproducibility of results. They found for 360 hydrology-related studies in 2017 that only 44 % provide any kind of digital materials at all. Only in 1.6 % of cases, results were reproducible using the provided materials.

Reason 5: Lack of freely accessible model codes and documentation.

The performance of a model is important for its usage. Well-coded and efficient models with short run times are favourable used. It allows users to try out models and to become acquainted with them. Physical soil hydrological models with a complicated, non-performant code structure can require several hours to days for simulation, even on smaller plot scales. This is inappropriate for testing multiple scenarios and thus, they may be less attractive than some easy-to-apply Darcy-Richards models.

Reason 6: Non-performant codes hinder users to become acquainted with models.

Conclusive remarks

In conclusion, there are some options that could help to improve the visibility and to strengthen the influence of new approaches in soil hydrological modelling:

- The establishment of a more rigorous validating of new model approaches. Testing several hypotheses and application cases, also with the option for a falsification of hypotheses, can strengthen the reliability of models. Many currently published models seem to be not properly evaluated but only statistically tested against one observation, which increases the vulnerability to error-prone measurements (Beven, 2010; Beven, 2018).
- The generation of a comprehensive database that contains several datasets from lysimeter and tracer experiments. Such a database

Suggestions for improving the shortcomings of new approaches.

could serve to validate and compare consistently soil hydrological models with standard benchmark tests. Similar evaluation databases already exist for hydro-meteorological and land surface models on larger scales, e.g. CAMELS (Newman et al., 2015) or PLUMBER (Best et al., 2015).

- The publication of one collective study instead of splitting it up to several small studies. This could help to decrease the large number of publications and to increase the visibility of single studies.
- The obligation to provide model codes and additional materials (data, documentations, simulation examples etc.) in a freely accessible online repository when publishing a model study.
- Active promotion of models. Besides the classical ways for presenting your work on scientific conferences and workshops, modern tools like social networks are promising for promotion and gaining outreach. It is also meaningful to include own model approaches into the teaching of students. They could perspectively transfer new ideas to future research and practice.

*Suggestions in terms
of LAST-Model.*

In terms of the LAST-Model framework, some of these suggestions are realised. Model codes and relevant data are provided on Github (Sternagel, 2022) and hypotheses are tested against several observations, benchmark models and sensitivity analyses. LAST is part of a student's exercise. However, the LAST-Model would benefit from further validations and a proper re-structuring of the code to make it more user-friendly.

If at all, it will probably still need several years to decades until real model alternatives become prevalent and challenge the Darcy-Richards models in the practice. This requires a renewed thinking of present hydrologists and the transfer of novel knowledge to the next generations of researchers. My thesis should be part of this knowledge transfer and serve as stimulus for future research on soil hydrological modelling.

Part VI

APPENDIX A

APPENDIX A

A.1 APPENDIX OF PART II

A.1: Further sensitivity analyses with time series

We performed additional sensitivity analyses to determine the effect of different k_s values and macropore diameters on the temporal development of the solute concentration profile. We moved the results of these time series to the Appendix as they generally provide no new insights but confirm the findings presented in the results section.

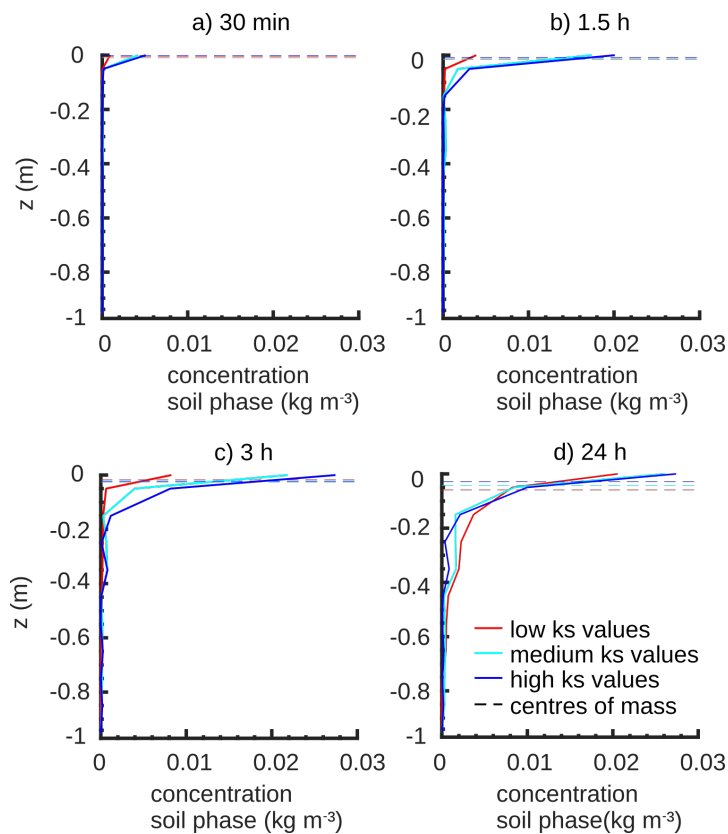


Figure A.1: Time series of bromide tracer concentration profiles and centres of mass at different k_s values during the rainfall event (a, b), shortly after it (c) and at the end of simulation (d).

Fig. A.1 generally confirms the findings of the sensitivity analyses with different k_s values (cf. Sect. 2.4.4.1). The four temporal snapshots show the development of the concentration profiles at low ($1 \times 10^{-6} \text{ m s}^{-1}$), medium ($2.5 \times 10^{-6} \text{ m s}^{-1}$) and high ($1 \times 10^{-5} \text{ m s}^{-1}$) k_s values

throughout the simulation time with (a) and (b) during the rainfall event and (c) and (d) shortly after it and after 1 d, respectively. It is obvious how rapidly solute concentrations increase, especially in the upper soil part at high k_s values. Shortly after the rainfall event almost all of the water and solute masses have infiltrated the matrix due to the higher infiltration capacity. At low k_s values, water and solutes notably need more time to infiltrate completely. The differences of the centres of mass and the deeper shift of the mass centre at low k_s values confirm the increased macropore infiltration and penetration of solutes through them to greater depths (cf. Fig. 2.7).

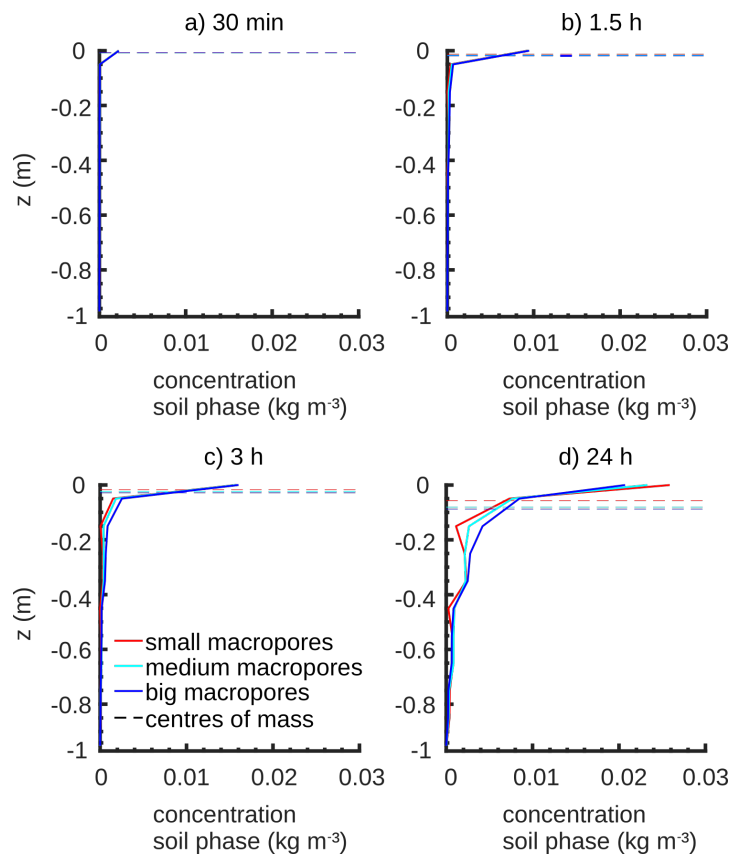


Figure A.2: Time series of bromide tracer concentration profiles and centres of mass at different macropore diameters (d_{mac}) during the rainfall event (a, b), shortly after it (c) and at the end of simulation (d).

Moreover, the temporal development of the concentrations is similar for all macropore diameters, with just marginal differences arising shortly after the rainfall event (Fig. A.2). While the macropore diameter has a minor influence in the initial phase, stronger differences occur at the end of the simulation when the residual water and solute amounts of the fictive surface storage have finally infiltrated. Thus, mainly at the end of the simulations the influence of the macropores on the infiltration and the macropore–matrix mixing processes are

remarkable, because the storage volume of the preferential flow domain is small and hence it can only collect small amounts of water and solutes in relation to the matrix domain. The centres of mass corroborate the results of Fig. 2.9a, b in a way that the big macropores have the tendency to transport more solute masses into the subsoil.

A.2 APPENDIX OF PART III

A 2: Detailed description of the macropore domain of LAST

The following descriptions and the equations in Tab. A.1 should complement the presentation of the macropore domain of LAST in Sect. 3.2.2.2 and Fig. 3.2 as well as serve to understand better the model theory. In this context, it is important to recall that we have already introduced the macropore domain of LAST in our previous study (Sternagel et al., 2019).

A 2.1: Structure of the macropore domain

LAST offers a structured macropore/preferential flow domain (pfd) consisting of a certain number of macropores. Each macropore has the shape and structure of a straight circular cylinder with a predefined length L_M (m) and diameter d_{mac} (m) containing spherically shaped particles (cf. Fig. 3.2a) (Sternagel et al., 2019). The parameterization of the preferential flow domain is based on observable field data, such as the mean numbers of macropores of certain diameters, their hydraulic properties, and length distribution. These structural data can be directly obtained from field observations or inverse modelling with tracer data but must not be spatially resolved because LAST operates on the 1-D scale. From these observable parameters, it is further possible to calculate additional pfd parameters like the total volume, stored water mass at saturation, the circumference C (m), and the flux rate. The total number of macropores at a study site is classified and distributed over three depth classes (big, medium, or small) to allow for a depth-dependent mass exchange with the matrix domain. To calculate water contents and tracer concentrations, the macropores of the pfd are vertically subdivided into grid elements of certain length dz_{pfd} (m). Similar to the matrix domain, water contents and solute concentrations are also regarded as averaged over these grid elements (Sternagel et al., 2019). Within a grid element of a macropore, a certain number of particles is packed, each having a mass and being geometrically defined by a diameter and volume. These properties can be derived from the total water mass and predefined number of maximum possible particles stored in a fully saturated macropore as well as the water density.

A 2.2: Infiltration and macropore filling

At the upper boundary of the soil domain a variable flux condition dependent on the incoming precipitation intensity prevails. First, the incoming precipitation water mass (m_{rain}) accumulates in a fictive surface storage from which, subsequently, infiltrating water masses into the matrix (m_{matrix}) and the pfd (m_{pfd}) and related particle numbers are calculated (cf. Eqs. A1–A3 in Tab. A.1). The presented equations refer to masses and not fluxes as LAST generally works with discrete particles and their masses. The actual water content and the flux densities of the topsoil control infiltration and distribution of water particles to both domains. The two processes are further determined by the matric potential gradient and hydraulic conductivity of the topsoil matrix (following principles of Darcy's law), together with the friction and gravity within the macropores. After the infiltration, macropores are filled from the bottom to the top, comparable to the filling of an empty bottle with water (cf. Fig. 3.2b), by assuming purely advective flow in the macropore domain as we assume a steady-state balance between gravity and dissipative energy loss by friction at the macropore walls. This advective macropore flow is determined by the hydraulic conductivity k_{pfd} ($m s^{-1}$) in a macropore. Zehe and Flühler (2001a) measured the velocity of water flow in undisturbed soil samples from the Weiherbach catchment (cf. Sect. 3.4.1) dominated by macropore influence. They found a clear proportionality of macropore flux rate and the square of macropore radius $\frac{d_{mac}}{2}$ (m), which can be described by a linear relationship. This leads to the calculation of k_{pfd} ($m s^{-1}$) (cf. Eq. A5 in Tab. A.1) under the assumption that the macropore flux rate and hydraulic conductivity as well as the advective velocity of a water particle in a macropore are equal as we presume purely gravity-driven flow.

A 2.3: Exchange between macropores and the matrix

Interactions at the interface between the pfd and the matrix with the exchange of water particles and thus also solutes are assumed to be mainly driven by matric potential gradients and hydraulic conductivity of both domains, which depend on an exchange length and flow velocities in the respective domains. We assume that exchange is only possible from the saturated parts/grid elements of the pfd into the matrix as it is expected that the purely advective downward flow of water in macropores is much larger than lateral exchange fluxes.

As described above, the total observed number of macropores n_{mac} at a study site is distributed over three depth classes. Hence, the total macropore number is multiplied by a distribution factor f for big (f_{big}), medium (f_{med}), and small (f_{sml}) macropores, respectively (cf. Fig. 3.2c). The saturated grid elements (blue filled squares in Fig. 3.2c)

of the respective three macropore classes are coupled due to their depth order. For instance, the red and black framed grid elements of the three macropore classes are respectively coupled because they are saturated and have the same position in depth order. The coupling thereby enables the simultaneous calculation of diffusive water fluxes q_{mix} (m s^{-1}) (cf. Eq. A4 in Tab. A.1) out of the respective grid elements of all three macropore classes.

In the current version, LAST works with a no-flow condition at the lower boundary of the pfd. For the lower matrix boundary, however, we actually assume a soil domain of 1.5 m length in total, which is larger than the soil space (0–1 m) we concentrate on in the simulations to avoid boundary effects. That means water particles may freely pass the lower boundary depth of 1 m.

Table A.1: Relevant LAST-Model equations and related parameters.

Name	Equation	Parameters
Eq. (A1): incoming precipitation mass m_{rain} (kg)	$m_{rain} = q_{rain} \cdot \rho_w \cdot \Delta t \cdot A$	q_{rain} (m s^{-1}): precipitation flux density; ρ_w (kg m^{-3}): water density; Δt (s): simulation time step; A (m^2): soil plot area
Eq. (A2): infiltrating water mass into matrix m_{matrix} (kg)	$m_{matrix} = \left(\frac{k_{m1} + k_s}{2} \right) \cdot \left(\frac{\psi_1 - \psi_2}{dz} + 1 \right) \cdot A \cdot \rho_w \cdot \Delta t$	k_{m1} (m s^{-1}): hydraulic conductivity of first matrix grid element; k_s (m s^{-1}): saturated hydraulic conductivity of matrix; $\psi_1 - \psi_2$ (m): matric potential difference between the surface and first matrix grid element; dz (m): matrix grid element length
Eq. (A3): infiltrating water mass into pfd m_{pfd} (kg)	$m_{pfd} = k_{pfd} \cdot \pi \cdot \left(\frac{d_{mac}}{2} \right)^2 \cdot \rho_w \cdot \Delta t \cdot n_{mac}$	k_{pfd} (m s^{-1}): hydraulic conductivity of a macropore; d_{mac} (m): diameter of a macropore; n_{mac} (-): total number of macropores within pfd
Eq. (A4): mixing flux between pfd and matrix q_{mix} (m s^{-1})	$q_{mix} = \frac{2 \cdot k_s \cdot k_{mi}}{k_s + k_{mi}} \cdot \frac{\psi_i}{d_{mac}} \cdot C \cdot dz_{pfd}$	k_s (m s^{-1}): saturated hydraulic conductivity of matrix; k_{mi} (m s^{-1}): current hydraulic conductivity of the respective matrix grid element; ψ_i (m): matric potential of the actual matrix grid element; d_{mac} (m): macropore diameter; C (m): circumference of a macropore grid element; dz_{pfd} (m): length of macropore grid element
Eq. (A5): hydraulic conductivity pfd k_{pfd} (m s^{-1})	$k_{pfd} = 2884.2 \cdot \left(\frac{d_{mac}}{2} \right)^2$	$\frac{d_{mac}}{2}$: macropore radius

BIBLIOGRAPHY

- Ackermann, M. (1998). "Hydrogeologische Systemanalyse und Grundwasserhaushalt des Weiherbach-Einzugsgebietes." PhD thesis. Karlsruhe, Germany: University of Karlsruhe.
- Adams, R. E. et al. (2020). "Bound and mobile soil water isotope ratios are affected by soil texture and mineralogy, whereas extraction method influences their measurement." In: *Hydrological Processes* 34.4, pp. 991–1003. DOI: [10.1002/hyp.13633](https://doi.org/10.1002/hyp.13633).
- Addor, N. and L. A. Melsen (2019). "Legacy, rather than adequacy, drives the selection of hydrological models." In: *Water resources research* 55.1, pp. 378–390. DOI: [10.1029/2018WR022958](https://doi.org/10.1029/2018WR022958).
- Allen, S. T. and J. W. Kirchner (2021). "Potential effects of cryogenic extraction biases on inferences drawn from xylem water deuterium isotope ratios: case studies using stable isotopes to infer plant water sources." In: *Hydrology and Earth System Sciences Discussions*, pp. 1–15. DOI: [10.5194/hess-2020-683](https://doi.org/10.5194/hess-2020-683).
- Arias-Estévez, M. et al. (2008). "The mobility and degradation of pesticides in soils and the pollution of groundwater resources." In: *Agriculture, Ecosystems & Environment* 123.4, pp. 247–260. DOI: [10.1016/j.agee.2007.07.011](https://doi.org/10.1016/j.agee.2007.07.011).
- Bear, J. (2013). *Dynamics of Fluids in Porous Media*. New York, USA: Courier Corporation.
- Bending, G. D. and M. S. Rodriguez-Cruz (2007). "Microbial aspects of the interaction between soil depth and biodegradation of the herbicide isoproturon." In: *Chemosphere* 66.4, pp. 664–671. DOI: [10.1016/j.chemosphere.2006.07.099](https://doi.org/10.1016/j.chemosphere.2006.07.099).
- Bending, G. D., E. Shaw, and A. Walker (2001). "Spatial heterogeneity in the metabolism and dynamics of isoproturon degrading microbial communities in soil." In: *Biology and Fertility of Soils* 33.6, pp. 484–489. DOI: [10.1007/s003740100356](https://doi.org/10.1007/s003740100356).
- Bending, G. D. et al. (2003). "In-Field Spatial Variability in the Degradation of the Phenyl-Urea Herbicide Isoproturon Is the Result of Interactions between Degradative *Sphingomonas* spp. and Soil pH." In: *Applied and Environmental Microbiology* 69.2, pp. 827–834. DOI: [10.1128/aem.69.2.827-834.2003](https://doi.org/10.1128/aem.69.2.827-834.2003).
- Benettin, P. et al. (2021). "Tracing and closing the water balance in a vegetated lysimeter." In: *Water Resources Research* 57.4. DOI: [10.1029/2020WR029049](https://doi.org/10.1029/2020WR029049).
- Berkowitz, B., A. Cortis, M. Dentz, and H. Scher (2006). "Modeling non-Fickian transport in geological formations as a continuous time random walk." In: *Reviews of Geophysics* 44.2. DOI: [10.1029/2005rg000178](https://doi.org/10.1029/2005rg000178).

- Berkowitz, B., I. Dror, S. K. Hansen, and H. Scher (2016). "Measurements and models of reactive transport in geological media." In: *Reviews of Geophysics* 54.4, pp. 930–986. DOI: [10.1002/2016rg000524](https://doi.org/10.1002/2016rg000524).
- Best, M. J. et al. (2015). "The plumbing of land surface models: benchmarking model performance." In: *Journal of Hydrometeorology* 16.3, pp. 1425–1442. DOI: [10.1175/JHM-D-14-0158.1](https://doi.org/10.1175/JHM-D-14-0158.1).
- Beven, K. J. and R. T. Clarke (1986). "On the Variation of Infiltration Into a Homogeneous Soil Matrix Containing a Population of Macropores." In: *Water Resources Research* 22.3, pp. 383–388. DOI: [10.1029/wr022i003p00383](https://doi.org/10.1029/wr022i003p00383).
- Beven, K. J. and P. Germann (1981). "Water Flow in soil macropores II. A combined flow model." In: *Journal of Soil Science* 32.1, pp. 15–29. DOI: [10.1111/j.1365-2389.1981.tb01682.x](https://doi.org/10.1111/j.1365-2389.1981.tb01682.x).
- Beven, K. J. and P. Germann (1982). "Macropores and water flow in soils." In: *Water Resources Research* 18.5, pp. 1311–1325. DOI: [10.1029/wr018i005p01311](https://doi.org/10.1029/wr018i005p01311).
- Beven, K. J. and P. Germann (2013). "Macropores and water flow in soils revisited." In: *Water Resources Research* 49.6, pp. 3071–3092. DOI: [10.1002/wrcr.20156](https://doi.org/10.1002/wrcr.20156).
- Beven, K. (2010). "Preferential flows and travel time distributions: defining adequate hypothesis tests for hydrological process models." In: *Hydrological Processes* 24.12, pp. 1537–1547. DOI: [10.1002/hyp.7718](https://doi.org/10.1002/hyp.7718).
- Beven, K. (2018). "A century of denial: Preferential and nonequilibrium water flow in soils, 1864-1984." In: *Vadose Zone Journal* 17.1, pp. 1–17. DOI: [10.2136/vzj2018.08.0153](https://doi.org/10.2136/vzj2018.08.0153).
- Binet, F. et al. (2006). "Lumbricid macrofauna alter atrazine mineralization and sorption in a silt loam soil." In: *Soil Biology and Biochemistry* 38.6, pp. 1255–1263. DOI: [10.1016/j.soilbio.2005.09.018](https://doi.org/10.1016/j.soilbio.2005.09.018).
- Blouin, M. et al. (2013). "A review of earthworm impact on soil function and ecosystem services." In: *European Journal of Soil Science* 64.2, pp. 161–182. DOI: [10.1111/ejss.12025](https://doi.org/10.1111/ejss.12025).
- Boivin, A., R. Cherrier, and M. Schiavon (2005). "A comparison of five pesticides adsorption and desorption processes in thirteen contrasting field soils." In: *Chemosphere* 61.5, pp. 668–676. DOI: [10.1016/j.chemosphere.2005.03.024](https://doi.org/10.1016/j.chemosphere.2005.03.024).
- Bolduan, R. and E. Zehe (2006). "Abbau von Isoproturon in Regenwurm-Makroporen und in der Unterbodenmatrix – Eine Feldstudie." In: *Journal of Plant Nutrition and Soil Science* 169.1, pp. 87–94. DOI: [10.1002/jpln.200521754](https://doi.org/10.1002/jpln.200521754).
- Bonell, M., A. J. Pearce, and M. K. Stewart (1990). "The identification of runoff-production mechanisms using environmental isotopes in a tussock grassland catchment, eastern Otago, New Zealand." In: *Hydrological Processes* 4.1, pp. 15–34. DOI: [10.1002/hyp.3360040103](https://doi.org/10.1002/hyp.3360040103).
- Boso, F., A. Bellin, and M. Dumbser (2013). "Numerical simulations of solute transport in highly heterogeneous formations: A com-

- parison of alternative numerical schemes." In: *Advances in Water Resources* 52, pp. 178–189. DOI: [10.1016/j.advwatres.2012.08.006](https://doi.org/10.1016/j.advwatres.2012.08.006).
- Bowers, W. H. and J. J. Mercer (2020). "A combination of soil water extraction methods quantifies the isotopic mixing of waters held at separate tensions in soil [data files and R code]." In: *Open Science Framework*. DOI: [10.17605/OSF.IO/ET3G5](https://doi.org/10.17605/OSF.IO/ET3G5).
- Bowers, W. H., J. J. Mercer, M. S. Pleasants, and D. G. Williams (2020). "A combination of soil water extraction methods quantifies the isotopic mixing of waters held at separate tensions in soil." In: *Hydrology and Earth System Sciences* 24.8, pp. 4045–4060. DOI: [10.5194/hess-24-4045-2020](https://doi.org/10.5194/hess-24-4045-2020).
- Buckingham, E. (1907). *Studies on the movement of soil moisture*. US Department of Agriculture.
- Bundt, M., F. Widmer, M. Pesaro, J. Zeyer, and P. Blaser (2001). "Preferential flow paths: biological 'hot spots' in soils." In: *Soil Biology and Biochemistry* 33.6, pp. 729–738. DOI: [10.1016/s0038-0717\(00\)00218-2](https://doi.org/10.1016/s0038-0717(00)00218-2).
- Bücker-Gittel, M., U. Mohrlock, and G. Jirka (2003). "Calibration and Reliability in Groundwater Modelling: A Few Steps Closer to Reality: Proceedings of the ModelCARE 2002 Conference: Held in Prague, Czech Republic." In: Wallingford, UK: IAHS Press. Chap. Modelling unsaturated water transport using a random walk approach, pp. 17–21.
- Carter, A. (2000). "How pesticides get into water - and proposed reduction measures." In: *Pesticide Outlook* 11.4, pp. 149–156. DOI: [10.1039/b006243j](https://doi.org/10.1039/b006243j).
- Chou, H., L. Wu, L. Zeng, and A. Chang (2012). "Evaluation of solute diffusion tortuosity factor models for variously saturated soils." In: *Water Resources Research* 48.10. DOI: [10.1029/2011WR011653](https://doi.org/10.1029/2011WR011653).
- Clay, S. A. and W. C. Koskinen (2002). "Effect of Variability of Soil Properties as a Function of Depth on Pesticide Sorption-Desorption." In: *ACS Symposium Series*. American Chemical Society, pp. 102–116. DOI: [10.1021/bk-2002-0842.ch008](https://doi.org/10.1021/bk-2002-0842.ch008).
- Cui, Z., C. Welty, and R. M. Maxwell (2014). "Modeling nitrogen transport and transformation in aquifers using a particle-tracking approach." In: *Computers & Geosciences* 70, pp. 1–14. DOI: [10.1016/j.cageo.2014.05.005](https://doi.org/10.1016/j.cageo.2014.05.005).
- Currie, I.G. (2002). *Fundamental Mechanics of Fluids*. Boca Raton, USA: CRC Press.
- Davies, J. and K. J. Beven (2012). "Comparison of a Multiple Interacting Pathways model with a classical kinematic wave subsurface flow solution." In: *Hydrological Sciences Journal* 57.2, pp. 203–216. DOI: [10.1080/02626667.2011.645476](https://doi.org/10.1080/02626667.2011.645476).
- Davies, J., K. J. Beven, A. Rodhe, L. Nyberg, and K. Bishop (2013). "Integrated modeling of flow and residence times at the catchment

- scale with multiple interacting pathways." In: *Water Resources Research* 49.8, pp. 4738–4750. DOI: [10.1002/wrcr.20377](https://doi.org/10.1002/wrcr.20377).
- De Jonge, L. W., P. Moldrup, G. H. Rubaek, K. Schelde, and J. Djurhuus (2004). "Particle Leaching and Particle-Facilitated Transport of Phosphorus at Field Scale." In: *Vadose Zone Journal* 3.2, pp. 462–470. DOI: [10.2136/vzj2004.0462](https://doi.org/10.2136/vzj2004.0462).
- Dechesne, A., N. Badawi, J. Amand, and B. F. Smets (2014). "Fine scale spatial variability of microbial pesticide degradation in soil: scales, controlling factors, and implications." In: *Frontiers in Microbiology* 5. DOI: [10.3389/fmicb.2014.00667](https://doi.org/10.3389/fmicb.2014.00667).
- Delay, F. and J. Bodin (2001). "Time domain random walk method to simulate transport by advection-dispersion and matrix diffusion in fracture networks." In: *Geophysical Research Letters* 28.21, pp. 4051–4054. DOI: [10.1029/2001gl013698](https://doi.org/10.1029/2001gl013698).
- Dentz M., J. J. Hidalgo and D. Lester (2022). "Mixing in Porous Media: Concepts and Approaches Across Scales." In: *Transport in Porous Media*, pp. 1–49. DOI: [10.1007/s11242-022-01852-x](https://doi.org/10.1007/s11242-022-01852-x).
- Dingman, S. L. (2015). *Physical hydrology*. Long Grove, USA: Waveland press.
- Dubus, I. G., C. D. Brown, and S. Beulke (2003). "Sources of uncertainty in pesticide fate modelling." In: *Science of The Total Environment* 317.1-3, pp. 53–72. DOI: [10.1016/s0048-9697\(03\)00362-0](https://doi.org/10.1016/s0048-9697(03)00362-0).
- Dusek, J. et al. (2015). "Transport of bromide and pesticides through an undisturbed soil column: A modeling study with global optimization analysis." In: *Journal of Contaminant Hydrology* 175-176, pp. 1–16. DOI: [10.1016/j.jconhyd.2015.02.002](https://doi.org/10.1016/j.jconhyd.2015.02.002).
- Edery, Y., A. Guadagnini, H. Scher, and B. Berkowitz (2014). "Origins of anomalous transport in heterogeneous media: Structural and dynamic controls." In: *Water Resources Research* 50.2, pp. 1490–1505. DOI: [10.1002/2013WR015111](https://doi.org/10.1002/2013WR015111).
- Eilers, K. G., S. Debenport, S. Anderson, and N. Fierer (2012). "Digging deeper to find unique microbial communities: The strong effect of depth on the structure of bacterial and archaeal communities in soil." In: *Soil Biology and Biochemistry* 50, pp. 58–65. DOI: [10.1016/j.soilbio.2012.03.011](https://doi.org/10.1016/j.soilbio.2012.03.011).
- El-Sebai, T., B. Lagacherie, J. F. Cooper, G. Soulas, and F. Martin-Laurent (2005). "Enhanced isotopuron mineralisation in a clay silt loam agricultural soil." In: *Agronomy for Sustainable Development* 25.2, pp. 271–277. DOI: [10.1051/agro:2005003](https://doi.org/10.1051/agro:2005003).
- Engdahl, N. B., D. A. Benson, and D. Bolster (2017). "Lagrangian simulation of mixing and reactions in complex geochemical systems." In: *Water Resources Research* 53.4, pp. 3513–3522. DOI: [10.1002/2017wr020362](https://doi.org/10.1002/2017wr020362).
- Engdahl, N. B., J. L. McCallum, and A. Massoudieh (2016). "Transient age distributions in subsurface hydrologic systems." In: *Journal of Hydrology* 543, pp. 88–100. DOI: [10.1016/j.jhydrol.2016.04.066](https://doi.org/10.1016/j.jhydrol.2016.04.066).

- Engdahl, N. B., M. J. Schmidt, and D. A. Benson (2019). "Accelerating and Parallelizing Lagrangian Simulations of Mixing-Limited Reactive Transport." In: *Water Resources Research* 55.4, pp. 3556–3566. DOI: [10.1029/2018wr024361](https://doi.org/10.1029/2018wr024361).
- Ewen, J. (1996a). "'SAMP' model for water and solute movement in unsaturated porous media involving thermodynamic subsystems and moving packets: 2. Design and application." In: *Journal of Hydrology* 182.1-4, pp. 195–207. DOI: [10.1016/0022-1694\(95\)02926-5](https://doi.org/10.1016/0022-1694(95)02926-5).
- Ewen, J. (1996b). "'SAMP' model for water and solute movement in unsaturated porous media involving thermodynamic subsystems and moving packets: 1. Theory." In: *Journal of Hydrology* 182.1-4, pp. 175–194. DOI: [10.1016/0022-1694\(95\)02925-7](https://doi.org/10.1016/0022-1694(95)02925-7).
- Farenhorst, A. (2006). "Importance of Soil Organic Matter Fractions in Soil-Landscape and Regional Assessments of Pesticide Sorption and Leaching in Soil." In: *Soil Science Society of America Journal* 70.3, pp. 1005–1012. DOI: [10.2136/sssaj2005.0158](https://doi.org/10.2136/sssaj2005.0158).
- Flury, M. (1996). "Experimental Evidence of Transport of Pesticides through Field Soils—A Review." In: *Journal of Environmental Quality* 25.1, pp. 25–45. DOI: [10.2134/jeq1996.00472425002500010005x](https://doi.org/10.2134/jeq1996.00472425002500010005x).
- Flury, M., H. Flühler, W. A. Jury, and J. Leuenberger (1994). "Susceptibility of soils to preferential flow of water: A field study." In: *Water Resources Research* 30.7, pp. 1945–1954. DOI: [10.1029/94wr00871](https://doi.org/10.1029/94wr00871).
- Fomsgaard, I. S. (1995). "Degradation of Pesticides in Subsurface Soils, Unsaturated Zone—a Review Of Methods and Results." In: *International Journal of Environmental Analytical Chemistry* 58.1-4, pp. 231–245. DOI: [10.1080/03067319508033127](https://doi.org/10.1080/03067319508033127).
- Frey, M. P., M. K. Schneider, A. Dietzel, P. Reichert, and C. Stamm (2009). "Predicting critical source areas for diffuse herbicide losses to surface waters: Role of connectivity and boundary conditions." In: *Journal of Hydrology* 365.1-2, pp. 23–36. DOI: [10.1016/j.jhydrol.2008.11.015](https://doi.org/10.1016/j.jhydrol.2008.11.015).
- Gassmann, M. et al. (2013). "Model-based estimation of pesticides and transformation products and their export pathways in a headwater catchment." In: *Hydrology and Earth System Sciences* 17.12, pp. 5213–5228. DOI: [10.5194/hess-17-5213-2013](https://doi.org/10.5194/hess-17-5213-2013).
- Gerke, H. H. (2006). "Preferential flow descriptions for structured soils." In: *Journal of Plant Nutrition and Soil Science* 169.3, pp. 382–400. DOI: [10.1002/jpln.200521955](https://doi.org/10.1002/jpln.200521955).
- Gerke, H. H. and M. Th. van Genuchten (1993). "A dual-porosity model for simulating the preferential movement of water and solutes in structured porous media." In: *Water Resources Research* 29.2, pp. 305–319. DOI: [10.1029/92wr02339](https://doi.org/10.1029/92wr02339).
- Germann, P. (2018). *Preferential Flow – Stokes Approach to Infiltration and Drainage*. Bern, Switzerland: Geographica Bernensia, University of Bern.

- Gill, H. K. and H. Garg (2014). "Pesticides: Environmental Impacts and Management Strategies." In: *Pesticides - Toxic Aspects*. Ed. by M. L. Larramendy and S. Soloneski. Rijeka, Croatia: InTechOpen. DOI: [10.5772/57399](https://doi.org/10.5772/57399).
- Gish, T. J. and A. Shirmohammadi (1991). *Preferential flow: proceedings of the national symposium: 16-17 December 1991, Chicago, Illinois*. American Society of Agricultural Engineers.
- Gouet-Kaplan, M. and B. Berkowitz (2011). "Measurements of interactions between resident and infiltrating water in a lattice micro-model." In: *Vadose Zone Journal* 10.2, pp. 624–633. DOI: [10.2136/vzj2010.0103](https://doi.org/10.2136/vzj2010.0103).
- Green, C. T., E. M. LaBolle, G. E. Fogg, and C. Davis (2002). "Randomwalk particle tracking for simulating reactive transport in heterogeneous aquifers: effects of concentration averaging." In: *Proceedings of the International Groundwater Symposium, International Association of Hydraulic Research and American Geophysical Union, 25-28 March 2002*. Berkeley, California, USA, pp. 446–450.
- Hansen, S. K. and B. Berkowitz (2020). "Modeling Non-Fickian Solute Transport Due to Mass Transfer and Physical Heterogeneity on Arbitrary Groundwater Velocity Fields." In: *Water Resources Research* 56.10. DOI: [10.1029/2019wr026868](https://doi.org/10.1029/2019wr026868).
- Harman, C. J. (2015). "Time-variable transit time distributions and transport: Theory and application to storage-dependent transport of chloride in a watershed." In: *Water Resources Research* 51.1, pp. 1–30. DOI: [10.1002/2014wr015707](https://doi.org/10.1002/2014wr015707).
- Hasegawa, T., K. Nakata, and R. Gwynne (2021). "Measurement on Diffusion Coefficients and Isotope Fractionation Factors by a Through-Diffusion Experiment." In: *Minerals* 11.2, 208. DOI: [10.3390/min11020208](https://doi.org/10.3390/min11020208).
- Haws, N. W., P. S. C. Rao, J. Simunek, and I. C. Poyer (2005). "Single-porosity and dual-porosity modeling of water flow and solute transport in subsurface-drained fields using effective field-scale parameters." In: *Journal of Hydrology* 313.3-4, pp. 257–273. DOI: [10.1016/j.jhydrol.2005.03.035](https://doi.org/10.1016/j.jhydrol.2005.03.035).
- Holden, P. A. and N. Fierer (2005). "Microbial Processes in the Vadose Zone." In: *Vadose Zone Journal* 4.1, pp. 1–21. DOI: [10.2113/4.1.1](https://doi.org/10.2113/4.1.1).
- Hrachowitz, M., H. Savenije, T. A. Bogaard, D. Tetzlaff, and C. Soulsby (2013). "What can flux tracking teach us about water age distribution patterns and their temporal dynamics?" In: *Hydrology and Earth System Sciences* 17.2, pp. 533–564. DOI: [10.5194/hess-17-533-2013](https://doi.org/10.5194/hess-17-533-2013).
- Ioannidis, J., R. Klavans, and K. W. Boyack (2018). "Thousands of scientists publish a paper every five days." In: *Nature* 561(7722), pp. 167–169. DOI: [10.1038/d41586-018-06185-8](https://doi.org/10.1038/d41586-018-06185-8).

- Jackisch, C. and E. Zehe (2018). "Ecohydrological particle model based on representative domains." In: *Hydrology and Earth System Sciences* 22.7, pp. 3639–3662. DOI: [10.5194/hess-22-3639-2018](https://doi.org/10.5194/hess-22-3639-2018).
- Jarvis, N. J. (2007). "A review of non-equilibrium water flow and solute transport in soil macropores: principles, controlling factors and consequences for water quality." In: *European Journal of Soil Science* 58.3, pp. 523–546. DOI: [10.1111/j.1365-2389.2007.00915.x](https://doi.org/10.1111/j.1365-2389.2007.00915.x).
- Jarvis, N. and M. Larsbo (2012). "MACRO (v5.2): Model Use, Calibration, and Validation." In: *Transactions of the ASABE* 55.4, pp. 1413–1423. DOI: [10.13031/2013.42251](https://doi.org/10.13031/2013.42251).
- Jensen, P. H., H. C. B. Hansen, J. Rasmussen, and O. S. Jacobsen (2004). "Sorption-Controlled Degradation Kinetics of MCPA in Soil." In: *Environmental Science & Technology* 38.24, pp. 6662–6668. DOI: [10.1021/es0494095](https://doi.org/10.1021/es0494095).
- Kapetas, L., I. Dror, and B. Berkowitz (2014). "Evidence of preferential path formation and path memory effect during successive infiltration and drainage cycles in uniform sand columns." In: *Journal of contaminant hydrology* 165, pp. 1–10. DOI: [10.1016/j.jconhyd.2014.06.016](https://doi.org/10.1016/j.jconhyd.2014.06.016).
- Klaus, J., K. P. Chun, K. J. McGuire, and J. J. McDonnell (2015). "Temporal dynamics of catchment transit times from stable isotope data." In: *Water Resources Research* 51.6, pp. 4208–4223. DOI: [10.1002/2014wr016247](https://doi.org/10.1002/2014wr016247).
- Klaus, J. and J. J. McDonnell (2013). "Hydrograph separation using stable isotopes: Review and evaluation." In: *Journal of hydrology* 505, pp. 47–64. DOI: [10.1016/j.jhydrol.2013.09.006](https://doi.org/10.1016/j.jhydrol.2013.09.006).
- Klaus, J. and E. Zehe (2010). "Modelling rapid flow response of a tile-drained field site using a 2D physically based model: assessment of 'equifinal' model setups." In: *Hydrological Processes* 24.12, pp. 1595–1609. DOI: [10.1002/hyp.7687](https://doi.org/10.1002/hyp.7687).
- Klaus, J. and E. Zehe (2011). "A novel explicit approach to model bromide and pesticide transport in connected soil structures." In: *Hydrology and Earth System Sciences* 15.7, pp. 2127–2144. DOI: [10.5194/hess-15-2127-2011](https://doi.org/10.5194/hess-15-2127-2011).
- Klaus, J., E. Zehe, M. Elsner, C. Külls, and J. J. McDonnell (2013). "Macropore flow of old water revisited: experimental insights from a tile-drained hillslope." In: *Hydrology and Earth System Sciences* 17.1, pp. 103–118. DOI: [10.5194/hess-17-103-2013](https://doi.org/10.5194/hess-17-103-2013).
- Klaus, J. et al. (2014). "Controls of event-based pesticide leaching in natural soils: A systematic study based on replicated field scale irrigation experiments." In: *Journal of Hydrology* 512, pp. 528–539. DOI: [10.1016/j.jhydrol.2014.03.020](https://doi.org/10.1016/j.jhydrol.2014.03.020).
- Knabner, P., K. U. Totsche, and I. Kögel-Knabner (1996). "The modeling of reactive solute transport with sorption to mobile and immobile sorbents: 1. Experimental evidence and model development."

- In: *Water Resources Research* 32.6, pp. 1611–1622. DOI: [10.1029/95wr02994](https://doi.org/10.1029/95wr02994).
- Koutsoyiannis, D. (2010). “HESS Opinions ”A random walk on water”.” In: *Hydrology and Earth System Sciences* 14.3, pp. 585–601. DOI: [10.5194/hess-14-585-2010](https://doi.org/10.5194/hess-14-585-2010).
- Kutílek, M. and D. R. Nielsen (1994). *Soil hydrology*. Cremlingen-Destedt, Germany: Catena-Verlag.
- Köhne, J. M., S. Köhne, and J. Šimůnek (2009a). “A review of model applications for structured soils: a) Water flow and tracer transport.” In: *Journal of Contaminant Hydrology* 104.1-4, pp. 4–35. DOI: [10.1016/j.jconhyd.2008.10.002](https://doi.org/10.1016/j.jconhyd.2008.10.002).
- Köhne, J. M., S. Köhne, and J. Šimůnek (2009b). “A review of model applications for structured soils: b) Pesticide transport.” In: *Journal of Contaminant Hydrology* 104.1-4, pp. 36–60. DOI: [10.1016/j.jconhyd.2008.10.003](https://doi.org/10.1016/j.jconhyd.2008.10.003).
- Leistra, M. (1977). “A model for the transport of pesticides in soil with diffusion-controlled rates of adsorption and desorption.” In: *Agriculture and Environment* 3.4, pp. 325–335. DOI: [10.1016/0304-1131\(77\)90028-5](https://doi.org/10.1016/0304-1131(77)90028-5).
- Lewis, K. A., J. Tzilivakis, D. J. Warner, and A. Green (2016). “An international database for pesticide risk assessments and management.” In: *Human and Ecological Risk Assessment: An International Journal* 22.4, pp. 1050–1064. DOI: [10.1080/10807039.2015.1133242](https://doi.org/10.1080/10807039.2015.1133242).
- Liess, M., R. Schulz, M.H.-D. Liess, B. Rother, and R. Kreuzig (1999). “Determination of insecticide contamination in agricultural headwater streams.” In: *Water Research* 33.1, pp. 239–247. DOI: [10.1016/s0043-1354\(98\)00174-2](https://doi.org/10.1016/s0043-1354(98)00174-2).
- Lin, Y. and J. Horita (2016). “An experimental study on isotope fractionation in a mesoporous silica-water system with implications for vadose-zone hydrology.” In: *Geochimica et Cosmochimica Acta* 184, pp. 257–271. DOI: [10.1016/j.gca.2016.04.029](https://doi.org/10.1016/j.gca.2016.04.029).
- Lin, Y., J. Horita, and O. Abe (2018). “Adsorption isotope effects of water on mesoporous silica and alumina with implications for the land-vegetation-atmosphere system.” In: *Geochimica et Cosmochimica Acta* 223, pp. 520–536. DOI: [10.1016/j.gca.2017.12.021](https://doi.org/10.1016/j.gca.2017.12.021).
- Liu, Y.-J., A. Zaprasis, S.-J. Liu, H. L. Drake, and M. A. Horn (2010). “The earthworm *Aporrectodea caliginosa* stimulates abundance and activity of phenoxyalkanoic acid herbicide degraders.” In: *The ISME Journal* 5.3, pp. 473–485. DOI: [10.1038/ismej.2010.140](https://doi.org/10.1038/ismej.2010.140).
- Loritz, R. et al. (2017). “Picturing and modeling catchments by representative hillslopes.” In: *Hydrology and Earth System Sciences* 21.2, pp. 1225–1249. DOI: [10.5194/hess-21-1225-2017](https://doi.org/10.5194/hess-21-1225-2017).
- McGlynn, B. L. and J. Seibert (2003). “Distributed assessment of contributing area and riparian buffering along stream networks.” In: *Water resources research* 39.4. DOI: [10.1029/2002WR001521](https://doi.org/10.1029/2002WR001521).

- McGlynn, B., J. McDonnell, M. Stewart, and J. Seibert (2003). "On the relationships between catchment scale and streamwater mean residence time." In: *Hydrological Processes* 17.1, pp. 175–181. DOI: [10.1002/hyp.5085](https://doi.org/10.1002/hyp.5085).
- McGuire, K. J. and J. J. McDonnell (2006). "A review and evaluation of catchment transit time modeling." In: *Journal of Hydrology* 330.3-4, pp. 543–563. DOI: [10.1016/j.jhydrol.2006.04.020](https://doi.org/10.1016/j.jhydrol.2006.04.020).
- Mennekes, D., M. Rinderer, S. Seeger, and N. Orłowski (2021). "Ecohydrological travel times derived from in situ stable water isotope measurements in trees during a semi-controlled pot experiment." In: *Hydrology and Earth System Sciences* 25.8, pp. 4513–4530. DOI: [10.5194/hess-25-4513-2021](https://doi.org/10.5194/hess-25-4513-2021).
- Mills, R. (1973). "Self-diffusion in normal and heavy water in the range 1-45. deg." In: *The Journal of Physical Chemistry* 77.5, pp. 685–688.
- Mualem, Y. (1976). "A new model for predicting the hydraulic conductivity of unsaturated porous media." In: *Water Resources Research* 12.3, pp. 513–522. DOI: [10.1029/wr012i003p00513](https://doi.org/10.1029/wr012i003p00513).
- Nadezhdina, N. et al. (2010). "Trees never rest: the multiple facets of hydraulic redistribution." In: *Ecohydrology* 3.4, pp. 431–444. DOI: [10.1002/eco.148](https://doi.org/10.1002/eco.148).
- Neuweiler I., D. Erdal and M. Dentz (2012). "A non-local Richards equation to model unsaturated flow in highly heterogeneous media under nonequilibrium pressure conditions." In: *Vadose Zone Journal* 11.3. DOI: [10.2136/vzj2011.0132](https://doi.org/10.2136/vzj2011.0132).
- Newman, A. J. et al. (2015). "Development of a large-sample watershed-scale hydrometeorological data set for the contiguous USA: data set characteristics and assessment of regional variability in hydrologic model performance." In: *Hydrology and Earth System Sciences* 19.1, pp. 209–223. DOI: [10.5194/hess-19-209-2015](https://doi.org/10.5194/hess-19-209-2015).
- Nimmo, J. R. (2016). "Quantitative Framework for Preferential Flow Initiation and Partitioning." In: *Vadose Zone Journal* 15.2, pp. 1–12. DOI: [10.2136/vzj2015.05.0079](https://doi.org/10.2136/vzj2015.05.0079).
- Oerter, E. et al. (2014). "Oxygen isotope fractionation effects in soil water via interaction with cations (Mg, Ca, K, Na) adsorbed to phyllosilicate clay minerals." In: *Journal of Hydrology* 515, pp. 1–9. DOI: [10.1016/j.jhydrol.2014.04.029](https://doi.org/10.1016/j.jhydrol.2014.04.029).
- Ogden, F. L. et al. (2017). "The soil moisture velocity equation." In: *Journal of Advances in Modeling Earth Systems* 9.2, pp. 1473–1487. DOI: [10.1002/2017MS000931](https://doi.org/10.1002/2017MS000931).
- Orłowski, N. and L. Breuer (2020). "Sampling soil water along the pF curve for $\delta^2\text{H}$ and $\delta^{18}\text{O}$ analysis." In: *Hydrological Processes* 34.25, pp. 4959–4972. DOI: [10.1002/hyp.13916](https://doi.org/10.1002/hyp.13916).
- Orłowski, N., H.-G. Frede, N. Brüggemann, and L. Breuer (2013). "Validation and application of a cryogenic vacuum extraction system for soil and plant water extraction for isotope analysis."

- In: *Journal of Sensors and Sensor Systems* 2.2, pp. 179–193. DOI: [10.5194/jsss-2-179-2013](https://doi.org/10.5194/jsss-2-179-2013).
- Palm, J., L. van Schaik, and B. Schröder (2013). “Modelling distribution patterns of anecic, epigeic and endogeic earthworms at catchment-scale in agro-ecosystems.” In: *Pedobiologia* 56.1, pp. 23–31. DOI: [10.1016/j.pedobi.2012.08.007](https://doi.org/10.1016/j.pedobi.2012.08.007).
- Penna, D., J. Geris, L. Hopp, and F. Scandellari (2020). “Water sources for root water uptake: Using stable isotopes of hydrogen and oxygen as a research tool in agricultural and agroforestry systems.” In: *Agriculture, Ecosystems & Environment* 291, 106790. DOI: [10.1016/j.agee.2019.106790](https://doi.org/10.1016/j.agee.2019.106790).
- Pimentel, D. et al. (1992). “Environmental and Economic Costs of Pesticide Use.” In: *BioScience* 42.10, pp. 750–760. DOI: [10.2307/1311994](https://doi.org/10.2307/1311994).
- Plate, E. J. and E. Zehe (2008). *Hydrologie und Stoffdynamik kleiner Einzugsgebiete. Prozesse und Modelle*. Stuttgart, Germany: Schweizerbart.
- Radcliffe, D. E. and J. Simunek (2010). *Soil Physics with HYDRUS. Modelling and applications*. Boca Raton, USA: CRC Press.
- Richards, L. A. (1931). “Capillary conduction of liquids through porous mediums.” In: *Physics* 1.5, pp. 318–333. DOI: [10.1063/1.1745010](https://doi.org/10.1063/1.1745010).
- Rinaldo, A. et al. (2015). “Storage selection functions: A coherent framework for quantifying how catchments store and release water and solutes.” In: *Water Resources Research* 51.6, pp. 4840–4847. DOI: [10.1002/2015WR017273](https://doi.org/10.1002/2015WR017273).
- Risken, H. (1984). *The Fokker-Planck Equation*. Berlin, Germany: Springer.
- Rodríguez-Cruz, M. S., J. Jones, and G. D. Bending (2006). “Field-scale study of the variability in pesticide biodegradation with soil depth and its relationship with soil characteristics.” In: *Soil Biology and Biochemistry* 38.9, pp. 2910–2918. DOI: [10.1016/j.soilbio.2006.04.051](https://doi.org/10.1016/j.soilbio.2006.04.051).
- Rodríguez, N. B. and J. Klaus (2019). “Catchment travel times from composite StorAge Selection functions representing the superposition of streamflow generation processes.” In: *Water Resources Research* 55.11, pp. 9292–9314. DOI: [10.1029/2019WR024973](https://doi.org/10.1029/2019WR024973).
- Rodríguez, N. B., L. Pfister, E. Zehe, and J. Klaus (2021). “A comparison of catchment travel times and storage deduced from deuterium and tritium tracers using StorAge Selection functions.” In: *Hydrology and Earth System Sciences* 25.1, pp. 401–428. DOI: [10.5194/hess-25-401-2021](https://doi.org/10.5194/hess-25-401-2021).
- Roth, K. (2008). “Scaling of water flow through porous media and soils.” In: *European journal of soil science* 59.1, pp. 125–130. DOI: [10.1111/j.1365-2389.2007.00986.x](https://doi.org/10.1111/j.1365-2389.2007.00986.x).
- Roth, K. and K. Hammel (1996). “Transport of conservative chemical through an unsaturated two-dimensional Miller-similar medium

- with steady state flow." In: *Water Resources Research* 32.6, pp. 1653–1663. DOI: [10.1029/96wr00756](https://doi.org/10.1029/96wr00756).
- Russian, A., M. Dentz, T. Le Borgne, J. Carrera, and J. Jimenez-Martinez (2013). "Temporal scaling of groundwater discharge in dual and multicontinuum catchment models." In: *Water Resources Research* 49.12, pp. 8552–8564. DOI: [10.1002/2013wr014255](https://doi.org/10.1002/2013wr014255).
- Sander, T. and H. H. Gerke (2009). "Modelling field-data of preferential flow in paddy soil induced by earthworm burrows." In: *Journal of Contaminant Hydrology* 104.1-4, pp. 126–136. DOI: [10.1016/j.jconhyd.2008.11.003](https://doi.org/10.1016/j.jconhyd.2008.11.003).
- Sarkar, B. et al. (2020). "Sorption and desorption of agro-pesticides in soils." In: *Agrochemicals Detection, Treatment and Remediation*. Elsevier, Oxford, UK, pp. 189–205. DOI: [10.1016/b978-0-08-103017-2.00008-8](https://doi.org/10.1016/b978-0-08-103017-2.00008-8).
- Schmidt, M. J., S. D. Pankavich, A. Navarre-Sitchler, and D. A. Benson (2019). "A Lagrangian method for reactive transport with solid/aqueous chemical phase interaction." In: *Journal of Computational Physics* 2, p. 100021. DOI: [10.1016/j.jcp.2019.100021](https://doi.org/10.1016/j.jcp.2019.100021).
- Schneider, A.-K. et al. (2018). "Variability of earthworm-induced biopores and their hydrological effectiveness in space and time." In: *Pedobiologia* 71, pp. 8–19. DOI: [10.1016/j.pedobi.2018.09.001](https://doi.org/10.1016/j.pedobi.2018.09.001).
- Schäfer, D. (1999). "Bodenhydraulische Eigenschaften eines Kleineinzugsgebietes. Vergleich und Bewertung unterschiedlicher Verfahren." PhD thesis. Karlsruhe, Germany: University of Karlsruhe.
- Shipitalo, M. J. and K. R. Butt (1999). "Occupancy and geometrical properties of *Lumbricus terrestris* L. burrows affecting infiltration." In: *Pedobiologia* 43, pp. 782–794.
- Šimůnek, J. and M. Th. van Genuchten (2008). "Modeling Nonequilibrium Flow and Transport Processes Using HYDRUS." In: *Vadose Zone Journal* 7.2, pp. 782–797. DOI: [10.2136/vzj2007.0074](https://doi.org/10.2136/vzj2007.0074).
- Šimůnek, J., M. Th. van Genuchten, and M. Šejna (2008). "Development and Applications of the HYDRUS and STANMOD Software Packages and Related Codes." In: *Vadose Zone Journal* 7.2, pp. 587–600. DOI: [10.2136/vzj2007.0077](https://doi.org/10.2136/vzj2007.0077).
- Šimůnek, J., N. J. Jarvis, M. Th. van Genuchten, and A. Gärdenäs (2003). "Review and comparison of models for describing non-equilibrium and preferential flow and transport in the vadose zone." In: *Journal of Hydrology* 272.1-4, pp. 14–35. DOI: [10.1016/s0022-1694\(02\)00252-4](https://doi.org/10.1016/s0022-1694(02)00252-4).
- Sklash, M. G., K. J. Beven, K. Gilman, and W. G. Darling (1996). "Isotope studies of pipeflow at Plynlimon, Wales, UK." In: *Hydrological Processes* 10.7, pp. 921–944. DOI: [10.1002/\(SICI\)1099-1085\(199607\)10:7<921::AID-HYP347>3.0.CO;2-B](https://doi.org/10.1002/(SICI)1099-1085(199607)10:7<921::AID-HYP347>3.0.CO;2-B).
- Sprenger, M., H. Leistert, K. Gimbel, and M. Weiler (2016). "Illuminating hydrological processes at the soil-vegetation-atmosphere

- interface with water stable isotopes." In: *Reviews of Geophysics* 54.3, pp. 674–704. DOI: [10.1002/2015RG000515](https://doi.org/10.1002/2015RG000515).
- Sprenger, M., D. Tetzlaff, J. Buttle, H. Laudon, and C. Soulsby (2018a). "Water ages in the critical zone of long-term experimental sites in northern latitudes." In: *Hydrology and Earth System Sciences* 22.7, pp. 3965–3981. DOI: [10.5194/hess-22-3965-2018](https://doi.org/10.5194/hess-22-3965-2018).
- Sprenger, M. et al. (2018b). "Measuring and modeling stable isotopes of mobile and bulk soil water." In: *Vadose zone journal*. DOI: [10.2136/vzj2017.08.0149](https://doi.org/10.2136/vzj2017.08.0149).
- Sprenger, M. et al. (2019). "The demographics of water: A review of water ages in the critical zone." In: *Reviews of Geophysics* 57.3, pp. 800–834. DOI: [10.1029/2018RG000633](https://doi.org/10.1029/2018RG000633).
- Stagge, J. H. et al. (2019). "Assessing data availability and research reproducibility in hydrology and water resources." In: *Scientific data* 6.1, pp. 1–12. DOI: [10.1038/sdata.2019.30](https://doi.org/10.1038/sdata.2019.30).
- Sternagel, A. (2022). *Code of the LAST-Model, Version 0.1.1*. DOI: [10.5281/zenodo.6375769](https://doi.org/10.5281/zenodo.6375769). URL: <https://github.com/KIT-HYD/last-model>.
- Sternagel, A., R. Loritz, J. Klaus, B. Berkowitz, and E. Zehe (2021). "Simulation of reactive solute transport in the critical zone: a Lagrangian model for transient flow and preferential transport." In: *Hydrology and Earth System Sciences* 25.3, pp. 1483–1508. DOI: [10.5194/hess-25-1483-2021](https://doi.org/10.5194/hess-25-1483-2021).
- Sternagel, A., R. Loritz, W. Wilcke, and E. Zehe (2019). "Simulating preferential soil water flow and tracer transport using the Lagrangian Soil Water and Solute Transport Model." In: *Hydrology and Earth System Sciences* 23.10, pp. 4249–4267. DOI: [10.5194/hess-23-4249-2019](https://doi.org/10.5194/hess-23-4249-2019).
- Talbot, C. A. and F. L. Ogden (2008). "A method for computing infiltration and redistribution in a discretized moisture content domain." In: *Water Resources Research* 44.8. DOI: [10.1029/2008WR006815](https://doi.org/10.1029/2008WR006815).
- Tang, Q. et al. (2012). "Augmentation of tribenuron methyl removal from polluted soil with *Bacillus* sp. strain BS2 and indigenous earthworms." In: *Journal of Environmental Sciences* 24.8, pp. 1492–1497. DOI: [10.1016/s1001-0742\(11\)60947-9](https://doi.org/10.1016/s1001-0742(11)60947-9).
- Uffink, G. J. M. (1990). "Analysis of dispersion by the random walk method." PhD thesis. Delft, Netherlands: Delft University of Technology.
- Uhlenbrook, S. (2006). "Catchment hydrology—a science in which all processes are preferential." In: *Hydrological Processes* 20.16, pp. 3581–3585. DOI: [10.1002/hyp.6564](https://doi.org/10.1002/hyp.6564).
- Villholth, K. G., N. J. Jarvis, O. H. Jacobsen, and H. Jonge (2000). "Field Investigations and Modeling of Particle-Facilitated Pesticide Transport in Macroporous Soil." In: *Journal of Environmental Quality* 29.4, pp. 1298–1309. DOI: [10.2134/jeq2000.00472425002900040037x](https://doi.org/10.2134/jeq2000.00472425002900040037x).
- van Dam, J. C., P. Groenendijk, R. F. A. Hendriks, and J. G. Kroes (2008). "Advances of Modeling Water Flow in Variably Saturated

- Soils with SWAP." In: *Vadose Zone Journal* 7.2, pp. 640–653. DOI: [10.2136/vzj2007.0060](https://doi.org/10.2136/vzj2007.0060).
- van Genuchten, M. Th. (1980). "A Closed-form Equation for Predicting the Hydraulic Conductivity of Unsaturated Soils." In: *Soil Science Society of America Journal* 44.5, pp. 892–898. DOI: [10.2136/sssaj1980.03615995004400050002x](https://doi.org/10.2136/sssaj1980.03615995004400050002x).
- van Schaik, L., J. Palm, J. Klaus, E. Zehe, and B. Schröder (2013). "Linking spatial earthworm distribution to macropore numbers and hydrological effectiveness." In: *Ecohydrology* 7.2, pp. 401–408. DOI: [10.1002/eco.1358](https://doi.org/10.1002/eco.1358).
- van der Velde, Y. et al. (2014). "Consequences of mixing assumptions for time-variable travel time distributions." In: *Hydrological Processes* 29.16, pp. 3460–3474. DOI: [10.1002/hyp.10372](https://doi.org/10.1002/hyp.10372).
- WRB, IUSS Working Group (2014). *World Reference Base for Soil Resources 2014. International soil classification system for naming soils and creating legends for soil maps*. Tech. rep. Rome, Italy.
- Weiler, M. (2001). "Mechanisms controlling macropore flow during infiltration. Dye tracer experiments and simulations." PhD thesis. Zürich, Switzerland: ETH Zürich.
- Weiler, M. (2005). "An infiltration model based on flow variability in macropores: development, sensitivity analysis and applications." In: *Journal of Hydrology* 310.1-4, pp. 294–315. DOI: [10.1016/j.jhydrol.2005.01.010](https://doi.org/10.1016/j.jhydrol.2005.01.010).
- Weiler, M., B. L. McGlynn, K. J. McGuire, and J. J. McDonnell (2003). "How does rainfall become runoff? A combined tracer and runoff transfer function approach." In: *Water Resources Research* 39.11. DOI: [10.1029/2003WR002331](https://doi.org/10.1029/2003WR002331).
- Whitmer, S., L. Baker, and R. Wass (2000). "Loss of Bromide in a Wetland Tracer Experiment." In: *Journal of Environmental Quality* 29.6, pp. 2043–2045. DOI: [10.2134/jeq2000.00472425002900060043x](https://doi.org/10.2134/jeq2000.00472425002900060043x).
- Wienhöfer, J. and E. Zehe (2014). "Predicting subsurface stormflow response of a forested hillslope – the role of connected flow paths." In: *Hydrology and Earth System Sciences* 18.1, pp. 121–138. DOI: [10.5194/hess-18-121-2014](https://doi.org/10.5194/hess-18-121-2014).
- Willmann, M., J. Carrera, and X. Sánchez-Vila (2008). "Transport up-scaling in heterogeneous aquifers: What physical parameters control memory functions?" In: *Water Resources Research* 44.12. DOI: [10.1029/2007WR006531](https://doi.org/10.1029/2007WR006531).
- Workman, S. R. and R. W. Skaggs (1990). "PREFLO: A water management model capable of simulating preferential flow." In: *Transactions of the ASAE* 33.6, pp. 1939–1948. DOI: [10.13031/2013.31562](https://doi.org/10.13031/2013.31562).
- Zehe, E. (1999). "Stofftransport in der ungesättigten Bodenzone auf verschiedenen Skalen." PhD thesis. Karlsruhe, Germany: University of Karlsruhe.

- Zehe, E. and G. Blöschl (2004). "Predictability of hydrologic response at the plot and catchment scales: Role of initial conditions." In: *Water Resources Research* 40.10. DOI: [10.1029/2003wr002869](https://doi.org/10.1029/2003wr002869).
- Zehe, E. and H. Flühler (2001a). "Preferential transport of isotoproturon at a plot scale and a field scale tile-drained site." In: *Journal of Hydrology* 247.1-2, pp. 100–115. DOI: [10.1016/s0022-1694\(01\)00370-5](https://doi.org/10.1016/s0022-1694(01)00370-5).
- Zehe, E. and H. Flühler (2001b). "Slope scale variation of flow patterns in soil profiles." In: *Journal of Hydrology* 247.1-2, pp. 116–132. DOI: [10.1016/s0022-1694\(01\)00371-7](https://doi.org/10.1016/s0022-1694(01)00371-7).
- Zehe, E. and C. Jackisch (2016). "A Lagrangian model for soil water dynamics during rainfall-driven conditions." In: *Hydrology and Earth System Sciences* 20.9, pp. 3511–3526. DOI: [10.5194/hess-20-3511-2016](https://doi.org/10.5194/hess-20-3511-2016).
- Zehe, E., R. Loritz, Y. Edery, and B. Berkowitz (2021). "Preferential pathways for fluid and solutes in heterogeneous groundwater systems: self-organization, entropy, work." In: *Hydrology and earth system sciences* 25.10, pp. 5337–5353. DOI: [hess-25-5337-2021](https://doi.org/hess-25-5337-2021).
- Zehe, E., T. Maurer, J. Ihringer, and E. Plate (2001). "Modeling water flow and mass transport in a loess catchment." In: *Physics and Chemistry of the Earth, Part B: Hydrology, Oceans and Atmosphere* 26.7-8, pp. 487–507. DOI: [10.1016/s1464-1909\(01\)00041-7](https://doi.org/10.1016/s1464-1909(01)00041-7).
- Zehe, E. et al. (2014). "HESS Opinions: From response units to functional units: a thermodynamic reinterpretation of the HRU concept to link spatial organization and functioning of intermediate scale catchments." In: *Hydrology and Earth System Sciences* 18.11, pp. 4635–4655. DOI: [10.5194/hess-18-4635-2014](https://doi.org/10.5194/hess-18-4635-2014).
- Zinn, B. and C. F. Harvey (2003). "When good statistical models of aquifer heterogeneity go bad: A comparison of flow, dispersion, and mass transfer in connected and multivariate Gaussian hydraulic conductivity fields." In: *Water Resources Research* 39.3. DOI: [10.1029/2001WR001146](https://doi.org/10.1029/2001WR001146).

ACKNOWLEDGMENTS

Many thanks and appreciation to my family, friends and (former) colleagues for all the support, which made this thesis possible.

My deepest gratitude goes to my supervisor Prof. Dr. Zehe. Your passion and expertise in your lectures awakened my interest in hydrology during my Master's. Throughout the years, we always had a valuable and pleasant relationship on a professional and also interpersonal level. I really appreciate that you create such a scientifically fruitful working atmosphere and that you spent endless time for helping your PhD students. Erwin, thank you very much for making this thesis possible and in general, for everything you have done for me.

Furthermore, special thanks go to my scientific collaborators and co-authors of my research articles, namely Ralf Loritz, Brian Berkowitz, Wolfgang Wilcke and Julian Klaus. Thank you for providing data, proofreading and your scientific input. Particularly, I would like to mention the great influence of Ralf Loritz on my work. Ralf, your enthusiasm for science, your creativity and countless ideas significantly increased the quality of my work. I really enjoy our scientific and non-scientific discussions. Thank you.

I would also like to acknowledge the Karlsruhe Institute of Technology and its Open Access Publishing Fund for funding the publication of my research articles.

Last but not least, I am deeply grateful for all my friends of "Team Thorben" and the good time we share together every Wednesday evening. Thanks to Nadja, Goldberger, Michi, Jän, Thomas, Jonas, Consti, Vali and Thorbinho.

OWN PUBLICATIONS

FIRST AUTHOR; PEER-REVIEWED INTERNATIONAL PUBLICATIONS

Sternagel, A., R. Loritz, W. Wilcke, and E. Zehe (2019). "Simulating preferential soil water flow and tracer transport using the Lagrangian Soil Water and Solute Transport Model." In: *Hydrology and Earth System Sciences* 23.10, pp. 4249–4267. <https://doi.org/10.5194/hess-23-4249-2019>.

Sternagel, A., R. Loritz, J. Klaus, B. Berkowitz, and E. Zehe (2021). "Simulation of reactive solute transport in the critical zone: a Lagrangian model for transient flow and preferential transport." In: *Hydrology and Earth System Sciences* 25.3, pp. 1483–1508. <https://doi.org/10.5194/hess-25-1483-2021>.

Sternagel, A., R. Loritz, B. Berkowitz, and E. Zehe (2022). "Stepping beyond perfectly mixed conditions in soil hydrological modelling using a Lagrangian approach." In: *Hydrology and Earth System Sciences* 26, pp. 1615–1629. <https://doi.org/10.5194/hess-26-1615-2022>.

CONFERENCE CONTRIBUTIONS (POSTER)

Sternagel, A., R. Loritz, W. Wilcke and E. Zehe (2019): "Simulation von präferentiellem Wasserfluss und Stofftransport in makroporösen Böden unter Verwendung des partikelbasierten LAST-Modells", Tag der Hydrologie 2019, Karlsruhe, Germany.

Sternagel, A., R. Loritz, W. Wilcke and E. Zehe (2019): "Simulating preferential soil water flow and tracer transport using the Lagrangian Soil Water and Solute Transport Model (LAST)", 10th EGU Leonardo Conference 2019, Esch-sur-Alzette, Luxembourg.

Sternagel, A., R. Loritz, W. Wilcke, and E. Zehe (2020): "Simulating preferential soil water flow and reactive solute transport using the Lagrangian Soil Water and Solute Transport Model (LAST)", EGU General Assembly 2020, online.

DECLARATION

Authors contributions:

Section 2: Sternagel, A., R. Loritz, W. Wilcke, and E. Zehe (2019). “Simulating preferential soil water flow and tracer transport using the Lagrangian Soil Water and Solute Transport Model.” In: *Hydrology and Earth System Sciences* 23.10, pp. 4249–4267. <https://doi.org/10.5194/hess-23-4249-2019>.

Alexander Sternagel wrote the paper, did the main code developments and carried out the analysis. Ralf Loritz, Wolfgang Wilcke and Erwin Zehe contributed to the theoretical framework and helped with interpreting and editing.

Section 3: Sternagel, A., R. Loritz, J. Klaus, B. Berkowitz, and E. Zehe (2021). “Simulation of reactive solute transport in the critical zone: a Lagrangian model for transient flow and preferential transport.” In: *Hydrology and Earth System Sciences* 25.3, pp. 1483–1508. <https://doi.org/10.5194/hess-25-1483-2021>.

Alexander Sternagel wrote the paper, did the main code developments, and carried out the analysis. Julian Klaus and Erwin Zehe provided the data. Ralf Loritz, Julian Klaus, Brian Berkowitz and Erwin Zehe contributed to the theoretical framework and helped with interpreting and editing.

Section 4: Sternagel, A., R. Loritz, B. Berkowitz, and E. Zehe (2022). “Stepping beyond perfectly mixed conditions in soil hydrological modelling using a Lagrangian approach.” In: *Hydrology and Earth System Sciences* 26, pp. 1615–1629. <https://doi.org/10.5194/hess-26-1615-2022>.

Alexander Sternagel wrote the paper, did the main code developments, and carried out the analysis. Ralf Loritz, Brian Berkowitz, and Erwin Zehe contributed to the theoretical framework and helped with the interpreting and editing of the paper.

Data availability:

The code of the LAST-Model (Version 0.1.1) is available in a GitHub repository: <https://github.com/KIT-HYD/last-model> (Sternagel, 2022).

Eidesstattliche Versicherung gemäß § 13 Absatz 2 Satz 1 Ziffer 4 der Promotionsordnung des Karlsruher Instituts für Technologie (KIT) für die KIT-Fakultät für Bauingenieur-, Geo- und Umweltwissenschaften:

1. Bei der eingereichten Dissertation zu dem Thema *A Lagrangian model framework for the simulation of fluid flow and solute transport in soils* handelt es sich um meine eigenständig erbrachte Leistung.
2. Ich habe nur die angegebenen Quellen und Hilfsmittel benutzt und mich keiner unzulässigen Hilfe Dritter bedient. Insbesondere habe ich wörtlich oder sinngemäß aus anderen Werken übernommene Inhalte als solche kenntlich gemacht.
3. Die Arbeit oder Teile davon habe ich bislang nicht an einer Hochschule des In- oder Auslands als Bestandteil einer Prüfungs- oder Qualifikationsleistung vorgelegt.
4. Die Richtigkeit der vorstehenden Erklärungen bestätige ich.
5. Die Bedeutung der eidesstattlichen Versicherung und die strafrechtlichen Folgen einer unrichtigen oder unvollständigen eidesstattlichen Versicherung sind mir bekannt.

Ich versichere an Eides statt, dass ich nach bestem Wissen die reine Wahrheit erklärt und nichts verschwiegen habe.

Karlsruhe, 2023

Alexander Sternagel

COLOPHON

This document was typeset using the typographical look-and-feel classicthesis developed by André Miede. The style was inspired by Robert Bringhurst's seminal book on typography "*The Elements of Typographic Style*". classicthesis is available for both L^AT_EX and L^yX:

<https://bitbucket.org/amiede/classicthesis/>

Happy users of classicthesis usually send a real postcard to the author, a collection of postcards received so far is featured here:

<http://postcards.miede.de/>

Final Version as of April 19, 2023 (classicthesis v4.6).